

## An analytical model for predicting the natural frequency of retaining structures

Lyazid Guechi, Smaïn Belkacemi

Ecole Nationale Polytechnique d'Alger, Algeria  
Civil Engineering Department  
e-mail: [gue28091@gmail.com](mailto:gue28091@gmail.com), [lyazidguechi@g.enp.edu.dz](mailto:lyazidguechi@g.enp.edu.dz)

### Abstract

The importance of the retaining structures is crucial in geotechnical engineering and the accurate determination of static and seismic earth pressures and natural frequency is important for study the dynamic behavior of these structures. Usually analytical formulas which do not consider the earth pressures behind retaining structure are used. An analytical model for predicting the natural frequency of retaining structures including the earth pressures by failure wedges is proposed in the present analysis. The model considers the effect of Coulomb and Mononobe Okabe failure wedges. Backfill material is considered in the analysis as cohesionless. The failure wedge is an important factor which should be considered in determining the natural frequency of retaining structures. As the weight of failure wedge increases the natural frequency decreases significantly. The current model is validated using several analytical models reported in the literature of the earlier researcher.

**Key words:** Analytical model, dynamic behavior, retaining structures, natural frequency, failure wedge.

## 1 Introduction

An adequate determination of the natural frequency of retaining structures plays a primordial role in the study of its dynamic behavior in earthquake prone regions. Many researchers have developed several methods to determine the natural frequency of retaining structures. In these methods, the natural frequency is often calculated by the elastic wave theory and based on two parameters namely height of the backfill and the soil shear wave velocity. The effect of the properties of earth pressures didn't get any attention till today. In the last few years, there has been increased interest in the study of the effects of soil on the natural frequency of structures: for free spanning offshore pipelines [1], for soil-foundation system [2] and for foundations of offshore wind turbines [3].

In this paper, a complete analysis is carried out to determine the natural frequency of retaining structures analytically in a more general way by introducing the Coulomb and Mononobe

Okabe active failure wedge. An analytical model is proposed to determine the natural frequency of retaining structures. This model estimates the natural frequency of wall-backfill soil system by using the Coulomb [4] and Mononobe Okabe [5, 6] to evaluate soil wedge created by active earth pressure behind retaining structures in both static and seismic cases. The validity of the proposed model will demonstrate by using results within the Scott [7] and Ghanbari et al [8] models.

## 2 Model formulation

### 2.1 General model description

The importance of the retaining structures is crucial in geotechnical engineering and the accurate determination of seismic earth pressures and natural frequency is important for study the dynamic behavior of these structures. In the most previous investigations, the soil backfill was considered sufficient width as rectangular wedge whereas in the real, the backfill behind retaining structures repartitioned as triangular wedge. Rectifying this weakness, this study proposed an analytical model for calculating the natural frequency of retaining structures by considering the triangular active static and seismic failure wedges.

This work is first include the active failure wedges in determination of natural frequency of retaining structures and proposed a new model; a complete study has been carried out to determine the natural frequency in a more general way.

It is possible and common to obtain equivalent natural frequency for a backfill soil-retaining structure system from results of analytical analysis assuming the system has a single degree of freedom.

The normalized form of first vibration mode in a retaining wall without considering failure wedge has been used as the shape function for determining the natural frequency of retaining wall with considering failure wedges.

### 2.2 Mathematical Formulation of the Problem

The proposed retaining structure model is illustrated schematically in Fig. 1 for static case and under seismic pseudo static conditions, and it is defined by (a) structure's characteristics: weight per unit length, modulus of elasticity, thickness and height (b) backfill soil characteristics: Poisson's ratio, soil friction angle, Young modulus and weight per unit mass and (c) seismic excitation characteristics: horizontal and vertical seismic accelerations.

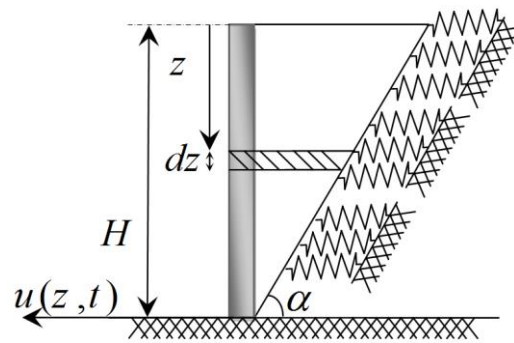


Figure 1: Description of model

In view of analytical studies, this model is designed to be as simple as possible, including Coulomb and Mononobe Okabe active failure wedges. More precisely, figure 2 represent the dynamic equilibrium and resultant forces acting on differential element of the modeled system. The following assumptions are adopted:

- the retaining wall behaves as a flexible structure [9];
- the static thrust is evaluated by Coulomb method [4];
- the seismic thrust is evaluated by Mononobe Okabe method [5,6];
- the inclined failure plane is modeled as a series of Winkler's springs [10];
- the natural frequency of wall-backfill soil system is estimated by Rayleigh method [11];and
- the backfill soil is assumed dry and cohesionless.

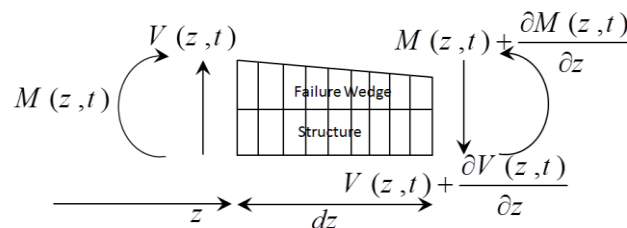


Figure 2: Dynamic equilibrium and resultant forces acting on differential element of the modeled system.

The kinetic energy can be calculated by integrating the mass through height of the retaining structure with failure wedge model and the potential energy by integrating the stiffness through the height of the model.

The kinetic energy in the system can be written as follows:

$$T_{\max} = \frac{1}{2} \int_0^H m(z) \left( \frac{\partial u}{\partial t} \right)^2 dz = \frac{\omega^2}{2} \int_0^H m(z) U^2(z) dz \quad (1)$$

The total potential energy, V, in the structure and backfill is written as follows:

$$V_{\max} = \frac{1}{2} \int_0^H E_m I(z) \left( \frac{\partial^2 U(z)}{\partial z} \right)^2 dz + \frac{1}{2} \int_0^H k U^2(z) dz \quad (2)$$

In this model, the mass of a thin element of thickness  $dz$  'soil & structure' at depth  $z$  is given by:

$$m(z) = \left( \rho_{soil} \cdot \frac{H-z}{\tan \alpha} + \rho_{str} \cdot e \right) dz \quad (3)$$

The inertial moment of model can be expressed as,

$$I(z) = \frac{1}{12} \left( \frac{H-z}{\tan \alpha} + e \right)^3 \quad (4)$$

The equivalent elastic soil-structure modulus of model  $E_m$  may be calculated as follows:

$$E_m(z) = \frac{E_{soil} E_{str} (H-z+e)}{(H-z) E_{str} + e E_{soil}} \quad (5)$$

The circular natural frequency, ( $\omega$ ) is defined as,

$$\omega^2 = \frac{\int_0^H E_m I(z) \left( \frac{d^2 U(z)}{dz^2} \right)^2 dz + \int_0^H k U^2(z) dz}{\int_0^H m(z) U^2(z) dz} \quad (6)$$

In equation (6), the stiffness per unit length of Winkler's spring ( $k$ ) can be computed using subgrade reaction modulus ( $K$ ) by Galin expression [8].

### 2.3 Solution for the retaining structure including soil failure wedge

Similar to the analysis of [8] using the Rayleigh's quotient method, the natural circular frequency of retaining structures can be obtained in the following manner.

The extension of the method for including failure wedge is not presented. A detailed methodology of calcul is already reported in [8].

Combining Eqs. (3), (4), (5) and (6), and integrating over the height of the wall, it is straightforward to show that the first circular natural frequency ( $\omega$ ) of system is given by:

$$\omega^2 = \frac{\frac{E_m}{12} \left[ 3.11 \left( \frac{e}{H} \right)^3 + \frac{7.54}{\tan(\alpha)} \left( \frac{e}{H} \right)^2 + \frac{6.31}{\tan^2(\alpha)} \frac{e}{H} + \frac{1.80}{\tan^3(\alpha)} \right] + \frac{Hk}{4}}{\frac{0.049}{\tan(\alpha)} \rho_{soil} \cdot H^2 + 0.252 \rho_{str} e H} \quad (7)$$

Equation (7) takes into account changes in soil wedge geometry and was used in the analysis given below.

From this equation (7), it is seen that  $\omega$  is function of the retaining structure parameters, backfill soil parameters and failure wedge behind retaining structure.

### 3 Validation and comparison with available solutions

To verify the validity of the proposed model, the calculated natural frequencies were compared with those reported in literature ‘Scott’ [7] and ‘Ghanbari et al.’ [8]. For different values of wall height (Fig.3.a) and backfill friction angle (Fig.3.b), natural angular frequency associated with Coulomb and Mononobe Okabe failure wedges models computed in the present study is located between that of ‘Scott’ [7] and ‘Ghanbari et al.’ [8] methods with  $\nu_{soil}=0.2$ ,  $E_{soil}=15$  MPa,  $E_{str}=26$  GPa,  $\rho_{soil}=1900$  kg/m<sup>3</sup>,  $\rho_{str}=2320$  kg/m<sup>3</sup>,  $H=7$  m and  $a_h=0.3$ ,  $a_v=0.5a_h$ .

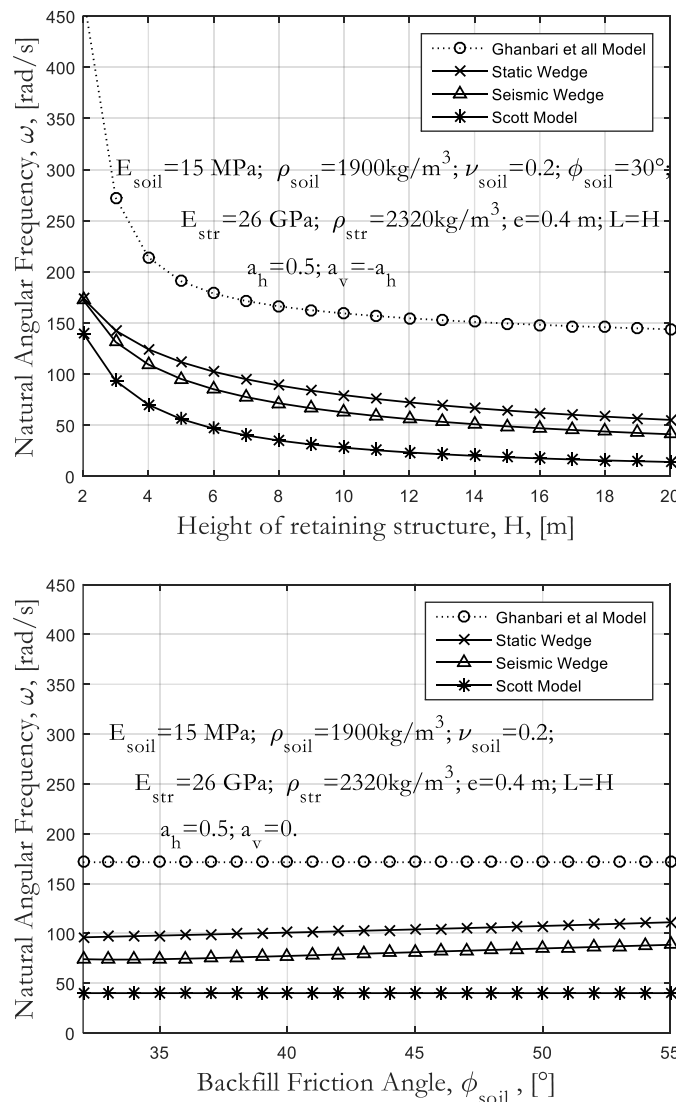


Figure 3: Scott, Ghanbari et al. and present study verification of naturel angular frequency

Scott (1973) [7] and Ghanbari et al. (2013) [8] methods do not consider the effect of backfill friction angle on the natural frequency of retaining structures.

## 4 Conclusion

In this research, by considering the earth pressures of the soil backfill behind retaining structures the natural frequency of retaining structures obtained. An analytical model using the Coulomb and Mononobe-Okabe failure wedges, to determine the natural frequency of retaining structures, is developed. In addition to the consideration of horizontal and vertical seismic acceleration coefficients, height and thickness of structure, Young modulus and density of the soil and the structure material and also Poisson ratio and friction angle of soil backfill are considered. Both static and seismic active thrusts are considered and it is found that values of natural frequency decreases significantly with the increase in the values of failure wedges.

The consideration of failure wedge plays an important role in determining the natural frequency of retaining structures, each variation of soil backfill and seismic accelerations changed the system and naturally the natural frequency.

The proposed model is reliable and is expected to give useful results for retaining structures.

## References

- [1] Yaghoobi, M. Mazaheri, S. & Dabbari, E. (2012). Determining natural frequency of free spanning offshore pipelines by considering the seabed soil characteristics. *J. Par. Gulf. Mar. Scie.* 3, 25-34. DOI: .
- [2] Ahn. J. Biscontin, G. & Roësset, J.M. (2011). Natural frequency and damping ratio of a vertically vibrated surface foundation. *Soil. Dyn. Earth. Eng.* 31, 674-681. DOI: .
- [3] Bhattacharya, S. (2014). Challenge in design of foundations for Offshore wind turbines. *Eng. Tech. Ref.* 31, 1-9. DOI: .
- [4] Coulomb, C. (1776). *Essai sur une application des règles de Maximis & Minimis à quelques problèmes de statique relatives à l'architecture*. Mémoires de Mathématiques et de physique, Académie Royale des sciences, Paris, France.
- [5] Okabe, S. (1926). General theory of earth pressure. *J. Jap. Soc. Civ. Eng.* 12(1). DOI: .
- [6] Mononobe, N. (1929). On the determination of earth pressure during earthquakes. In Proceedings of the IX world Engineering Congress.
- [7] Scott, R.F. (1973). Earthquake-induced earth pressures on retaining walls. In 5th World Conference on Earthquake Engineering. Rome, Italy.
- [8] Ghanbari, A. Hoomaan, E. & Mojallal, M. (2013). An analytical method for calculating the natural frequency of retaining walls. *Inter. J. Civ. Eng. Geotech.* 11, 1-9. DOI: .
- [9] Sitar, N. & Wagner, N (2015). On Seismic Response of Stiff and Flexible Retaining Structures. In 6th International Conference on Earthquake Geotechnical Engineering, New Zealand.
- [10] Xu, Q. (2017). Investigation of Stability Alarming for Retaining Wall Structures with Damage. *Shock. Vib.* 1-12. DOI:org/10.1155/2017/4691947.
- [11] Bakhtiari-Nejad, F. Khorram, A. & Rezaeian, M. (2014). Analytical estimation of natural frequencies and mode shapes of a beam having two cracks. *Inter. J. Mech. Scie.* 78, 193-202. DOI: .

## Using water wall like air humidifier

Katarína Čákyová, František Vranay, Zuzana Vranayová

Technical University of Košice, Slovakia  
Faculty of Civil Engineering, Institute of Architectural Engineering  
e-mail: [katarina.cakyova@tuke.sk](mailto:katarina.cakyova@tuke.sk), [frantisek.vranay@tuke.sk](mailto:frantisek.vranay@tuke.sk), [zuzana.vranayova@tuke.sk](mailto:zuzana.vranayova@tuke.sk)

### Abstract

This paper presents experimental results of the study of falling water film evaporation from water wall. The contribution is divided into several parts. The introduction is devoted to the theoretical part of the use, then the prototype of the water wall is presented and its most important parts are described. In order to verify the humidification performance of the water wall, experimental verification under laboratory conditions (climate chamber) was chosen. One task for the definition of water wall evaporation potential is to determine and develop the measuring system, which is clearly defined in article. The present document describes the methodology and boundary conditions during experiments. Plate heat exchanger ensured a water temperature in the system approximately 23 °C hot during all measurements. A total of 4 measurements were performed at different air temperatures and relative humidity. The results showed that at different temperatures and relative humidity of air, the water wall has a different humidification performance.

**Key words:** evaporation process, water wall, experimental measurements, climate chamber,

## 1 Introduction

To achieve satisfying thermal comfort we use different ventilation, heating or cooling systems, which are responsible for half of the energy demands in relation to the buildings sector. Main parameters of the six primary factors of thermal comfort are humidity and air temperature. Achieving a satisfactory level of air humidity is not just a parameter influencing the energy consumption of buildings but also overall satisfaction with the indoor environment quality, health and work productivity.

In the climatic area of Slovakia, the problem with a low RH in buildings occurs mainly during winter season. Although the relative humidity of the outside air is high, due to low temperatures, water vapour content in the outside air is low. Then after heating to the internal temperature, the relative humidity of indoor air is too low. A low level of indoor humidity leads to dry air and the symptoms such as dryness, irritation or itching of the skin and eyes,

dry throat and nose, and irritation in the upper airways [1]. In accordance with official regulations of the Ministry of Health of the Slovak Republic, the permissible relative humidity is in the range of 30-70%. However, in some cases, there was dissatisfaction with air humidity as dry or sore throat and itching, burning or irritation to the eyes, although these limit values were observed. [2].

Moisture sources, airflows, moisture exchange with materials and state of water vapour in the exterior affect the level of indoor humidity. One of the sources can be also decorative elements like water features. In the interior, we can find the water elements in different forms, like fountains, decorative pools but also water walls, with using various materials. Benefit of water wall (Fig. 1) is lower spatial requirement in interior of building. Water walls represent one of the pattern of biophilic design. Presence of water feature in interior can lead to increasing of concentration and productivity, but also have health benefits [3].

The aim of this article is to present the water wall as a humidifier inside buildings which can increase air humidity by evaporation process. The physics of these processes is quite complex, involving conjugate heat and mass transfer among liquid-gaseous phase together with the change of phase associated with evaporation. Evaporation process depends on several things for example concentration of the water evaporating in the air. If the air already has a high concentration of evaporated water, then the given water will evaporate more slowly, so evaporation is slower with higher relative humidity. Another important parameter is temperature of water. With higher temperature of water, there is greater kinetic energy of molecules at its surface and therefore rate of evaporation is faster [4]. Due to these facts, the water wall performance was tested under different air temperatures and relative humidity.



Fig. 1: Examples of water wall (shopping centre, Vienna; office building, Baku; railway station, Vienna; library, Brno)

## 2 Methodology

The goal of this work is to verify the potential of water wall for humidification of indoor air. To achieve this goal, the water wall prototype was developed and tested under laboratory condition with using climate chamber, where is possible to set steady boundary conditions. The temperature range is from - 20°C to +125 °C and the climatic range is from 20% to 95%. Its inner dimensions are 3.95\*1.60\*2.85m and the volume of the air in the chamber is



18.01m<sup>3</sup>. The climatic chamber has been chosen to avoid mass exchange between chamber's walls, which are made from stainless steel and air. Due to this fact, the moisture buffer effect of materials can be neglected and clean humidification potential of water wall can be determined. The climate chamber was adapted for measurement purposes to avoided a large draft. In the chamber was created a textile tunnel that was deployed to the air supply. This intervention contributed to a uniform air distribution.

## 2.1 Prototype of water wall

A lot of different designs of water wall and possibilities how to create water film exist. In the present work a water film is formed by perfect overflow. Through the overflow edge, made by glass pane, water runs down and makes continual water film, which is in constant motion.

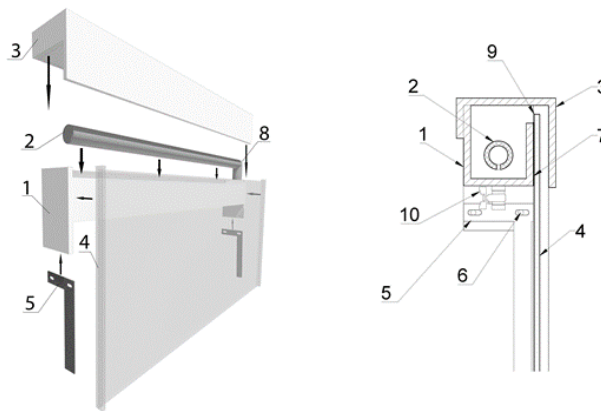


Fig. 2: Main elements of the upper part of prototype: collecting tank (1), perforated pipe (2), cover (3), glass pane (4), supporting metal structure (5), screws (6), silicone adhesive (7), water supply (8), overflow edge (9), ball valve (10)

Among other things, the geometry of the upper part of the water wall affects formation and thickness of the water film (Fig. 2). To construct the upper and down collection tanks, the method based on fusion welding of polypropylene was used, this ensured the watertight tanks. Into upper tank is inserted a perforated pipe for supply of water. The orientation of perforation is downwards what is essential for smooth inlet of water to tank and for forming a water film in the entire width of the water wall. Created water film takes area of one square meter. To connect the collecting tank and glass pane was used silicone adhesive.

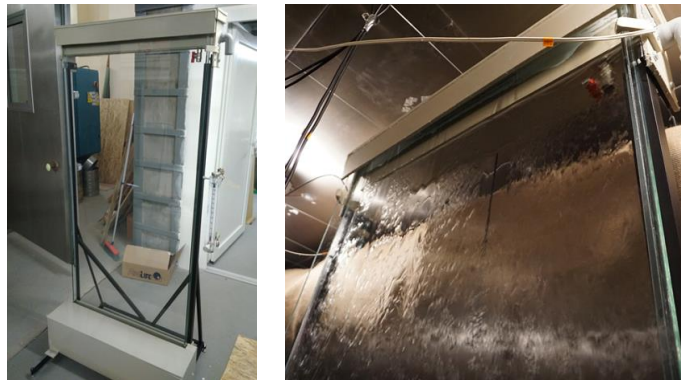


Fig. 3: Final water wall prototype

## 2.2 Measuring instruments

For the recording of boundary conditions, different sensors have been used in the chamber. AHLBORN control unit was used to link sensors and by AMR Win Control software was possible to obtain and collect measured data. The measured values were recorded continuously in a 2 minute time step. Temperature of water was measured by two sensors in upper collecting tank and by two sensors in the lower tank (NTC sensor FN 0001 K with an accuracy of 0.01°C). Installed sensors allow determination of average temperatures of water for lower and upper collecting tanks. Regarding physical air parameters (temperature, relative humidity), two sensors are located in front of water film, and one was placed behind the glass (sensor FHAD 46-C0 with an accuracy of 0.01°C and 0.1 %).

## 2.3 Measuring system of evaporation performance

To investigate the evaporation potential of water wall was used the system based on principle of communicating vessels (Fig. 4). A glass tank was placed on the laboratory scale (RADWAG with an accuracy of 0.01g), which is in an elevated position relative to the measuring cylinder. From glass tank were led two pipes. The end of air supply pipe was located at the water level in measuring cylinder, the end of water supply pipe was 150 mm lower than the air supply pipe. After the start of experiment, individual parts of the prototype are flooded. Water flows from the lower collecting tank to the measuring cylinder, from where it is supplied into the upper collecting tank by pump. It means that water circulates in the system. At the moment water evaporates from the film, the water level in the measuring cylinder drops. Due to this fact, pressure equalization occurs and thus water flows from a glass tank placed on the scale into the measuring cylinder until it reaches the level of the air supply pipe. By this system it is possible to accurately and continuously record evaporation rate in time.



Fig. 4: Measuring system of evaporation performance

In the system is also shut-off valve which offers control of flow rate velocity and for its accurately monitoring the flow meter is used. During experimental measurements the flow rate was 450 l/h what had been found like optimal flow rate during past experiments [5]. Part of the measuring system is a plate heat exchanger which was connected to a tank for hot water located outside the climate chamber. Thanks to the thermostat, it was ensured that the water was heated to 23 °C during all time.

### 3 Results and discussion

Two series of measurements were carried out. Actively using of climate chamber provided steady boundary conditions during the experiments. For one series two measurements were carried out. During measurements temperature of water in the system was same 22.65 °C (TH2O), the air temperature and relative humidity were different (TAIR; RH). Throughout the first series the average air temperature was set at 21.15°C and was two measurements were carried out with relative humidity: 36.4 % (RH\_1) what represents specific humidity 5.802 g/kg and 46.4% (RH\_2) what represents specific humidity 7.415 g/kg. During the second series the average air temperature was 19.19°C and two measurements were carried out with relative humidity: 42.43 % (RH\_1) what represents specific humidity 5.994 g/kg and 56.32% (RH\_2) what represents specific humidity 7.981 g/kg. The graphs (Fig. 5, 6) represent the courses of evaporation weight created by water film in time dependence.

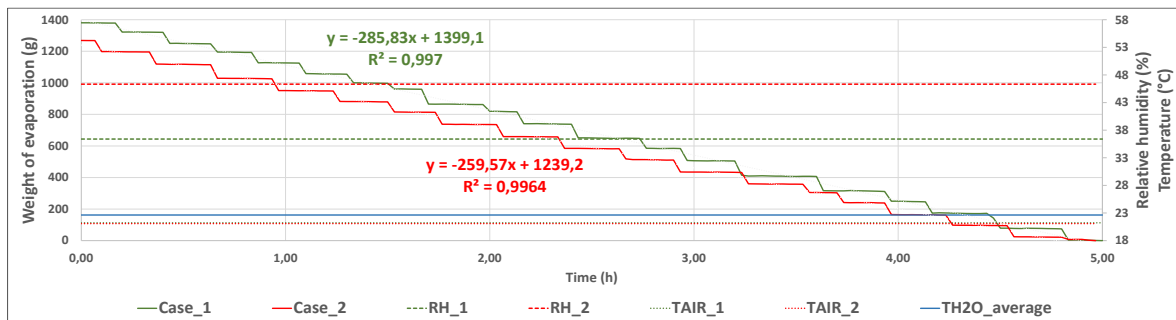


Fig. 5: Curves of evaporation weight when air temperature is 21.15 °C

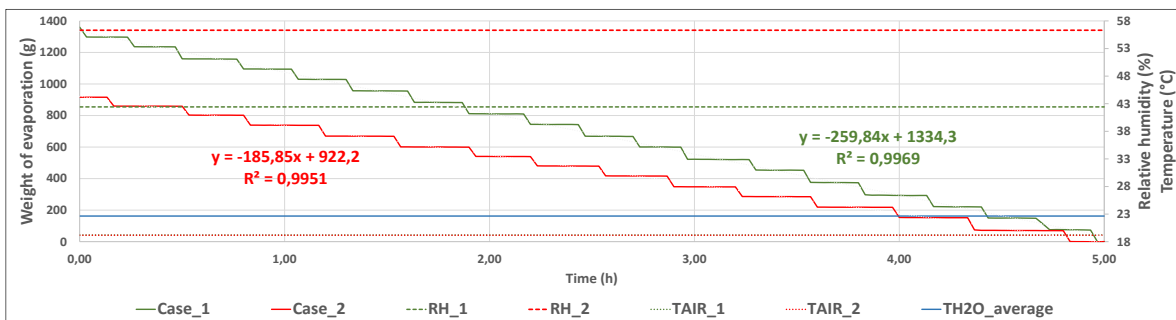


Fig. 6: Curves of evaporation weight when air temperature is 19.19 °C

During first investigation (Fig. 5) with relative humidity 36.4 %, the hourly water loss from glass tank was 285.83 g/h and when the relative humidity was 46.34%, the hourly weight of evaporated water was 259.57 g/h. In the second case (Fig. 6), when relative humidity was 42.43 %, the hourly water loss from glass tank was 259.84 g/h and when relative humidity

was 56.32 % evaporation performance was 185.85 g/h. The presented humidification performance of the water wall refers to the area of the water film which is 1 m<sup>2</sup>.

## 4 Conclusion

Because similar as temperature, air humidity may affect people's thermal comfort it is important to deal with it. Nowadays when we deal more and more with sustainable architecture and new technologies it is important to focus on each element in buildings and use its potential and use it effectively. Water wall isn't able to cover all needs but combination with conventional systems can lead to decreasing of energy consumptions of buildings. The article presents the humidification capacity of the water wall with a water film area of 1 m<sup>2</sup>. In the first case when air temperature was 21.15°C and relative humidity 36.4 % the evaporation performance was 285.83 g/h. Increase of relative humidity by 10% represents a reduction in hourly weight of vapour by 26.26 g, which is 1.1 times less compared when relative humidity is 36.4 %. When air temperature decrease by 1.96°C to 19.19°C humidification performance for relative humidity 42.43% was 259.84 g/h. Increase of relative humidity by 13.89% represents a rise in evaporation weight by 73.99 g, which is 1.4 times less compared to the case when relative humidity is 42.43%. It was shown there is dependence between air temperature, relative humidity and evaporation potential of water wall. Also, hypothesis was verified that with higher air temperature and lower relative humidity the evaporation performance will be higher. The presented contribution is part of the doctoral study. Together was carried out 14 measurements under different boundary conditions from which the general equation for humidification performance of water wall was determined.

## Acknowledgements

This research was supported by grant project APVV-18-0360 “Active hybrid infrastructure towards to sponge city” and by grant project VEGA 1/0217/19 “Research of Hybrid Blue and Green Infrastructure as Active Elements of a 'Sponge City'”

## References

- [1] Jokl M. (2011). *Teorie vnútorného prostredia budov*. ČVUT. 22.11.2019, <https://docplayer.cz/1933879-Teorie-vnutrniho-prostredi-budov.html>
- [2] Vilcekova, S., Meciarova, L., Burdova Kridlova, E., Katunská, J., Kosicanova, D., Doroudiani, S. (2017). Indoor environmental quality of classrooms and occupants' comfort in a special education school in Slovak Republic. *Building and Environment*. Vol.120. 29-40.
- [3] Browning W., Ryan C., Clancy J. (2014). *14 patterns of biophilic design*. Terrapin Bright Green, LLC, 22.11.2019 <http://www.terrapinbrightgreen.com/wp-content/uploads/2014/09/14-Patterns-of-Biophilic-Design-Terrapin-2014p.pdf>
- [4] Bird R. B., Steward W. E., Lightfoot E. N. (2007). *Transport phenomena*. John Wiley & Sons, Inc. ISBN 978-0-470-11539-8.
- [5] Čákyová K., Vranay F., Kusnir M. (2019). Impact of flow rate to water film thickness of water wall. In: *Advances and Trends in Engineering Sciences and Technologies III*. (337-342). London: CRC Press. ISBN 9780367075095.

## Parasitic architecture

Tomáš Baroš, Dušan Katunský

Technical University of Košice, Slovakia  
Faculty of Civil Engineering, Institute of Architectural Engineering  
e-mail: tomas.baros@tuke.sk, dusan.katunsky@tuke.sk

### Abstract

This paper could be considered as a general overview of current examples of realization, research, in architecture which could be called parasitic. Also, as an outline of possible new perspectives on current issues through the biomimicry design philosophy. The aim was also to clearly articulate the intent of the research I am dealing with while opening up a discourse on the subject.

**Key words:** parasitic architecture, biomimicry, parasitic architectural forms

## 1 Introduction

The basis for the whole theme of parasitic architecture and the direction of my research was the initial question, "What if architecture could be self-designed, self-growing, self-developed, and self-healing?" We are currently facing the fundamental challenges of climate change, whose solutions today are reflected in the future direction of humanity. The solutions with that, we try to mitigate the negative impact of our consumer way of living seem to be on a larger scale than slow and inefficient. The building, as a CO<sub>2</sub> producer, the consumer of energy, and the work of man, contributes significantly to the deterioration. The impact of global warming is transforming our environment. In the last two decades, we have experienced eighteen of the hottest years, increases in intensity and frequency of extreme weather events. Europe experienced extreme heatwaves in four of the last five years. An increase in temperatures of 5 ° C as usual above the Arctic Circle in summer has led to a rapid loss of Arctic sea ice. These changes have also harmed Nordic biodiversity, severe droughts in other parts of Europe, floods [1,2]. Transport, electricity and heat generation accounted for two-thirds of total CO<sub>2</sub> emissions, and since 2010 they have also been responsible for almost all global emissions growth. The buildings sector uses half of the world's electricity (21,000 TWh) [3]. Building and construction are responsible for 39% of all carbon emissions in the

world. Of these, operating emissions account for 28% and embodied emissions 11%. The aim of WorldGBC's is fully decarbonising the sector. That requires eliminating embodied and operational carbon emissions [4]. This paper aims to present the current state of knowledge, building practice examples and ongoing research on biomimicry. It also aims to present my vision and concept of Parasitic Architectural Forms as part of biomimicry design.

## **2 What is parasitic architecture, or what we can consider of as parasitic architecture?**

### **2.1 Parasite and parasitism**

Most ecologists harbour a classic, taxonomic view of parasites; that is, parasites are protozoans or metazoans that occupy and harm their free-living hosts. Parasites are typically small-sized organisms that exploit their host both as a food resource and as a habitat. Parasite life inevitably involves an interaction with adverse conditions, as is the case for free-living organisms. Essential in perception is the duality of parasites, which goes through the whole ecology of parasitism. Parasites can, on the one hand, create diversity, but on the other, they can cause extinction. They can neuter the host, but also increase its growth rate and also stimulate the immune response, but can stimulate secondary chronic infection. Parasites inhabit individual hosts and also they are distributed as discrete patches, similar to metapopulation, but these hosts also nested in a spatially structured metapopulation and these in the meta-community of competent hosts. They often divert host resources to themselves and other consumers, changing the patterns of energy flow, the use of critical resources, and thus affecting the functioning of the ecosystem. Most living organisms are parasitic, and their role as specialized consumers and their impact on biodiversity can become essential actors in many ecosystems. Parasitism is a dominant part of many ecosystems. Although there may be few relative biomass of parasites in the system, we should be aware that parasites often have a tremendous turnover rate so that parasites can have a relatively significant effect on energy flow [5].

### **2.2 Parasitic architecture – formally**

As in nature, the parasitic relationship is based on the host-parasite relationship, the parasitic architecture would, in this sense, represent the relationship of an existing building and a new extension, adaptive reuse, superstructure, installation. The existing building stock constituting a significant percentage of all buildings can thus be considered as a rich source of adepts as potential hosts. Such a perception of parasitic architecture is formalistic. It deals only the form, its aesthetics and expands the host only spatially, utmost programmatically. The relationship in question could therefore also be called ectoparasitic, where the parasite lives only on the surface or outside the host. It uses the host, the existing building as the base, its statics as the skeleton, and the only enrichment of the host I see only in the extension of layout and utility space.



Figure 1, 2: The Green Exhibition House, Rotterdam, Korteknie Stuhlmacher Architekten; Figure 3: Manifest Destiny, San Francisco, Mark Reigelman; Figure 4: Cabin, Athens, Panos Dragonas Christopoulou Architects; Figure 5: Homes for the Homeless, London, James Furzer

## 2.3 Parasitic architecture – contentually

### 2.3.1 Urban acupuncture

An excellent example of parasitic architecture could be the concept of Urban acupuncture, the idea of micro intervention in the urban structure to improve the overall functioning of urban organisms. Urban acupuncture is an ideology, only as a mixture of urbanism and traditional eastern treatment [6]. The affected sites will be selected based on an overall analysis of the environment and its socio-economic-ecological factors. Interventions are developed through a dialogue between designers and the community. Acupuncture relieves stress in the body. Urban acupuncture relieves stress in the environment [7]. The result should be the production of small but socially catalytic inputs into the urban structural scheme [8]. The theory thus offers the possibility of minimal contact with the absolute impact [9]. A small-scale but socially catalytic interventions (City Acupuncture), tailored for the particular environment and community for which they are created and designed to solve particular local issues may cause positive ripple effects. In this way, they are best adapted for creative solutions and design, to respond to and influences the context in which it forms part [10]. Such a mutually beneficial relationship then represents mutualism. The intervention of the parasite is sensitive, in this case, it keeps the space of the existing building layer in memory, respects the host and at the same time enriches it. Contextual and historical layers can even affect the expression of intervention. Thus, the host uses the parasite for its benefit.

### 2.3.2 Parasite at scene

If we consider the scale factor of the building itself and its architecture, we can consider all installations as a parasite in the vicinity of existing buildings, contrasting expression to the surrounding, an existing urban area.



Figure 6: Balcony, Zalewski Architecture Group; Figure 7, 8: Hutong Bubble, Beijing, MAD Architects

### 2.3.3 Parasite as building's architectural elements

Green facades, elements that parasitize on the building, its structures and the skeleton as the underlay for vegetation can be considered as parasitic architecture in an even smaller scale factor, in the scale of architectural elements. For example, One Central Park building by Jean Nouvel, is covered by a vertical landscape. Approximately 50% of the whole facade is green. The vegetation of the building is connected to the adjacent city park. The green icon thus positively affects the Sydney skyline. It creates a unique environment not only for building users. Facade's support cables, hydroponic walls with low-profile stackers support various climbing and spreading devices for vegetation. Here the plant becomes a natural shade and a regulator of solar radiation [11]. Another good example is the concept of the vertical forest by Stefano Boeri in collaboration with ethologists and botanists. It is a prototype of a new format of biodiversity and re-colonization of fauna and flora in the urban structure. The plant envelope does not reflect the sun's rays, filters them, and creates a favourable internal microclimate. The envelope regulates moisture, absorbs CO<sub>2</sub> and microparticles, produces oxygen. The type, colour, shape of the plants vary concerning the application on the different sides of the towers and the different floors. Direction and height of facades affect this selection. It is also a habitat colonized by numerous animal species [12]. Or also porous structured facades as a base for vertical greening of buildings. The façade of the Green Cast building by Kengo Kuma is made of inclined aluminium panels, while the castings of the individual panels are made of crumbled styrene foam. The facade as a whole conceals equipment for irrigation, ventilation and drainage [13]. Although the above examples took into account the vegetation layer "green parasite" already in the initial design of the buildings, we can indirectly consider this designation, as the aim is not to precisely define such a relationship in a biological sense, but how we can perceive and change the point of view of what appears to be immutable, to point out to initially invisible links.



Figure 9: One Central Park, Sydney, Australia – Jean Nouvel – Ateliers Jean Nouvel; Figure 10: Vertical Forest Milan, Milan, Italy – Stefano Boeri – Boeri Studio; Figure 11: Green Cast, Odawara-shi, Kanagawa Pref., Japan – Kengo Kuma – Kengo Kuma Associates



## 2.4 Parasitic architecture as Biomimicry

As the definition of Biomimicry is an approach to innovation that seeks sustainable solutions to human challenges by emulating nature's time-tested patterns and strategies. The goal is to create products, processes, and policies - new ways of living - that are well-adapted to life on earth over the long haul. Nature has already solved many of the problems we are grappling with. After billions of years of nature's development, failures are fossils, and what surrounds us is the secret to survival [14]. What we can observe in nature today is many of the best structures, evolved throughout the history of life on earth. The principle for architecture that emerges from observing is: less materials, more design. Exploring this paradigm, we will see an array of examples showing how minimum materials can be used to maximum effect [15]. Unlike nature, our material strategies are ineffective, inefficient and unnecessary in terms of long-term sustainability, and our dependence on separate solutions for distinct functions. We mass-produce instead of customizing for particular conditions in a particular context. We produce in bulk without the possibility of variation, adaptation to change and diversity [16]. Grouping the biological relationships observed from nature into code-driven associative-parametric models allows creating new perspectives on architecture. The aim should not be the creation of a building, nor its design after a cellular structure, but rather learn from biological models that capture and cultivate the dynamic reciprocity of the organic life complexes of biological systems. Not just create cell-like or tissue-like [17].



Figure 12: The Eden Project: The Biomes, Cornwall, UK, Grimshaw Architects – mimic structure of pollen seed; Figure 13: The Eastgate Centre, Harare, Zimbabwe, Mick Pearce – mimic cooling mechanism of a termite mound; Figure 14: 30 St Mary Axe Tower, London UK, Foster+Partners – mimic shape and lattice structure of a Venus' flower basket

### 2.4.1 Research in the field and case-studies

London's architecture research studio Tonkin Liu deals with the development of structures through biomimicry. The Oval Court is an example of such a way of designing where research translates into realization. The court's canopy is the 'shell structure' is made of thin aluminium perforated sheets, which was laser cut and welded together to create an ultra-light canopy's structure. The structure behind the design uses biomimicry to abstract the principles of mollusks and plants and has been used since 2008 to create ultra-lightweight pavilions, bridges, and towers. The shape of the curvature and corrugation of the shell was achieved with the advanced geometry. Through structural analysis and generative scripting, the perforations of the pattern plates were determined to respond locally to stress in each piece. That means maximum design efficiency and maximum load reduction. [18]. The Pratt Institute Center of Experimental Structures, and its co-founder professor Lalvani, designs systems whose material contains information. Inspired by living creature genes to create perforated sheets, using a computer-controlled laser cutter, a combination of physical shaping processes can transform 2D perforated sheets into stable 3D structures. The initial action is

expected to stretch them into a three-dimensional object. To exert some force that further pulls the gaps created by the perforations. The element of the system is an inert perforated sheet containing information, geometry and shape which, as part of the whole, carries it as an instruction to assemble the overall shape of the system. The appearance of these systems has a smooth organic that mimics the shaping of the growth of living matter. Even as an inert sheet with some holes in it, these installations contain all the necessary information for self-coding encoded into their initial geometry, as well as the gene in the cell contains instructions for assembling the whole organism [19]. Progressive research and alternative perspectives seek to find practical expression for the design of new materials that are better, lighter, stronger, more resilient and thus able to move the industry further [16].

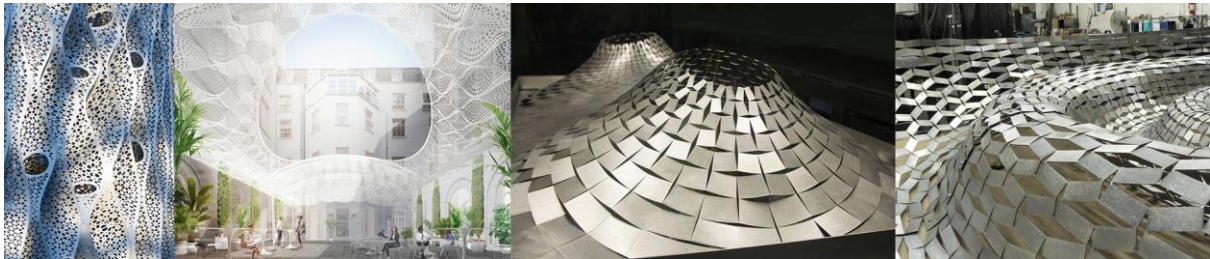


Figure 15, 166: Tonkin Liu's Oval Court; Figure 17, 18: Lalvani's perforated sheets 3D structures

#### 2.4.2 Visions and experiments

The research assumes that next-generation construction materials may support dynamic (in addition to their current, static) spatially-differentiated material compositions and structural forms. The aim is to combine structural, optical, and fluidic behaviours which are governed by the material architecture, as well as the interactions between materials and their environment. Such material architectures could simultaneously bear the large structural load, change their transparency so as to control light levels within a building or vehicle, and open and close embedded pores so as to ventilate a space [16]. As one of the next architectural frontiers, Biomimicry is quickly emerging. The drive to make buildings more environmentally friendly and new manufacturing processes such as 3D printing have led to a wave of ideas and projects that are constructed with biological materials. There are numerous precedents that demonstrate how animals can be biologically altered in this way, including silkworms that can produce coloured silk and genetically engineered goats that can produce spider-silk proteins for a new unbreakable super-fibre. The complexity of biological organisms is greater than any building or gadget that exist today. Nature response is able to changes over time, maintains self-sufficient systems, regenerates, and through it all creates beauty. The natural world around us gives us an infinite amount of knowledge to gain. Examining how animals utilize their own versions of 3D printing, at first glance, may seem like looking backwards. However, if it were possible to unlock the potential for biological materials and manufacturing processes already found in nature, we would be able live to see a built environment that is inherently linked to the natural world and contributes to it rather than threatening to destroy it [20]. Research led by materials scientist Debbie Chachra at New England's Olin College of Engineering has been known as "bee plastic": *Colletes inaequalis*, a cellophane-like biopolymer that produced by a species native to New England. Cocoon-like structures in the soil a special gland unique to its species is secreted by these bees. Non-fossil-

fuel-based natural polyester not only resists biodegradation, but it also survives the temperate extremes of New England. Possibility of using genetically modified bees to print concrete, was main target of Debbie Chachra's collaboration project with designer John Becker Initially inspired by a project published under the title "Bees Make Concrete Honey," which illustrate a series of science-fictional scenarios in which a new urban bee species, called *Apis caementicium*, could be used throughout the city as a cheap way to repair statues and fix architectural ornaments, or even to produce whole new structures [21]. MIT Media Lab's Mediated Matter Group's research integrates computational form-finding strategies with biologically inspired fabrication. The pavilion, inspired by the way silkworms weave delicate cocoons from a single strand of silk, was created using a base of threads wrapping a steel frame, completed by over 6,500 silkworms which were let loose upon this structure. The way Silk Pavilion connects the dots between the world of information technology and biology perhaps is the fascinating aspect of it. How the blind instinct of silkworms is sometimes revealed as almost machine-like, is shown by the recent study: "parallel basic research explored the use of silkworms as entities that can "compute" material organization based on external performance criteria." [22].



Figure 19, 20: MIT Media Lab's Silk Pavilion; Figure 21, 22: Project Bees Make Concrete Honey

### 3 Parasitic Architectural Forms (PAF)

Symbiosis is a reasonably peculiar way of coexistence of two or more different biological species. In this concept, there are two different architectural "species" in a mutualist relationship providing each other convenient services. Each symbiosis has a clearly defined relationship between parasite and host. Defining these relationships is free and in essence, does not have to identify with the usual links in nature, it is an opportunity to bring a new perspective to problems we do not know how to deal with that. After all, just like in nature, symbiotic interactions can be highly variable change from mutualistic to parasitic depending on local environmental conditions. In nature, if some force was changing the composition of the community or the functioning of the ecosystem, a mutualistic association could start functioning as a parasitic one [5]. In this case, the host would be an existing building, area, or environment as such. The theme would be the development and research of such forms. Parasitic architectural forms (PAF) would be able to independently self-design and create, self-grow and evolve with minimal initial human intervention. They would respect original input/definition (geometry, external influences, spatial planning, anything predefined by the creator). Fully autonomous development these forms based on cell division in specific geometric structures, and behaviour along with responses to external influences of the whole

form would provide generative geometry. The development of forms would precede the gradual development of the element with the given genomic instruction, the information of clustering into structures, and then structures into form/forms. It would probably be a fast-growing, expanding material structure based on biopolymers and bio-cement, which would gradually change from elastic to scaly, providing the basis for the micro-ecosystem. Like in nature, nothing arises without interacting with the environment and other organisms, the growth process should be accompanied by the mutually beneficial synergy between PAF, fauna and wildlife (birds, insects), thus returning a part of extruded nature from places. Such development of PAF will allow the emergence of new typological models that will be able to respond to changes in user needs. The idea of parasitic architecture is current within city and city structures. Nature is the driving force, resilience, adaptability and flexibility of species diversity. Individual PAF should differ from one another in content, formal, aesthetic, depending on the differences inputting information, data based on the environment, external influences, but also legislative, planning tools of the place of occurrence. PAF is, therefore, a system consisting of three inseparable, integral parts. Brain, Body and Life, representing Artificial Intelligence of PAF (PAF © A.I.), Material of PAF (PAF © DNA-BIO-MAT) and Process/Life cycle of PAF (PAF © RE.PROD.USE). Whole PAF research and development could take place in four stages. The first one sets a specific model of an Element, material concept, mapping of suitable implication locations within the environment (Modeling). In the second, virtual simulation is set and defined parameters for the development of PAF (Behavior), in the third one on scaled models under laboratory conditions experimentally test PAF (Test), and in the fourth in real conditions imply PAF (Usage). PAF can be used in various interactions, symbiosis depending on the host. We could hypothetically consider that the parasite invasively interferes with the authorship, and so we may open a discussion and view of the experienced perception on this topic as well. Nature does not ask for consent, and like Parasitic Architectural Forms based on biological basis and the idea of reproduction with genetic information, let us consider the oeuvre autonomous.



Figure 23: Illustration graphic of Parasitic Architectural Forms

## 4 Conclusion

To reduce the cost of advanced low-carbon energy carriers and technologies, a huge research and innovation effort is needed over the next two decades. A well-coordinated strategic research, innovation and investment agenda will make zero-carbon solutions economically workable while bringing about new ones [1]. As part of the 10<sup>th</sup> annual World Green Building Week, the World Green Building Council has issued a bold new vision for how buildings and infrastructure around the world can reach 40% less embodied carbon emissions by 2030, and achieve 100% net zero emissions buildings by 2050 [4]. Parasitic architecture as a new way can become a result and response to climate change in architecture and civil engineering. Perhaps it will become essential soon to refrain from experiencing alchemical solutions, inventing over-combined artificial solutions, changing mindset in designing. Less material, more design. As a paradigm, an approach to biomimicry design philosophy. This paper could be seen as an inspiration, an initial letter, an outline of my research that will attempt to manifest new interpretations of existing relationships in space, parasitic architecture. We can deduce from it a way of looking at solutions in which the openness of sources of inspiration, the possibilities of implied patterns and models observed from nature are virtually borderless. Professionals can draw inspiration for designing and conceptualization. For academics, it could be interesting by free and attractive research space and possible interdisciplinary collaborations. The layman can imagine possible solutions to existing problems and start to perceive nature again as a spatial-creative element that has been present here in the past, nowadays and inevitably must be in the future too.

## Acknowledgements

The paper presents author's own design and research - Parasitic Architectural Forms (PAF and its integral parts), and partial research results of project VEGA 1/0674/18 "Theoretical and experimental analysis of architectural-structural shapes and fragments of building envelope structures designed for harsh weather conditions".

## References

- [1] Directorate-General for Climate Action. (European Commission) (2018). COMMUNICATION FROM THE COMMISSION, COM(2018) 773 final, Brussels, 28.11.2018 *A Clean Planet for all A European strategic long-term vision for a prosperous, modern, competitive and climate neutral economy*. European Union, Brussels: EU publications. <https://eur-lex.europa.eu/legal-content/en/TXT/?uri=CELEX%3A52018DC0773>
- [2] Directorate-General for Climate Action. (European Commission) (2019). *Going climate-neutral by 2050, A strategic long-term vision for a prosperous, modern, competitive and climate-neutral EU economy*. European Union, Brussels: EU publications, ISBN 978-92-76-02037-0. <https://op.europa.eu/en/publication-detail/-/publication/92f6d5bc-76bc-11e9-9f05-01aa75ed71a1>
- [3] The International Energy Agency. (2019). *Global Energy and CO2 Status Report 2019*. <https://www.iea.org/statistics/co2emissions/>
- [4] World Green Building Council. (2019). *New report: the building and construction sector can reach net zerocarbon emissions by 2050*. <https://www.worldgbc.org/news-media/WorldGBC->

- embodied-carbon-report-published
- [5] Thomas F., Renaud F., Guégan J. (2005). *Parasitism and Ecosystems*. Oxford University Press, ISBN 0-19-852986-4
  - [6] Casagrande, M. (2020) From Urban Acupuncture to the Third Generation City. In Editors of book (Jana Revedin). *Nature Driven Urbanism* (pp.131-153). Cham: Springer, ISBN: 978-3-030-26716-2
  - [7] Casagrande M. (2009). *Urban Acupuncture*. Statement, Helsinki University of Art and Design Department of Environmental Art. <https://casagrandetext.blogspot.com/search?q=urban+acupuncture>
  - [8] Harrison A.L. (Ed.). (2013). *Architectural Theories of the Environment: Posthuman Territory*. Ruin Academy, Casagrande Lab, (pp.304-315). New York: Routledge. ISBN: 978-0-415-50619-9. <https://www.casagrandelaboratory.com/portfolio/ruin-academy/>
  - [9] Casagrande M. (2010). *Urban acupuncture*. <http://helsinkiacupuncture.blogspot.com/2008/12/blog-post.html>
  - [10] Floryn P., Madrecki K., Zyburka P. *City Acupuncture: Water front project for area around Zawalna street Wroclaw*. <http://futurearchitectureplatform.org/projects/9f196904-17ca-4bdb-9316-4bd7fdf406f0/>
  - [11] Jean Nouvel/Ateliers Jean Nouvel. (2014). *One Central Park*. <http://www.jeannouvel.com/en/projects/one-central-park/>
  - [12] Stefano Boeri/Boeri Studio. (2014). *Vertical Forest*. <https://www.stefanoboeriarchitetti.net/en/project/vertical-forest/>
  - [13] Kengo Kuma/Kengo Kuma Associates. (2011). *Green Cast*. <https://kkaa.co.jp/works/architecture/green-cast/>
  - [14] Biomimicry Institute. (2006). *Biomimicry*. <https://biomimicry.org/what-is-biomimicry/>
  - [15] PAWLYN, M. (2016). *Biomimicry in Architecture: 2nd edition*. London: RIBA Publishing
  - [16] Oxman N. (2010). *Material-based Design Computation*. Massachusetts: Massachusetts Institute of Technology
  - [17] Sabin J. E., Jones P. L. (2008). *Nonlinear Systems Biology and Design. Surface Design*. Nonlinear Systems Organization, ACADIA08
  - [18] Liu A., Tonkin M./TonkinLiu. (2000). *Oval court*. <https://tonkinliu.co.uk/oval-court>
  - [19] Mortice Z./Redshift by Autodesk. (2000). *Haresh Lalvani on Biomimicry and Architecture That Designs Itself*. [https://www.autodesk.com/redshift/haresh-lalvani/?utm\\_medium=website&utm\\_source=archdaily.com](https://www.autodesk.com/redshift/haresh-lalvani/?utm_medium=website&utm_source=archdaily.com)
  - [20] Rawn E./Archdaily (2014). *Animal Printheads, Biomimicry and More: How Nature Will Shape the Built Environment of the Future*. [https://www.archdaily.com/535674/animal-printheads-biomimicry-and-more-how-nature-will-shape-the-built-environment-of-the-future?ad\\_source=search&ad\\_medium=search\\_result\\_all](https://www.archdaily.com/535674/animal-printheads-biomimicry-and-more-how-nature-will-shape-the-built-environment-of-the-future?ad_source=search&ad_medium=search_result_all)
  - [21] Manaugh G./BLDGBLOG (2014). *Architecture-by-bee and Other Animal Printheads*. [http://www.bldgblog.com/2014/07/architecture-by-bee-and-other-animal-printheads/?utm\\_medium=website&utm\\_source=archdaily.com](http://www.bldgblog.com/2014/07/architecture-by-bee-and-other-animal-printheads/?utm_medium=website&utm_source=archdaily.com)
  - [22] MIT Media Lab. (2018). *Silk Pavilion, CNC Deposit Silk Fiber & Silkworm Construction*. Massachusetts: Massachusetts Institute of Technology, MIT Media Lab



## Analysis of short – term heavy rains in eastern Slovakia in the period 2003 - 2018

Adam Repel<sup>1</sup>, Martina Zeleňáková<sup>1</sup>, Vinayakam Jothiprakash<sup>2</sup>, Helena Hlavatá<sup>3</sup>, Slávka Galas<sup>4</sup> Maria Manuela Portela<sup>5</sup>

<sup>1</sup>Technical University of Košice, Faculty of Civil Engineering, Institute of Environmental Engineering  
e-mail: adam.repel@tuke.sk, martina.zelenakova@tuke.sk

<sup>2</sup>Indian Institute of Technology, Department of Civil Engineering  
e-mail: vprakash@iitb.ac.in

<sup>3</sup>Slovak Hydrometeorological Institute, Branch Office Košice  
e-mail: helena.hlavata@shmu.sk

<sup>4</sup>AGH Krakow, Department of Environmental Analysis, Geological Mapping and Economic Geology  
e-mail: slavka.galas@gmail.com

<sup>5</sup>Universidade de Lisboa, Instituto Superior Tecnico  
e-mail: maria.manuela.portela@ist.utl.pt

### Abstract

Short-term heavy rains are one the most important rains from a meteorological, hydrological, and also technical point of view. When designing rainwater drainage systems or rainwater management systems, the intensity of short-term rains is used as a design parameter, because of short-term rains usually reach the highest intensity. This paper is focused on analysis of short-term heavy rains occurrence in the last 15 years in 3 rainfall stations in eastern Slovakia. The data used in analysis are automatically collected 10-minute precipitation totals at rainfall stations Poprad, Kamenica nad Cirochou and Košice.

**Key words:** short-term heavy rains, rainwater drainage, rainfall intensity, rainwater management

## 1 Introduction

Climate change has been a topic of interest to many researchers with multiple areas of expertise. One of the most important necessities of research into climate change is to analyze and detect historical changes in the climatic system [1]. Distribution of rainfall and its changes during the time is one of the most important aspects of climate change and it needs to

be investigated. Rainfall is one of the most important climatic variables because it affects important hydrological events such as floods and droughts. Rainfall and other hydrologic processes are known as stochastic processes. This is because they evolve in space and time in a way that is partly predictable or deterministic and partly random [2]. Rainfall and other hydrological processes are characterized for their variability in space and in time. There are many ways how to analyze the variability, for example by examining trend, stationarity, homogeneity, periodicity or noise [3]. Long term rainfall data presents time series, which is a series of data points indexed in time order.

Analysis of rainfall data is very important in hydrology and also in engineering practice. Many authors in the world analyzed historical time series of rainfall in many countries in the world. In Asia, between Nepal and Tibet in the Himalayan region was showed that the annual precipitation amount is increasing in the period between 1943 and 1993 [4]. Similar results were presented also in other studies in many Canadian series [5] or in many places in South America, where authors analyze the number of rainy days per year and the daily rainfall amount [6]. In Europe, studies on Ireland series collected from 1940 to 1990 confirm the increasing of the total annual precipitation, in particular on the west coast [7]. Study from Ireland also shows how the intensity of rainfall is growing up and the return period of the extreme events is reducing. Results of this study is, that 30-year return period events are becoming 10-year events nowadays [8]. In Italy, it was proved that dry periods tend to be longer with increasing variability of the length of the dry spells and this is also associated with shorter duration of rain episodes with an evident effect on rainfall extremes [9]. In eastern Europe, there are some studies which documents the extremes of rainfall and their changes in time [10, 11].

In Slovakia, there are not many studies of rainfall time series in last years. Daily rainfall data were analyzed by Dub in 1950 and second, very complex analyze was done in 1973 by Šamaj and Valovič. Since these studies, not many authors have dealt with this issue. Statistical analysis of daily rainfall is very important for further use of data, for example for engineering practice. Rainfall, and its duration, intensity and frequency are very important in urban hydrology, for example in designing of sewerage or drainage system in cities.

Short-term precipitation, especially associated with storms, is a phenomenon in which the intensity of rain reaches a high value, while the duration of rain is usually short. Short-term precipitation is one of the main extremes in the weather [12]. Due to the high concentration of precipitation over time, short-term precipitation causes flash floods or landslides that cause large financial losses and casualties [13]. Events with high rainfall depths and durations of a few hours are most often associated with convective storms [14]. In Czech Republic, which is close neighbor of Slovak Republic it was reported, that the convective precipitation represents about 50% of the total precipitation in summer, and heavy rainfall events contribute significantly to precipitation in warm season [15]. Significant increasing trends in event rainfall rate and significant decreasing trends in event duration were found in Czech Republic [16]. This paper is focused on analysis of short-term heavy rains in Eastern Slovakia in the period from 2003 to 2018.



## 2 Study area and data

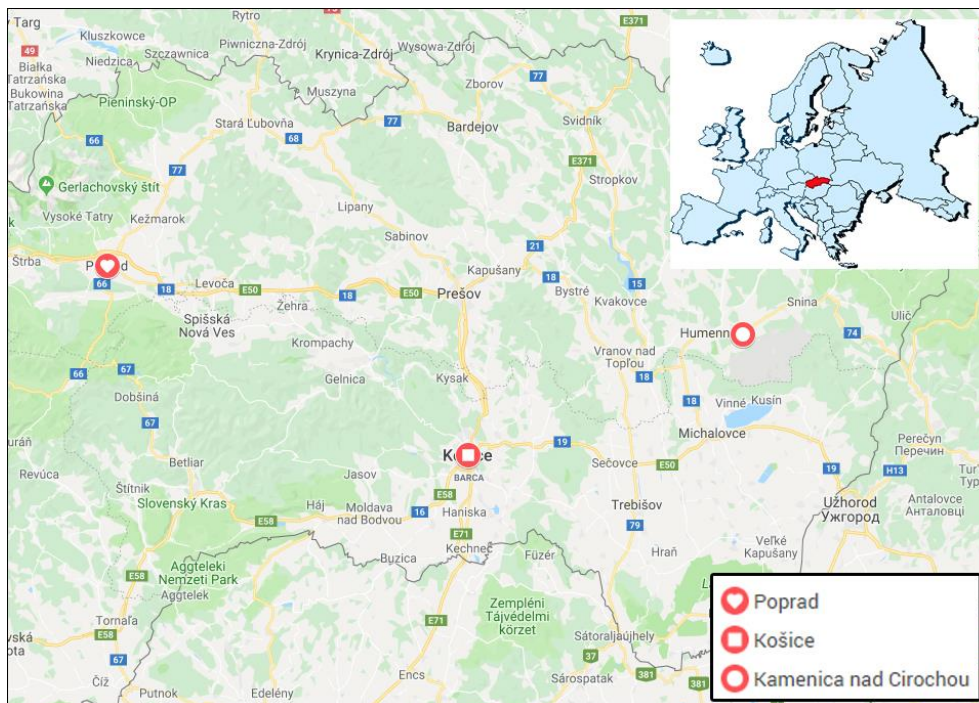
### 2.1 Study area

Analyzed rainfall stations are situated in the eastern part of Slovakia. These are the stations Kamenica, Košice and Poprad.

The Poprad city, where the first rainfall station is situated in the north of Slovakia, in altitude of 672 m close to the highest mountains of Slovakia, the High Tatras. Climate in this city is affected by topography of the terrain. Poprad is situated on the Poprad River in the Sub-Tatra Basin, and is a gateway to the High Tatras. Mountain ranges around the city include the Levoča Hills in the east, Kozie Chrbty in the south, and the Low Tatras in the southwest. The drainage divide between the Black Sea and Baltic Sea lies a bit to the west, near the village of Štrba [17].

The Košice is city situated in central part of eastern Slovakia near Hornád river in altitude of 208 m. It is situated on the river Hornád at the eastern reaches of the Slovak Ore Mountains, near the border with Hungary. Precipitation varies little throughout the year with abundance precipitation that falls during summer and only few during winter. The coldest month is January, with an average temperature of  $-2.6\text{ }^{\circ}\text{C}$ , and the hottest month is July, with an average temperature of  $19.3\text{ }^{\circ}\text{C}$ . [18].

Kamenica nad Cirochou is situated in eastern Slovakia in altitude of 178 m and there are two rivers, Kamenica and Cirocha that merge approximately 1 km off the village. The location of each precipitation (rainfall) station is shown in Figure 1.



## 2.2 Input data

Input data used in this study consist of total rainfall per 10 minutes interval in each station from 2003 to 2018. Length of time series is 15 years. These data were automatically recorded and were obtained from the Slovak Hydrometeorological Institute (SHI), regional centre Košice. The value of total rainfall for the ten minutes interval was recorded at the end of each interval. There are no missing data in datasets, precipitation from all 10 minutes intervals are included.

## 3 Methods and methodology

In this paper, the occurrence of heavy rains in eastern Slovakia were analyzed. Heavy rains can be characterized in several ways. The easiest way is to characterization by the intensity of the rain (height of the water layer that hits the earth's surface in a certain time) [17]. This means that any rain that reaches a higher intensity than the set value is characterized as heavy rain. Boundary intensity values for the identification of heavy rains and downpours by Berg are given in the table.

Table 1: Characterization of heavy rains and downpours according to Berg on the basis of minimum rainfall intensities ( $H_s$  and  $I$ ) for heavy rains and downpours **Chyba! Nenašiel sa žiaden zdroj odkazov.**

Duration (min)	5	10	15	20	25	30	45	60	120
<b>Heavy rain</b>									
$H_s$ (mm)	2,5	3,8	5,0	6,0	7,0	8,0	10,25	12	18
$I$ (mm/min)	0,5	0,38	0,33	0,30	0,27	0,27	0,23	0,2	0,15
<b>Downpour</b>									
$H_s$ (mm)	5,3	8,0	10,5	12,7	14,8	16,9	21,6	25,3	38,0
$I$ (mm/min)	1,06	0,8	0,7	0,64	0,59	0,56	0,48	0,42	0,32

It is clear from the table that a heavy rain for 10 minutes can be defined as any rain in which the rain intensity of 0.38 mm/min has been exceeded. Heavy rain is therefore characterized by a total rainfall of 3.8 mm per 10 minutes interval. Downpour is then characterized by a total rainfall of 8.0 mm per 10 minutes interval. In all three datasets (from Poprad, Košice and Kamenica stations for the period 2003 to 2018) all rainfalls with higher intensities than 0.38 mm/min and 0.80 mm/min were found and analyzed in this paper.

## 4 Results and discussion

For each station in every year, the number of occurrences of heavy rains (with more than 3.8 mm per 10 minutes) and downpours (with more than 8.0 mm per 10 minutes) were found. The number of heavy rains in observed period in the Kosice and in the Kamenica are more or less

the same (179 heavy rains in the Kamenica and 180 heavy rains in Kosice), but trend of heavy rains occurrences in these two stations are different. The fewest heavy rains occurred in Poprad station (134 heavy rains). The number of heavy rains in every year for every station is shown in Figure 2. There are also trend lines for each station. In Poprad and Kamenica station, there is positive trend in number of occurrences of heavy rains from 2003 to 2018. On the other hand, in the Kosice station, there is negative trend. The largest number of heavy rains in one year was 18 heavy rains in 2006 in Košice. In Poprad, the largest number of heavy rains was 17 in 2018 and the largest number of heavy rains in Kamenica was 15 in 2007. It is interesting that the largest number of heavy rains was observed in the Košice station in the years 2003 to 2011, while in the Poprad and Kamenica stations the number of heavy rains is constant or shows a slightly positive trend.

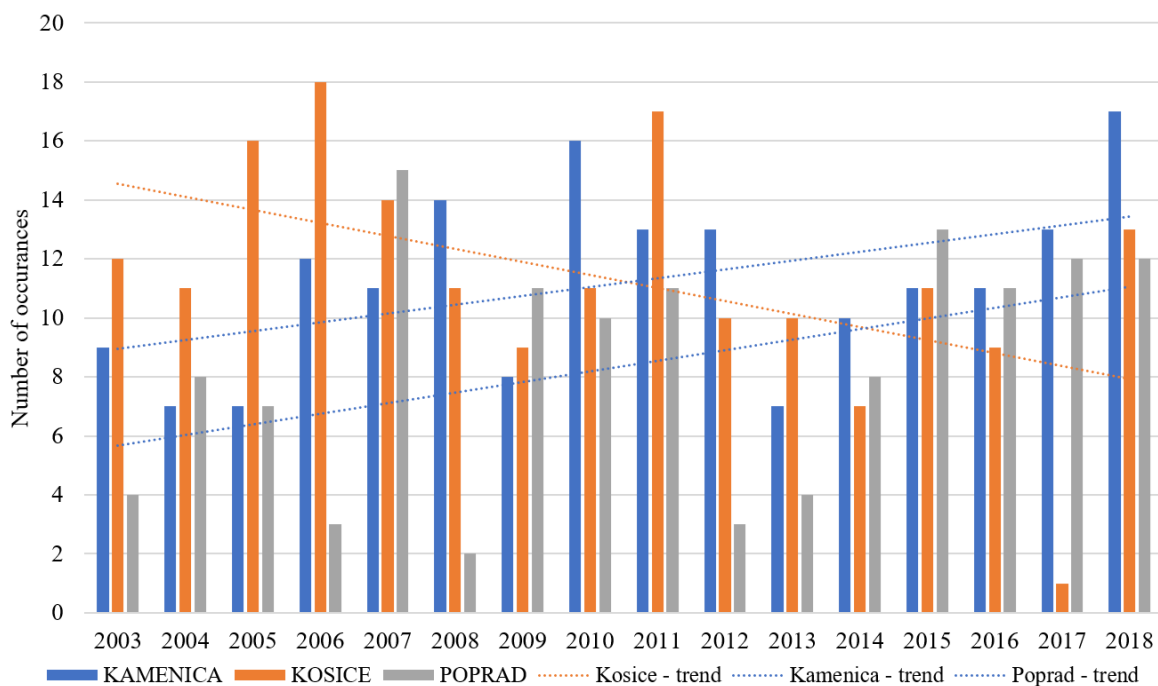


Figure 2: Number of occurrences of heavy rains for the period 2003 to 2018 in stations Kamenica, Kosice and Poprad

In the Figure 3 there is shown the number of occurrences of heavy rains in each month. It is clear from the graph in Figure 3 that heavy rains occur in all three stations in eastern Slovakia only in the summer season, very exceptionally in the spring and autumn season.

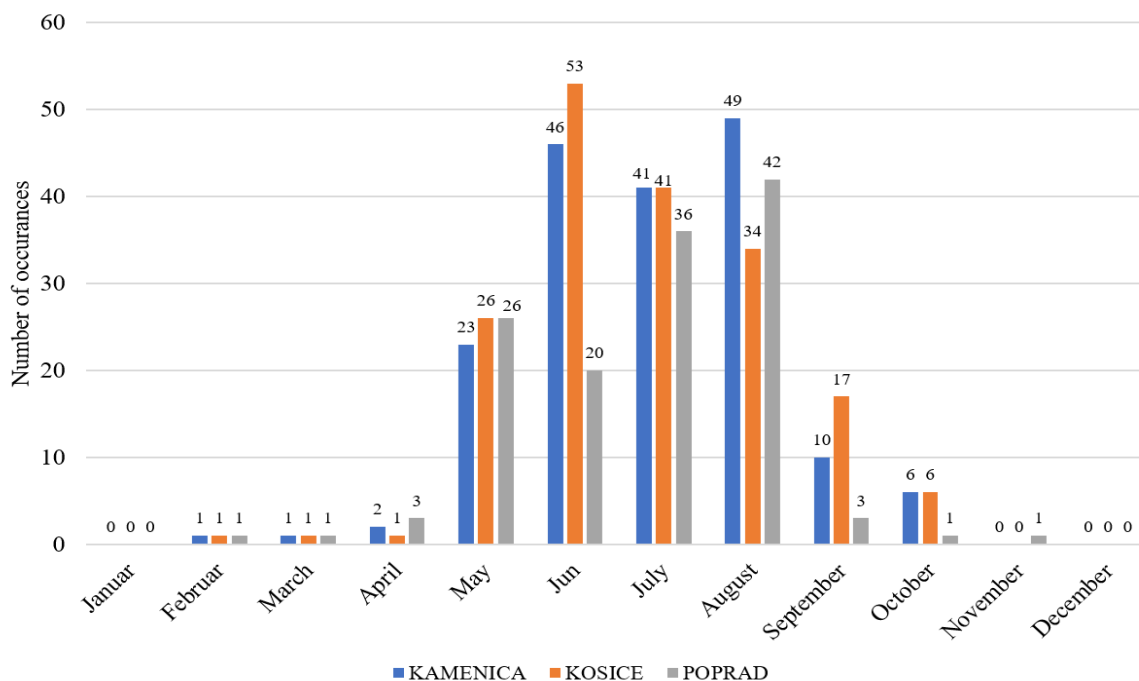


Figure 3: Number of occurrences of heavy rains in each month in stations Kamenica, Kosice and Poprad

In February, March and April, there were just few heavy rains in each station during the observed period. In May there is the start of the heavy rain season, which lasts until the end of August. This is due to the fact that heavy rains in the territory of eastern Slovakia occur mainly during storms, which occur during very warm weather. The largest number of heavy rains in Košice are in Jun, in Kamenica and Poprad station in August. In the Poprad station, the largest number of heavy rains are especially in second half of the summer, in July and August, it is because the climate of Poprad is affected by High Tatras mountains and climate here is affected, among other things by melting of snow in mountains. These two months, July and August, especially August, are also the warmest months of the year in Poprad.

The number of downpours with a total of rainfall more than 8.0 mm in 10 minutes is significantly lower than the occurrence of heavy rains with a total of more than 3.8 mm in 10 minutes. In total, downpours were observed at the Kamenica station 46 times during the observed period, at the Košice station 40 times and at the Poprad station 24 times. Significantly more downpours than in the Poprad station occurred in the Košice and Kamenica stations due to the higher temperatures that are reached in the summer months. The number of heavy rains in every year for every station is shown in Figure 4.

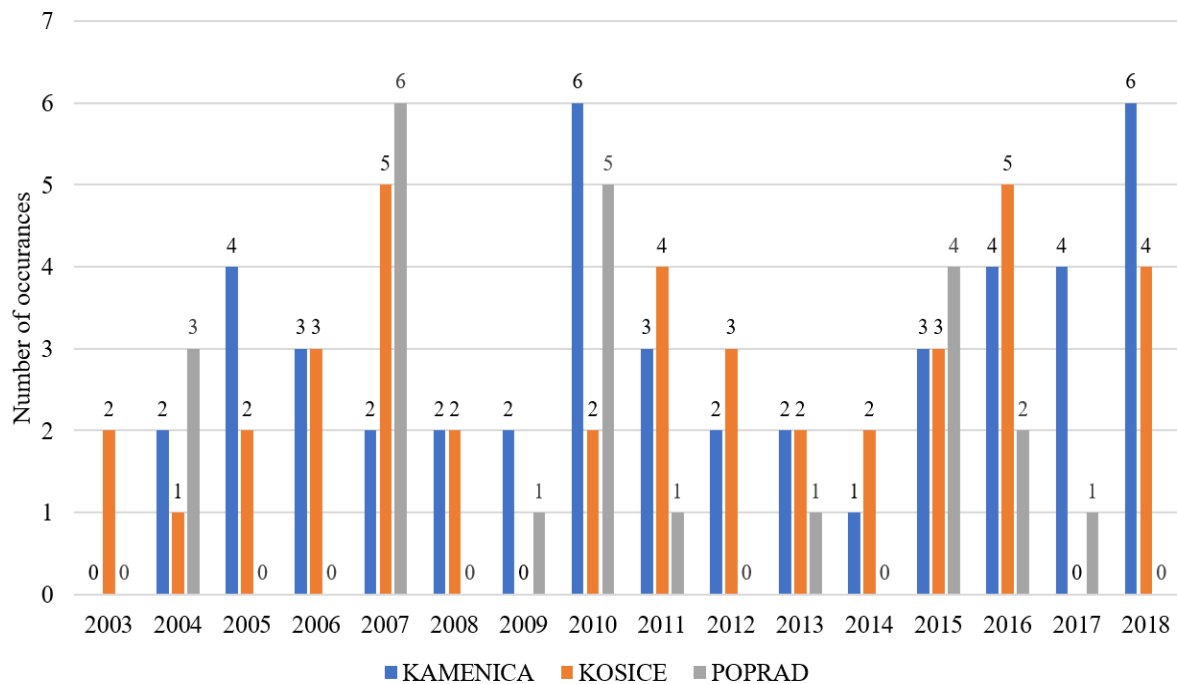


Figure 4: Number of occurrences of downpours for the period 2003 to 2018 in stations Kamenica, Kosice and Poprad

Downpours occur in all three stations exclusively in the summer months. The highest number of downpours (6) was observed at the Poprad station in 2007 and at the Kamenica station in 2010 and 2018. There were also many years during the observed period, when downpours did not occur at all throughout the year. Over the last 15 years (observed period) there has been no increase in the incidence of downpours in any of the observed stations.

## 5 Conclusion

Investigation of short-term heavy rainfall, which occurs in the Slovakia especially during summer storms, is very important, as these precipitations reach high intensities and cause considerable damage [20-23]. In this paper, the short-term precipitation was divided into heavy-rains and downpours, according to their intensities. Heavy rains and downpours were analyzed for the time period from 2003 to 2018 in three stations of eastern Slovakia. In Poprad and Kamenica station, there is positive trend in number of occurrences of heavy rains from 2003 to 2018. On the other hand, in the Kosice station, there is negative trend. The results showed, that heavy rains and downpours occur mainly in the summer months (from June to August), rarely in May and very exceptionally from Februar to April and in September and October. Heavy rains did not occur even once in the winter months during the observed period. The number of heavy rains during the year does not seem to have increased significantly. It seems that flash floods causing damage, which have occurred more frequently in eastern Slovakia in recent years, are mainly caused by changes in land use (urbanization, deforestation, monoculture agriculture), not an increase in the number of occurrences of

heavy rainfalls.

## **Acknowledgements**

This work was supported by projects of the Ministry of Education of the Slovak Republic VEGA 1/0217/19 Research of Hybrid Blue and Green Infrastructure as Active Elements of a Sponge City, VEGA 1/0308/20 Mitigation of hydrological hazards - floods and droughts - by exploring extreme hydroclimatic phenomena in river basins, the project of Slovak Research and Development Agency APVV-18-0360, APVV SL-PL-18-0033, APVV SK-PT-18-0008.

## **References**

- [1] Cannarozzo, M., Noto, L. V., & Viola, F. (2006). Spatial distribution of rainfall trends in Sicily (1921–2000). *Physics and Chemistry of the Earth, Parts A/B/C*, 31(18), 1201-1211.
- [2] Te Chow, V. (2010). *Applied hydrology*. Tata McGraw-Hill Education.
- [3] Drissia, T. K., Jothiprakash, V., & Anitha, A. B. (2019). Statistical classification of streamflow based on flow variability in west flowing rivers of Kerala, India. *Theoretical and Applied Climatology*, 137(3-4), 1643-1658.
- [4] Sharma, K. P., Moore, B., & Vorosmarty, C. J. (2000). Anthropogenic, climatic, and hydrologic trends in the Kosi Basin, Himalaya. *Climatic Change*, 47(1-2), 141-165.
- [5] Hamilton, J. P., Whitelaw, G. S., & Fenech, A. (2001). Mean annual temperature and total annual precipitation trends at Canadian biosphere reserves. *Environmental monitoring and assessment*, 67(1-2), 239-275.
- [6] Lucero, O. A., & Rozas, D. (2002). Characteristics of aggregation of daily rainfall in a middle-latitudes region during a climate variability in annual rainfall amount. *Atmospheric Research*, 61(1), 35-48.
- [7] Hoppe, H., & Kiely, G. (1999). Precipitation over Ireland—Observed change since 1940. *Physics and Chemistry of the Earth, Part B: Hydrology, Oceans and Atmosphere*, 24(1-2), 91-96.
- [8] Kiely, G. (1999). Climate change in Ireland from precipitation and streamflow observations. *Advances in water resources*, 23(2), 141-151.
- [9] Cislighi, M., De Michele, C., Ghezzi, A., & Rosso, R. (2005). Statistical assessment of trends and oscillations in rainfall dynamics: Analysis of long daily Italian series. *Atmospheric Research*, 77(1-4), 188-202.
- [10] Brázdil, R., Březina, L., Dobrovolný, P., Dubrovský, M., Halásová, O., Hostýnek, J., Kirchner, K. (2007). *Vybrané přírodní extrémny a jejich dopady na Moravě a ve Slezsku*. Masarykova universita, Český hydrometeorologický ústav, Ústav geoniky Akademie věd ČR.
- [11] Starkel, L. (1996). Geomorphic role of extreme rainfalls in the Polish Carpathians. *Studia Geomorphologica Carpatho-Balcanica*, 30, 21-38.
- [12] Tao, Y., Wang, W., Song, S., & Ma, J. (2018). Spatial and Temporal variations of precipitation extremes and seasonality over China from 1961~ 2013. *Water*, 10(6), 719.
- [13] Tian, X., Li, D., Zhou, J., Zhou, Y., & Zhang, Z. (2019). Characteristics Analysis on

- Short-Time Heavy Rainfall during the Flood Season in Shanxi Province, China. *Journal of Geoscience and Environment Protection*, 7(03), 190.
- [14] Hand, W. H., Fox, N. I., & Collier, C. G. (2004). A study of twentieth-century extreme rainfall events in the United Kingdom with implications for forecasting. *Meteorological Applications*, 11(1), 15-31.
- [15] Rulfová, Z., & Kyselý, J. (2013). Disaggregating convective and stratiform precipitation from station weather data. *Atmospheric research*, 134, 100-115.
- [16] Svoboda, V., Hanel, M., Máca, P., & Kyselý, J. (2016). Projected changes of rainfall event characteristics for the Czech Republic. *Journal of Hydrology and Hydromechanics*, 64(4), 415- 425.
- [17] Šatalová, B., & Kenderessy, P. (2017). Assessment of water retention function as tool to improve integrated watershed management (case study of Poprad river basin, Slovakia). *Science of the Total Environment*, 599, 1082-1089.
- [18] Poórová, Z., & Vranayová, Z. (2020). *Green Roofs and Water Retention in Košice, Slovakia*. Springer International Publishing.
- [19] Dub, O. (1957). *Hydrológia, hydrografia, hydrometria*. Slovenské vydavateľstvo technickej literatúry.
- [20] Alkhalaf, I., Sol'áková, T., Zeleňáková, M., & Gargar, I. (2018) Recent climate change in Syria: Seasonal rainfall and climatology of Syria for 1991-2009. *SSP - Journal of Civil Engineering*, 13(1) 77-96.
- [21] Zeleňáková, M., Gargar, I. A. K., & Purcz, P. (2012) Multicriteria analysis in hazards assessment in Libya. *Selected Scientific Papers: Journal of Civil Engineering*. 7(2) 59-70.
- [22] Kubiak-Wójcicka, K. (2018). Flow characteristics of the Vistula River at the Tczew gauging station in 1951–2010 based on Flashiness Index.pp. In Gastescu, P., Bretcan, P. (edit, 2018), *Water resources and wetlands, 4th International Conference Water resources and wetlands*, 5-9 September 2018, Tulcea (Romania), 119-129.
- [23] Svoboda, A., Pekarova, P. (1998) Katastrofálna povodeň z júla 1998 v povodí Malej Svinky–simulácia jej priebehu.(The July 1998 disastrous flood in the basin of the Malá Svinka–simulation of its course). *Vodohospodársky Casopis*. 46(6) 356-372.

## Drought indices and trend analysis

**Patrik Nagy, Martina Zelenáková**

Technical University of Košice, Slovakia  
Civil Engineering Faculty, Institute of Environmental Engineering  
e-mail: patrik.nagy@tuke.sk, martina.zelenakova@tuke.sk

### Abstract

In recent times, extremely dry seasons have been occurring more and more often in the eastern Slovakia, alternating with extremely wet seasons like torrential floods from extreme rainfall. Trend of reconnaissance drought index (RDI) and streamflow drought index (SDI) was evaluated in the paper using the Mann-Kendall test. The indices were evaluated at six climatic and river stations in the eastern Slovakia. The Mann-Kendall test results showed that the trend in the SDI index is not significant in 5 stations and only in one station the trend is significant. In the RDI index the trend is not significant in four stations and the trend is significant in two stations. The abstract is to indicate the subject of the paper, how the author proposes to develop the subject and its overall objective, aim or outcome.

**Key words:** Drought, Mann-Kendall test, Trend, Index

## 1 Introduction

Drought is a worldwide phenomenon that occurs due to lack of precipitation from normal or expected [1]. The lack of rainfall affects the environment and human activity. Drought can last several days, months to years, depending on the area in which it occurs. Water scarcity is manifested in reduced flow rates, water reservoir levels and lower groundwater levels [2 & 3]. Drought can be divided into hydrological, climatological, agricultural and socio-economic. The first three droughts are defined as a physical phenomenon [4]. The socio-economic drought addresses demand and supply and monitors the effects of water scarcity [5]. Hydrological drought has widespread impacts on water supply, deterioration of water quality, irrigation, energy production, habitat disturbance, reduction of recreational activities and affecting social and economic activities [6].



## 2 Study area and data

Drought indices are important elements for drought assessment and monitoring, which simplify the complex interrelationships between interdependent indicators. The drought indices that were evaluated are standardized streamflow drought index and reconnaissance drought index in 12 months' seasons. The Drinc software was used for SDI and RDI calculation. The Mann-Kendall test monitor the development of the trend in the evaluated indices [6 & 7].

### 2.1 Study area

Selected evaluated climatological and hydrological stations are located in the eastern Slovakia (figure 1). The stations Svit, Poprad, Chmeľnica and Červený kláštor are located in the catchment area of the river Poprad. The river Poprad is located in the north of eastern Slovakia. The stations Stratená, Švedlár, Mníšek nad Hnilcom are located in the Hnilec river basin. Košice is in the Hornád river basin and the Streda nad Bodrogom station is in the Bodrog basin. The Bodrog basin is located in the south-east of eastern Slovakia. The Laborce catchment area is a partial catchment area of Bodrog and in the Laborce catchment area there are stations Humenné, Kamenica nad Cirochou, Krásny brod and Tisinec.

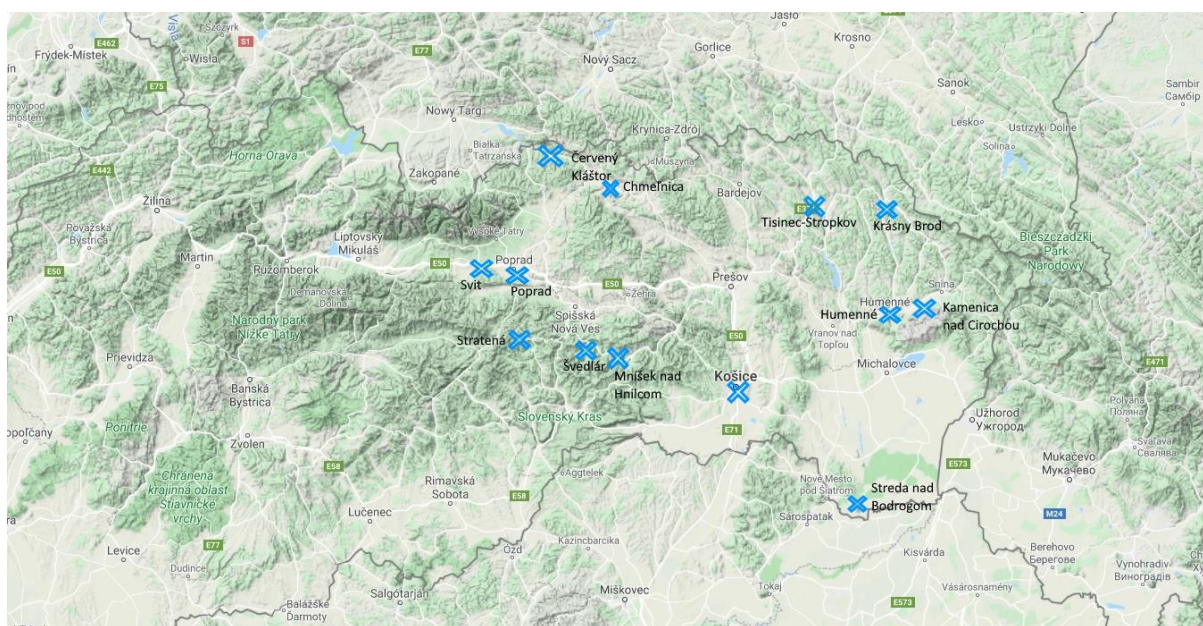


Figure 1: Station location map

### 2.2 Input data

The input data used in this study consist of monthly precipitation, temperature and streamflow from 1960-2015. The length of the time series is 55 years. Table 1 describes the input values for the evaluated streamflow drought index (SDI) and reconnaissance drought index (RDI). Table 1 describes the average, minimum and maximum streamflow, air temperatures and precipitation.

The highest average monthly streamflow was in the Bodrog basin at the station Streda nad Bodrogom 110 m<sup>3</sup>/s. The lowest average monthly streamflow was 0.05 m<sup>3</sup>/s in the Laborec basin at the station Krásny Brod. The Bodrog River is the largest river in the eastern Slovakia and is located in the south-east of Slovakia. The Bodrog basin forms the Laborec sub-basin. Two hydrological stations Humenné and Krásny Brod were evaluated on the Laborec river. In the Dunajec and Poprad basin, two hydrological stations on the Poprad River were evaluated, namely the stations Svit and Chmeľnica. The Stratená hydrological station was evaluated in the Hornád River basin on the Hnilec River. Data from hydrological stations were used to calculate the SDI. The climatological stations evaluated were located near the hydrological stations and these data were used to calculate the RDI index. The highest average monthly temperature of the evaluated climatological stations was in the climatological station Košice 29.75°C. The lowest average monthly temperature was at Červený Kláštor -29.75°C. Climatological station Kosice is located in the south of the eastern Slovakia, therefore there was the highest average monthly temperature and climatological station Červený Kláštor is located in the north of the eastern Slovakia near the High Tatras.

Table 1: Input data

Station	Value variables	Evaluated period	Min monthly	Max monthly	Average monthly
Poprad	Precipitation [mm]	1960-2014	0.4	220.4	50.1
	Air temperature [°C]	1960-2014	-24.7	25.65	6.15
Svit	Streamflow [m <sup>3</sup> /s]	1960-2015	0.21	4.82	1.29
Chmeľnica	Precipitation [mm]	1980-2010	4.6	259.3	64.7
	Streamflow [m <sup>3</sup> /s]	1960-2015	2.81	62.92	15.01
Červený Kláštor	Air temperature [°C]	1961-2014	-29.9	26.7	6.34
Mníšek nad Hnilcom	Precipitation [mm]	1980-2010	1.1	261.2	59.8
Švedlár	Air temperature [°C]	1961-2014	-22.4	25.4	6.56
Stratená	Streamflow [m <sup>3</sup> /s]	1960-2015	0.15	10.8	1.08
Humenné	Precipitation [mm]	1980-2014	4.8	271.7	61.4
	Streamflow [m <sup>3</sup> /s]	1960-2015	1.14	66.49	13.19
Kamenica nad Cirochou	Air temperature [°C]	1960-2014	-21.1	29.6	8.7
Krásny Brod	Precipitation [mm]	1986-2010	1.4	245.5	69.2
	Streamflow [m <sup>3</sup> /s]	1960-2015	0.05	16.73	2.05
Tisinec-Stropkov	Air temperature [°C]	1963-2010	-22.3	26.8	8.14
Streda nad Bodrogom	Precipitation [mm]	1980-2014	0.6	260	53.1
	Streamflow [m <sup>3</sup> /s]	1960-2015	10.1	629	110.85
Košice	Air temperature [°C]	1960-2014	-18.4	29.75	9.1

### 3 Methods and methodology

Drought indices are important elements for drought assessment and monitoring, which simplify the complex interrelationships between interdependent indicators. The drought indices that were evaluated are standardized streamflow drought index and reconnaissance drought index in 12 months' seasons. The Drinc software was used for SDI and RDI calculation. The Mann-Kendall test monitor the development of the trend in the evaluated indices [8 & 9].

The standardized streamflow index (SDI) uses monthly water flows and standardization methods associated with the standardized precipitation index (SPI). The reconnaissance drought index (RDI) is based on the ratio of two aggregate quantities: precipitation and the potential evapotranspiration. The Mann-Kendall test is non-parametric test. The Mann-Kendall test is used to determine the trend in indices SDI and RDI [10 & 11].

### 4 Results and discussion

Table 2 presents trends in the 12-month SDI index. The trend occurs only in the station Chmeľnica. There is no trend in other evaluated stations.

Table 2: Mann-Kendall trend test 12 months SDI

Hydrological station seasons	Mann-Kendall trend test	Test interpretation
Svit 1960-2015	Kendall's tau 0.091 S 135.000 Var(S) 18975.000 p-value (Two-tailed) 0.331 alpha 0.05	H0: There is no trend H1: There is a trend <b>There is no trend</b>
Stratená 1960-2015	Kendall's tau -0.140 S -208.000 Var(S) 1897.,000 p-value (Two-tailed) 0.133 alpha 0.05	H0: There is no trend H1: There is a trend <b>There is no trend</b>
Humenné 1980-2010	Kendall's tau -0.003 S -4.000 Var(S) 18974.000 p-value (Two-tailed) 0.983 alpha 0.05	H0: There is no trend H1: There is a trend <b>There is no trend</b>
Krásny Brod 1960-2015	Kendall's tau 0.101 S 146.000 Var(S) 18641.333 p-value (Two-tailed) 0.288	H0: There is no trend H1: There is a trend <b>There is no trend</b>

	alpha	0.05	
Chmeľnica 1960-2015	Kendall's tau	0.187	H0: There is no trend H1: There is a trend <b>There is a trend</b>
	S	267.000	
	Var(S)	17967.000	
	p-value (Two-tailed)	0.047	
	alpha	0.05	
Streda nad Bodrogom 1960-2015	Kendall's tau	-0.009	H0: There is no trend H1: There is a trend <b>There is no trend</b>
	S	-14.000	
	Var(S)	18974.000	
	p-value (Two-tailed)	0.925	
	alpha	0.05	

In station Poprad, Mníšek nad Hnilcom and Švedlár, Chmeľnica and Červený Kláštor there is trend. In station Humenné and Kamenica nad Cirochou, Krásny Brod and Tisinec-Stropkov, Streda nad Bodrogom there is no trend.

Table 3 Mann-Kendall trend test of 12 months RDI

Climatology station season	Mann-Kendall trend test		Test interpretation
Poprad 1960-2014	Kendall's tau	-0.201	H0: There is no trend H1: There is a trend <b>There is a trend</b>
	S	-393.000	
	Var(S)	28427.000	
	p-value (Two-tailed)	0.020	
	alpha	0.05	
Mníšek nad Hnilcom and Švedlár 1980-2010	Kendall's tau	0.310	H0: There is no trend H1: There is a trend <b>There is a trend</b>
	S	135.000	
	Var(S)	3141.667	
	p-value (Two-tailed)	0.017	
	alpha	0.05	
Humenné and Kamenica nad Cirochou 1989-2010	Kendall's tau	0.127	H0: There is no trend H1: There is a trend <b>There is no trend</b>
	S	59.000	
	Var(S)	3461.667	
	p-value (Two-tailed)	0.324	
	alpha	0.05	
Krásny Brod and Tisinec- Stropkov 1980-2010	Kendall's tau	0.058	H0: There is no trend H1: There is a trend <b>There is no trend</b>
	S	16.000	
	Var(S)	1625.333	
	p-value (Two-tailed)	0.710	
	alpha	0.05	
Chmeľnica and Červený Kláštor 1986-2010	Kendall's tau	0.306	H0: There is no trend H1: There is a trend <b>There is a trend</b>
	S	133.000	
	Var(S)	3141.667	
	p-value (Two-tailed)	0.019	
	alpha	0.05	
	Kendall's tau	0.030	

Streda nad Bodrogom and Košice 1980-2014	S	14.000	H0: There is no trend H1: There is a trend <b>There is no trend</b>
	Var(S)	3458.000	
	p-value (Two-tailed)	0.825	
	alpha	0.05	

The work was focused on the occurrence of a trend in the climatological indices Streamflow drought index (SDI) and reconnaissance drought index (RDI). The results show that in the SDI index there was a trend only in the station Humenné. There was a trend in the RDI index at the Poprad, Mníšek nad Hnilcom and Švedlár, Chmeľnica and Červený Kláštor stations. In stations where the trend did not occur, there could be an alternation of dry and wet periods. The results would be useful for further research into hydrological models and drought prediction and drought risk reduction.

## 5 Conclusion

Drought assessment is needed in terms of climate change. In recent times, drought has become more frequent, but also extreme rainfall, which is causing flash floods. Evaluating climatic variables using drought indices can help to improve water management in the country and make better use of water during droughts. The frequent occurrence of drought causes an increase in air temperature and a decrease in precipitation. Drought research should receive more attention. It would be possible to reduce the duration of drought and the intensity of drought if drought could be more accurately predicted.

## Acknowledgements

This work was supported by projects of the Ministry of Education of the Slovak Republic VEGA 1/0217/19 Research of Hybrid Blue and Green Infrastructure as Active Elements of a Sponge City, VEGA 1/0308/20 Mitigation of hydrological hazards - floods and droughts - by exploring extreme hydroclimatic phenomena in river basins and the projects of Slovak Research and Development Agency APVV-18-0360, APVV SL-PL-18-0033 and APVV SK-PT-18-0008.

## References

- [1] Mishra, A. K., & Singh, V. P. (2010). A review of drought concepts. *Journal of hydrology*, 391(1-2), 202-216.
- [2] Fendeková, M., Poórová, J., & Slivová, V. (2018). Hydrologické sucho na Slovensku a prognóza jeho vývoja. Bratislava: Comenius University.
- [3] Didovets, I., Krysanova, V., Bürger, G., Snizhko, S., Balabukh, V., & Bronstert, A. (2019). Climate change impact on regional floods in the Carpathian region. *Journal of Hydrology: Regional Studies*, 22, 100590.

- [4] Milanovic, M., Gocic, M., & Trajkovic, S. (2015). Analysis of Climatic Parameters in Serbia over the Period from 1981 to 2010. *Agriculture and agricultural science procedia*, 4, 167-174.
- [5] West, H., Quinn, N., & Horswell, M. (2019). Remote sensing for drought monitoring & impact assessment: Progress, past challenges and future opportunities. *Remote Sensing of Environment*, 232, 111291.
- [6] Tirivarombo, S., Osupile, D., & Eliasson, P. (2018). Drought monitoring and analysis: standardised precipitation evapotranspiration index (SPEI) and standardised precipitation index (SPI). *Physics and Chemistry of the Earth, Parts A/B/C*, 106, 1-10.
- [7] Svoboda, M., Hayes, M., & Wood, D. (2012). Standardized precipitation index user guide. *World Meteorological Organization Geneva, Switzerland*.
- [8] Mann, H. B. (1945). Nonparametric tests against trend. *Econometrica: Journal of the Econometric Society*, 245-259.
- [9] Thornthwaite, C. W. (1948). An approach toward a rational classification of climate. *Geographical review*, 38(1), 55-94.
- [10] Tigkas, D., Vangelis, H., & Tsakiris, G. (2015). DrinC: a software for drought analysis based on drought indices. *Earth Science Informatics*, 8(3), 697-709.
- [11] Svoboda, M., & Fuchs, B. (2016). Handbook of drought indicators and indices.

## Comparison of the strength development of binary and ternary cements containing perlite powder

Alena Sičáková, Erika Figmigová, Matej Špak

Technical University of Košice, Slovakia

Institute of Environmental Engineering, Institute of Technology, Economics and Management in Construction  
e-mail: alena.sicakova@tuke.sk, erika.figmigova@tuke.sk, matej.spak@tuke.sk

### Abstract

Currently, the consumption of blended cements is increasing all over the world. This is due to environmental, technical and economic reasons. Among the additives mixed with ordinary Portland cement, ground granulated blast furnace slag and fly ash are of particular significance. However, some regions may lack standard additives, and vice versa, may be rich in natural pozzolans. This paper is focused on the perlite as a natural pozzolanic material which is locally available. This study presents the results of the application of perlite as a component of blended cements in different proportions, representing binary and ternary compositions, and compares it with standard additives (fly ash and ground granulated blast furnace slag). The time development of both compressive and flexural strength, including results of 2, 7, 28 and 90-day testing, is analyzed. Perlite binders show acceptable time development of strengths, which is comparable to conventional blended binders based on ground granulated blast furnace slag and fly ash and do not constitute a technological barrier. With a higher dose of perlite, the time increase in flexural strength is slower, but the rate of increase in compressive strength does not change substantially. Flexural strength of 4.1–6.2 MPa and compressive strength of 18.8–38.5 MPa are sufficient for a number of practical applications and are expected to meet the required limits. An improvement of strengths in the later period (90 days) was also confirmed.

**Key words:** blended cements, perlite, blast furnace slag, fly ash, flexural strength, compressive strength

## 1 Introduction

Cement can currently be considered the most widely used binder in the construction sector. Several kinds of cement, as for the composition, are standardly used. The basic level is represented by Ordinary Portland Cement (OPC), and then different additives are considered to substitute the part of it, creating various blended cements. The standard range of such additives and compositions is given in STN EN 197-1 [1]. However, only a few types of all the defined options of cement compositions are commonly manufactured and used, like cements with blast furnace slag (CEM II/A-S or B-S, CEM III).

Currently, the consumption of blended cements is increasing all over the world. This is due to

three basic aspects [2, 3, 4]:

- energy saving and air quality: The cement industry contributes significantly to the imbalances of the environment; in particular, due to air quality and energy use. Partial substitution of cement clinker by other materials can help with this issue.
- conservation of natural resources: in case the used mineral additives are the waste products. By using these products, natural minerals like lime stone, clay and silica are saved.
- quality of cement-based products, like concrete: improvement of workability, mechanical properties and durability due to fineness and chemical actions.

Among the additives, ground granulated blast furnace slag (GGBFS) and fly ash (FA) are of particular significance throughout the world [2, 5].

**Fly ash** used in the production of cement and concrete is an inorganic product produced by the combustion of solid, usually finely ground, fuels in coal-fired power plants. Due to its fine particle size and generally non-crystalline character, fly ash usually has satisfactory pozzolanic properties or, in the case of a high lime content, both pozzolanic and latent hydraulic properties [6]. Oxide analysis is traditionally used to describe chemical composition in fly ash. The chemical composition can vary considerably, e.g. its mineralogical composition depending on the type and quantity of impurities present in the coal, method of combustion and method of collection. Fly ash obtained from anthracite is rich in silica ( $\text{SiO}_2$ ), alumina ( $\text{Al}_2\text{O}_3$ ) and iron oxide ( $\text{Fe}_2\text{O}_3$ ). The mineralogical parameters of the fly ash are of decisive impact on pozzolanic reaction, microstructure and nature of the hydrated products [6].

**Ground granulated blast furnace slag** is a by-product of the production of iron in a blast furnace. In terms of use in cement and concrete, the most important parameter is the glass-phase content. In almost completely glassy form, obtained by rapid cooling, GGBFS reaches a latent hydraulic and pozzolanic properties [6].

The effects of both FA and GGBFS on cement-based mixtures can generally be listed as follows [7-11]:

- on fresh mixtures: reduction of segregation and bleeding, better workability,
- on heat of hydration: additives reduce the heat of hydration in concrete. A substitution of 30 per cent fly ash may result in a reduction of 50-60% heat of hydration. This helps reduce the risk of thermal cracking,
- on setting time: setting time is typically longer; a 30 per cent substitution of fly ash may result in an increase of initial setting time up to 2 hours,
- on strength: since the pozzolanic action is slow, the early strengths at 7 and 28 days are lower, but may be about equal at 3 months and may further increase at ages greater than 3 months provided curing is continued,
- on durability: on addition of fly ash or GGBFS to cement, concrete is less permeable and chemically more stable than concrete from OPC. 28 days old concrete may be three times as permeable as ordinary concrete. It provides high resistance to attack by sulphates, chlorides and other chemicals thus durability is improved. High resistance to chloride ingress also reduces the risk of reinforcement corrosion.

However, some regions may lack standard additives, such as GGBFS due to high demand and consequent difficulties in securing supplies, or FA due to a lack of one that meets standard limits for concrete production. And vice versa, some regions or countries may be rich in natural pozzolans but do not generate substantial amounts of artificial pozzolans [12].



Therefore, other types of additives are increasingly being tested, like lime, perlite, artificial pozzolans (glass powder, brick powder...) and others [13 - 18].

**Perlite (P)** is amorphous volcanic glass, which has a relatively high-water content, usually formed by the hydration of obsidian. It occurs naturally and has the unusual property of expanding significantly when heated sufficiently. A typical perlite sample consists of 71% to 75% silicon dioxide, 12.5% to 18.0% alumina, 4% to 5% potassium oxide, 1% to 4% of sodium and calcium oxides and trace amounts of metal oxides [19]. Partial replacement of cement with perlite powder (PP) significantly reduces the initial strength of cement mortars during the first 7-28 days compared to CEM I samples. The optimal rate of cement substitution by perlite is declared in the values of 10% and 20%. This reduces sorptivity and porosity and also increases strength over time, due to the pozzolanic activity of perlite, which is slow at an early age and develops over time [20]. PP as a natural pozzolan is considered to be beneficial due to its low price and availability (depending on the region), as well as its ability to reduce the hydration heat and control the shrinkage of concrete mixtures. Nevertheless, its influence on the properties of concrete, including the reactivity (specifically in the early ages), strength, durability and so on, is still a concern [21]. There is also little information on how perlite interacts with other additives. With the trend of higher amounts of additives present in blended cements, different combinations need to be tested and optimized to achieve satisfactory performance.

This study presents the results of the application of perlite as a component of blended cements in different proportions, representing binary and ternary compositions, and compares it with standard additives (FA and GGBFS). The time development of both compressive and flexural strength, including results of 2, 7, 28 and 90-day testing, is analyzed. Testing was performed according to STN EN 196-1 [22].

## 2 Materials and methods

To verify the effect of perlite on the strength development of blended binders, binder mixtures were designed in different compositions, including the reference one with no any additive. Perlite (P) was applied as a component of OPC (CEM I) in three different percentage proportions:

- CEM/P = 70/30; the binder represents the CEM II/B-P type of cement according to STN EN 197-1 [1],
- CEM/P = 50/50; the binder represents the CEM IV/B type of cement according to STN EN 197-1,
- CEM/P/Ad = 70/15/15; the binder is of ternary composition and it represents the CEM II/B-M type of cement according to STN EN 197-1.

To compare the effect of perlite, two standard additives, FA and GGBFS, were used in such compositions, too. Ten compositions were tested in this way, including a reference sample – see table 1.

Table 1: Composition of blended binders

Samples	Components [%]			
	CEM I 42.5 R	Perlite (P)	Slag (S)	Fly ash (F)
<b>REF</b>	100	-	-	-
<b>C70P30</b>	70	30	-	-
<b>C70S30</b>	70	-	30	-
<b>C70F30</b>	70	-	-	30
<b>C50P50</b>	50	50	-	-
<b>C50S50</b>	50	-	50	-
<b>C50F50</b>	50	-	-	50
<b>C70/P15/S15</b>	70	15	15	-
<b>C70/S15/F15</b>	70	-	15	15
<b>C70/P15/F15</b>	70	15	-	15

For testing the properties, standard mortars according to STN EN 196-1 [22] were prepared using following materials:

- Sand (S): CEN Standard sand according to STN EN 196-1 [22],
- Cement (C): CEM I 42,5 R (CRH Turňa nad Bodvou, Slovakia),
- Mixing water (W): tap water,
- Mineral additives (Ad):
  - Ground granulated blast furnace slag (S): US Steel Košice, Slovakia,
  - Fly ash (F): energy segment of steel making factory, US Steel Košice, Slovakia,
  - Perlite (P): natural, finely ground perlite, Lehôtka pod Brehmi, Slovakia.

The powdery materials are characterised in table 2, including the presence of main oxides and grain size characteristics.

Table 2: Properties of cement, perlite, slag and fly ash

	SiO <sub>2</sub>	Al <sub>2</sub> O <sub>3</sub>	Fe <sub>2</sub> O <sub>3</sub>	CaO	Others	d (0.5)	d (0.9)
	(%)						
CEM I 42.5 R	20.3	4.0	3.0	64.1	8.6	26.7	67.9
P	53.9	9.3	1.3	1.3	34.2	33.7	78.0
S	41.3	6.3	0.4	36.0	16.0	19.0	111.5
F	56.4	19.9	7.3	4.4	12.0	19.1	94.8

Binders were prepared according to the proposed percentage composition by dry mixing. Furthermore, mixtures of standard composition ( $450 \pm 2$  g of binder,  $1\ 350 \pm 5$  g of CEN standard sand and  $225 \pm 1$  g of water) were prepared in accordance with STN EN 196-1 [20]. In the fresh state, differences in consistency were visually detected (with the presence of perlite powder and at higher amounts, the mixtures tended to be stiffer); however, for all mixtures, the

principle of a constant w/b ratio was kept to maintain the prescribed composition for testing the strength of binders. Following the moulding of the samples (40x40x160 mm), and after the appropriate curing time, the samples were tested for both flexural and compressive strength.

### 3 Results and discussion

To declare the flexural and compressive strength development of binders, results of 2, 7, 28 and 90-day values are given in tables 3 and 5. Results are next evaluated and discussed in two ways:

- as a percentage of the values of the reference sample, and
- as a percentage of 90-days values.

Data are given in tables 4 and 6.

#### 3.1 Flexural strength

Table 3: Results of flexural strength of blended binders

	<b>R<sub>f</sub> [MPa]</b>			
	2 days	7 days	28 days	90 days
<b>REF sample</b>	4.4	4.7	7.0	7.8
<b>C70 P30</b>	3.6	4.8	5.3	5.9
<b>C70 S30</b>	3.9	5.6	7.2	8.1
<b>C70 F30</b>	3.6	4.9	5.9	6.7
<b>C50 P50</b>	2.4	3.5	4.1	5.3
<b>C50 S50</b>	2.7	5.1	5.7	9.1
<b>C50 F50</b>	2.8	4.2	5.0	5.7
<b>C70 P15 S15</b>	3.8	5.4	5.9	6.8
<b>C70 S15 F15</b>	4.3	5.9	6.8	7.0
<b>C70 P15 F15</b>	3.6	5.2	6.2	6.2

Table 4: Expression of flexural strength as a percentage of the values of the reference sample and the values of 90 days, respectively

	<b>2 days</b>		<b>7 days</b>		<b>28 days</b>		<b>90 days</b>	
	share of REF value	share of 90- day value	share of REF value	share of 90- day value	share of REF value	share of 90- day value	share of REF value	share of 90- day value
	%							
<b>REF sample</b>	100	56	100	60	100	90	100	100

<b>C70 P30</b>	82	61	102	81	76	90	76	100
<b>C70 S30</b>	89	48	119	69	103	89	104	100
<b>C70 F30</b>	82	54	104	73	84	88	86	100
<b>C50 P50</b>	55	45	74	66	59	77	68	100
<b>C50 S50</b>	61	30	109	56	81	63	117	100
<b>C50 F50</b>	64	49	89	74	71	88	73	100
<b>C70 P15 S15</b>	86	56	115	79	84	87	87	100
<b>C70 S15 F15</b>	98	61	126	84	97	97	90	100
<b>C70 P15 F15</b>	82	58	111	84	89	100	79	100

The reference sample has the highest flexural strength after 2 days (4.4 MPa), but over time some of the blended binders acquire better strengths. After 90 days, C50S50 achieved the highest strength (9.1 MPa).

*Comparison of time development of flexural strength:*

- all samples show an increase over time, but to varying degrees,
- the fastest increase is in samples C70P30, C70S15F15 and C70P15F15, which in 2 days reach 61%, 61% and 58% of their 90-day strength, and in 7 days they reach 81%, 84% and 84% of 90-day strength,
- the slowest increase is in C50S50 and C50P50, which in 2 days have only 30% and 45% of their 90-day strength, and in 28-days only 63% and 77% of 90-day strength.

*Comparison with the reference sample:*

- at 2 days of setting, the blended cement samples reach from 55% (C50P50) to 98% (C70S15F15) of the value of the reference sample. In later times, some of the blended cements even exceed the value of the reference sample; e.g. after 7 days of setting and hardening, this is the case for all samples except C50P50 and C50F50,
- after 90 days of hardening, the samples of blended cements reach from 73% (C50F50) up to 104% (C70S30), and 117% (C50S50) of the value of the reference sample.

*Evaluation of perlite samples:*

- standard 28-day values of flexural strength of blended binders with perlite are in the range of 4.1 - 6.2 MPa, the best value being in combination with fly ash (C70P15F15),
- with a higher dose of perlite, the increase in flexural strength is slower; at 28 days, C70P30 has 90% of its 90-day strength, but C50P50 has only 59% of its 90-day strength. In combination with slag (C70P15S15) the value is at the level of 30% perlite, but in combination with fly ash (C70P15F15) the hardening is accelerated and the 28-day strength reaches the level of 90-day strength.
- perlite samples achieve lower strength than that of the reference sample; after 90 days of curing, the closest value to the reference sample is 87% (C70P15S15),
- perlite achieves the best results in combination with slag or fly ash.

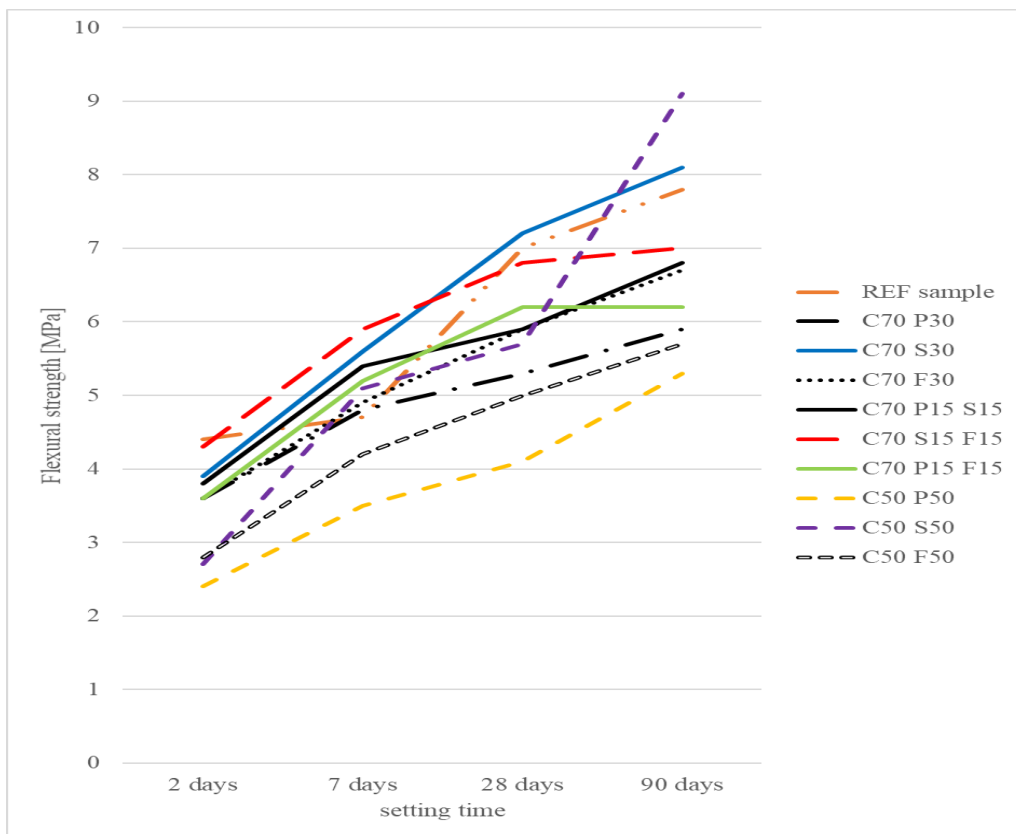


Figure 1: Development of flexural strength of blended binders

### 3.2 Compressive strength

Table 5: Results of compressive strength of blended binders

	$R_c$ [MPa]			
	2 days	7 days	28 days	90 days
<b>REF sample</b>	26.3	46.0	54.5	55.4
<b>C70 P30</b>	16.1	24.4	31.0	35.3
<b>C70 S30</b>	17.3	29.8	41.5	48.0
<b>C70 F30</b>	17.7	26.1	39.0	46.9
<b>C50 P50</b>	9.4	15.3	18.8	23.5
<b>C50 S50</b>	10.9	21.3	34.9	48.7
<b>C50 F50</b>	12.2	19.6	27.0	34.0
<b>C70 P15 S15</b>	16.8	29.2	38.0	42.9
<b>C70 S15 F15</b>	17.4	29.6	44.5	49.1
<b>C70 P15 F15</b>	16.5	25.3	38.5	41.4

Table 6: Expression of compressive strength as a percentage of the values of the reference sample and the values of 90 days, respectively

	2 days		7 days		28 days		90 days	
	share of REF value	share of 90- day value	share of REF value	share of 90- day value	share of REF value	share of 90- day value	share of REF value	share of 90- day value
	%							
<b>REF sample</b>	100	47	100	83	100	98	100	100
<b>C70 P30</b>	61	46	53	69	57	88	64	100
<b>C70 S30</b>	66	36	65	62	76	86	87	100
<b>C70 F30</b>	67	38	57	56	72	83	85	100
<b>C50 P50</b>	36	40	33	65	34	80	42	100
<b>C50 S50</b>	41	22	46	44	64	72	88	100
<b>C50 F50</b>	46	36	43	58	50	79	61	100
<b>C70 P15 S15</b>	64	39	63	68	70	89	77	100
<b>C70 S15 F15</b>	66	35	64	60	82	91	89	100
<b>C70 P15 F15</b>	63	40	55	61	71	93	75	100

The reference sample has the highest compressive strength at all tested times (26.3 - 55.4 MPa). Of the blended binders, they are C70S30 and C70S15F15, which have values at the same level (17.3 - 48.0 MPa) and (17.4 - 49.1 MPa) respectively.

*Comparison of time development of compressive strength:*

- all samples show an increase over time, but to varying degrees,
- the reference sample has the fastest increase. In the case of blended binders, the sharpest increase is in C70P30, C50P50 and C70P15F15, which in 2 days reach 46%, 41% and 40% of their 90-day strength,
- the slowest increase is in C50S50, which in 2 days has only 22% of 90-day strength, and in 28 days only 72% of 90-day strength.

*Comparison with the reference sample:*

- at 2 days of setting, the blended cement samples reach from 36% (C50P50) to 67% (C70F30) of the reference sample value. It can be stated that all blended binders with combinations at the level of 30% of additives have in principle the same result,
- after 90 days of hardening, the samples of blended cements reach from 42% (C50P50) up to 89% (C70S15F15) and 88% (C50S50) of the reference sample value.

*Evaluation of perlite samples:*

- standard 28-day values of compressive strength of blended binders with perlite are in the range of 18.8 - 38.5 MPa, with the best value in combination with fly ash (C70P15F15),
- with a higher dose of perlite, the increase in strength does not change substantially, even in combinations with slag and fly ash. The strength after 2 days of setting reaches the level of about 40% of 90-day strength, in 7 days about 67% and in 28 days about 90% of 90-day strength.

- perlite samples achieve lower strengths than the reference sample; after 90 days of curing, sample C70P15S15 was found to be closest to the reference sample by 77%,
- perlite achieves the best results in combination with slag or fly ash.

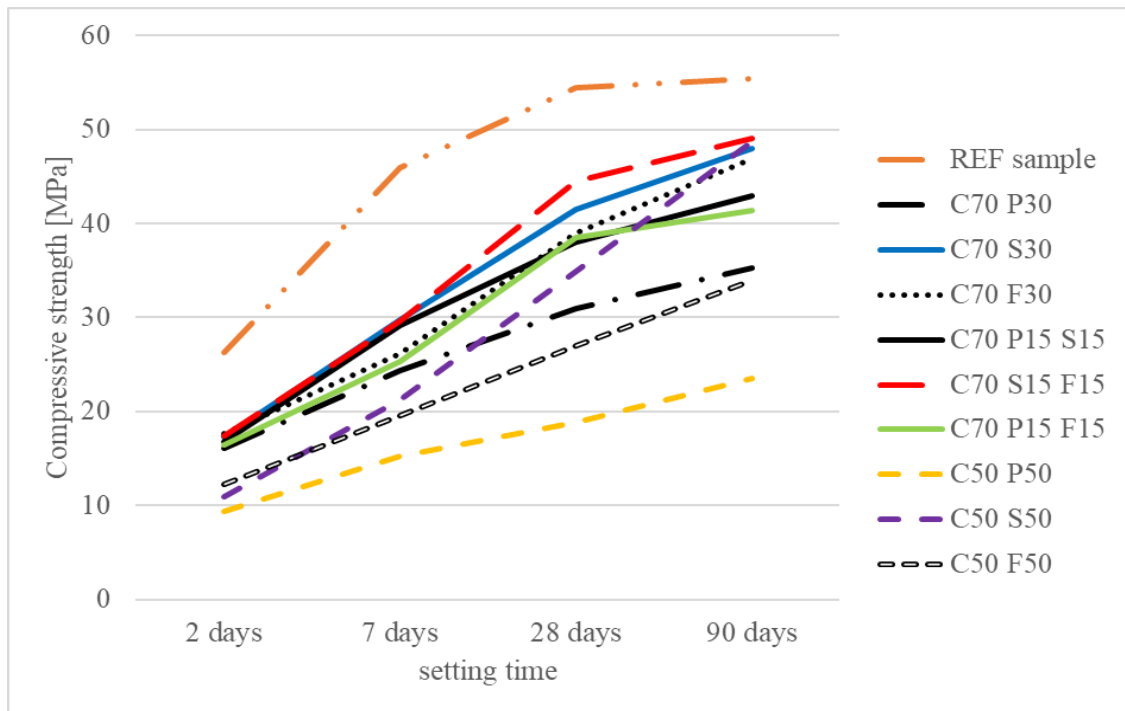


Figure 2: Development of compressive strength of blended binders

## 4 Conclusion

Perlite powder, a natural material with pozzolanic properties that is locally available, was the subject of the presented testing. The aim was to compare perlite performance with conventional additives (GGBFS and FA), while they were used in different compositions representing binary and ternary blended cements. Following percentage ratios of CEM I and additives (Ad) were tested: CEM I/Ad = 70/30, 50/50, and CEM I/Ad1/Ad2 = 70/15/15, while all possible combinations of three additives were applied. For testing the properties, standard mortars according to STN EN 196-1 were prepared. The time development of both the compressive and flexural strength, including results of 2, 7, 28 and 90-day testing, was evaluated. The following findings can be formulated:

- blended binders with different % of perlite, slag and fly ash show different rates of strength increase in the range of 90 days of setting and hardening,
- the fastest increases after 2 days of curing were found at the level of 61% and 58% of the 90-day flexural strength and at the level of 46% and 40% of 90-day compressive strength – this applies to samples C70P30 and C70P15F15,
- sample C50S50 has the slowest increases in strength: after 2 days of curing it was found at

the level of 30% of the 90-day flexural strength and at the level of 22% of the 90-day compressive strength; after 28 days at the level of 63% of the 90-day tensile strength and only 72% of the 90-day compressive strength,

- with a higher dose of perlite, the time increase in flexural strength is slower, but the rate of increase in compressive strength does not change substantially,

- perlite binders show acceptable time development of strengths, which is comparable to conventional blended binders based on GGBFS and FA and do not constitute a technological barrier,

- standard 28-day values of blended binders with perlite are in the range of 4.1 - 6.2 MPa (flexural strength), and 18.8 - 38.5 MPa (compressive strength), the best values being achieved in combination with fly ash (C70P15F15),

- perlite samples achieve lower strengths than the reference sample; after 90 days of hardening, the sample C70P15S15 is closest to the reference sample - it reached 87% of the reference flexural strength and 77% of reference compressive strength.

By comparing the results, it is generally possible to conclude that although perlite blended binders achieve lower strengths compared to conventional binders, they have a promising potential. Flexural strength of 4.1–6.2 MPa and compressive strength of 18.8–38.5 MPa are sufficient for a number of practical applications and are expected to meet the required limits. Also, their improvement in the later period (90 days) was confirmed.

## Acknowledgements

This research has been carried out within the project of Slovak Scientific Grant Agency VEGA (Grant No. 1/0524/18).

## References

- [1] STN EN 197-1. (2012). Cement. Part 1 Composition, specifications and conformity criteria for common cements.
- [2] Sivakumar A., Nair Nithya, Sounthararajan V.M. (2013). Hydration Characteristics of Pozzolan Substitutes in Cementitious Binder. *World Applied Sciences Journal* 25.8, 1166-1170. ISSN 1818-4952.
- [3] DEVI K. Syamala, LAKSHMI V. Vijaya, ALAKANANDANA A. (2017). Impacts of cement industry on environment-an overview. *Asia Pac. J. Res.* 1, 156-161.
- [4] NACERI A., HAMINA M. Chikouche, GROSSEAU P. (2009). Physico-Chemical Characteristics of Cement Manufactured with Artificial Pozzolan (Waste Brick). *World Academy of Science, Engineering and Technology.* 52, 41-43.
- [5] ZHAO Feng-Qing, et al. (2007). Activated fly ash/slag blended cement. *Resources, Conservation and recycling.* 52 (2), 303-313.
- [6] TOKYAY Mustafa. (2016). *Cement and concrete mineral admixtures.* CRC Press.
- [7] PAYA J., et al. (2000). Mechanical treatment of fly ashes: Part IV. Strength development of ground fly ash-cement mortars cured at different temperatures. *Cement and Concrete Research.* 30 (4), 543-551.



- [8] CHOI Young Cheol, KIM Jiyoung, CHOI Seongcheol. (2017). Mercury intrusion porosimetry characterization of micropore structures of high-strength cement pastes incorporating high volume ground granulated blast-furnace slag. *Construction and Building Materials*. 137, 96-103.
- [9] SURESH D., NAGARAJU K. (2015). Ground granulated blast slag (GGBS) in concrete—a review. *IOSR journal of mechanical and civil engineering*. 12(4), 76-82.
- [10] PANDEY Rajesh Kr, KUMAR Abhishek, AFAQUE KHAN M. (2016). Effect of ground granulated blast furnace slag as partial cement replacement on strength and durability of concrete: a review. *Int Res J Eng Technol (IRJET)*. 3 (2), 1662-1666.
- [11] KAGADGAR Sarfaraz Ahmed, SAHA Suman, RAJASEKARAN C. (2017). Mechanical and durability properties of fly ash based concrete exposed to marine environment. *Selected Scientific Papers-Journal of Civil Engineering*. 12 (1), 7-18.
- [12] ERDOĞAN Sinan Turhan, SAĞLIK Aslı Ünsal. (2013). Early-age activation of cement pastes and mortars containing ground perlite as a pozzolan. *Cement and Concrete Composites*. 38, 29-39.
- [13] BHEEL Naraindas, et al. (2019). Use of rice husk ash as cementitious material in concrete. *Engineering, Technology & Applied Science Research*. 9 (3), 4209-4212.
- [14] BHEEL Naraindas. et al. (2019). Effect of Tile Powder Used as a Cementitious Material on the Mechanical Properties of Concrete. *Engineering, Technology & Applied Science Research*. 9.5, 4596-4599.
- [15] ESFANDIARI J., LOGHMANI P. (2019). Effect of perlite powder and silica fume on the compressive strength and microstructural characterization of self-compacting concrete with lime-cement binder. *Measurement*. 147, 106846.
- [16] KAREIN S., Mahmoud Motahari, et al. (2018). Effects of the mechanical milling method on transport properties of self-compacting concrete containing perlite powder as a supplementary cementitious material. *Construction and Building Materials*. 172, 677-684.
- [17] FEDERICO L. M., CHIDIAC S. E. (2009). Waste glass as a supplementary cementitious material in concrete—critical review of treatment methods. *Cement and concrete composites*. 31 (8), 606-610.
- [18] SOBOL Khrystyna, MARKIV Taras, HUNYAK Oleksii. (2017). Effect of mineral additives on structure and properties of concrete for pavements. *Selected Scientific Papers-Journal of Civil Engineering*. 12 (2), 95-100.
- [19] SAMAR Mueena, SAXENA Shweta. (2016). Study of chemical and physical properties of perlite and its application in India. *Int J Sci Technol Manag*. 5, 70-80.
- [20] GUENANOU Farida, KHELAFI Hamid, AATTACHE Amel. (2019). Behavior of perlite-based mortars on physicochemical characteristics, mechanical and carbonation: Case of perlite of Hammam Boughrara. *Journal of Building Engineering*. 24, 100734.
- [21] KAREIN S. Mahmoud Motahari, et al. (2018). Effects of the mechanical milling method on transport properties of self-compacting concrete containing perlite powder as a supplementary cementitious material. *Construction and Building Materials*. 172, 677-684.
- [22] STN EN 196-1. (2019). Methods of testing cement. Part 1 Determination of strength.

# Wind flow around buildings of basic shapes with and without a wind-adaptive envelope

Lenka Kabošová, Stanislav Kmet', Dušan Katunský

Technical University of Košice, Slovakia  
Faculty of Civil Engineering, Institute of Architectural Engineering  
e-mail: [lenka.kabosova@tuke.sk](mailto:lenka.kabosova@tuke.sk), [stanislav.kmet@tuke.com](mailto:stanislav.kmet@tuke.com), [dusan.katunsky@tuke.sk](mailto:dusan.katunsky@tuke.sk)

## Abstract

Together with the natural environment, the built, artificial environment represents a barrier to the wind fluxes. Especially in the densely built cities, the wind flow pattern and the wind speed are considerably altered by buildings, which can lead to zones of an accelerated wind and turbulent flow. Incorporating the wind into the early conceptual stage of architectural design, this reciprocal interaction of the built environment and the wind fluxes can be analyzed and controlled to create zones of calmer wind around buildings. Presently, building envelopes are designed to withstand extreme load cases, which, however, demands thicker and bulkier structures. The subject of this study is a proposal and investigation of a lightweight, adaptive building envelope, which is able of a local, passive morphing in the wind. This local shape change leads to creating a textured, dimpled building surface; the final shape depends on the wind direction and force. The wind-induced dimpled surface influences the wind flow around the building, as well as surface wind pressure acting on the building, and the drag force. The analysis of three fundamental building shapes using the CFD (Computational Fluid Dynamics) simulation is performed for the variants with and without the proposed adaptive envelope. Concluding from the wind simulations, the wind flow can be decelerated, the turbulence reduced, and calmer zones around buildings can be created, by certain conditions. Moreover, the envelope, morphing with the instant wind force, can contribute to the reduction of the surface wind suction on buildings. Strikingly, the dimpled geometry of the wind-adaptive envelope can decrease the wind drag force by up to 28.4 %, which is again dependent on the global form, as well as the initial wind speed.

**Key words:** wind flow, adaptive building envelope, digital design, CFD analysis

## 1 Introduction

Designing architecture based on its performance in the wind was still a new approach in architectural practice not that long ago [1,2]. This method, however, slowly penetrates the architectural, as well as the civil engineering area [3]. Continuously advancing digital design and analysis tools contribute to the smooth integration of wind analysis to the design process. In the early conceptual design stage, fast decision-making is crucial. When it comes to the evaluation of the building performance in the wind, CFD simulations can help in estimating the wind-architecture interactions, and subsequently, in developing wind-formed designs.

When designing for arid lands, for instance, the wind can be utilized to provide natural ventilation [4]. Porous building envelopes, for example, can contribute to the natural ventilation of tall buildings and thus protect them from the heat load, as well as manage exhaust air [5]. Moreover, pollutant dispersion can be predicted by employing CFD simulations [6,7]. In the zones with the turbulent, cold and strong wind, both local and global building forms, together with the urban configuration of buildings, can influence the reduction of the unfavorable wind effects [8]. The small scale elements, creating a bumpy surface, can contribute to affecting the overall building aerodynamics [9].

### 1.1 Computational tools in the early design stage

Designing for the fluctuating wind conditions in the external environment, incorporating available computational tools in the early conceptual design stage leads to improving the performance of the design under the existing wind conditions [7,8,9] compared to evaluating the wind performance of the completed project in the later design stages, which is less effective, and the subsequent wind optimization of the design much costlier [9]. Among architects, Rhinoceros, as well as its algorithmic designing plug-in Grasshopper, are well-known 3D modeling software. Controlling the design parametrically according to the results of the design's performance in the wind, a wind-adaptive urban, architectural, or structural design can be created as a result of an iterative process. Creating more design alternatives varying in form, relative rotation, and scale means more options to choose from in the given wind conditions. The wind-driven form-finding using CFD (Computational Fluid Dynamics) analysis leads to the wind-based optimization of the intended design, which can retroactively control or modify the wind speed and flow pattern [10,11]. CFD simulations can either run through a stand-alone program or be integrated into a 3D software (e.g., Rhinoceros). If the design and the wind analysis can be completed in one working environment, the wind optimization is much more fluid, which speeds up the iterative process of finding the most suitable design option in the specific wind situation. When employing the simulations in the design process, a question might arise, whether the virtual simulation results are comparable with reality, and the physical wind tunnel experiments. Older studies [6,15], as well as new research, has already tested and validated the accuracy of CFD simulations compared to the wind tunnel measurements or field measurements [8,9,12,13]. The results obtained from modern CFD tools are in good agreement with wind tunnel experiments. This study proposes to engage the simulations in the early design phase for obtaining an idea of the interactions of the wind with the built environment. In the later design stages, after the best-performing designs are picked based on the CFD results, these can be then tested in the physical wind tunnel.

### 1.2 The Eurocode 1

The structural design of buildings exposed to the wind effects is coordinated by the Eurocode 1 EN 1991-1-4:2005. The guidelines are valid in most EU countries except Bulgaria, Croatia, and Romania. However, some of the non-EU countries, such as Iceland, Norway, as well as Switzerland, use Eurocode 1 to design building structures subjected to the wind. National annexes contain a country-specific wind map depicting the fundamental value of the basic wind velocity,  $v_{b0}$ . This value represents the characteristic 10-minute mean wind velocity,

irrespective of wind direction and season, at the height of 10 m above flat open country terrain with low vegetation. It is used for the structural design of buildings, as a maximum wind load that a structure has to withstand. The example of the Central and Mediterranean Europe wind map with values of  $v_{b0}$  is depicted in (Fig. 1) [18]. The value of 24 m/s (86.4 km/h), representing the fundamental value of the basic wind velocity for Slovakia is used in the wind analysis tests.

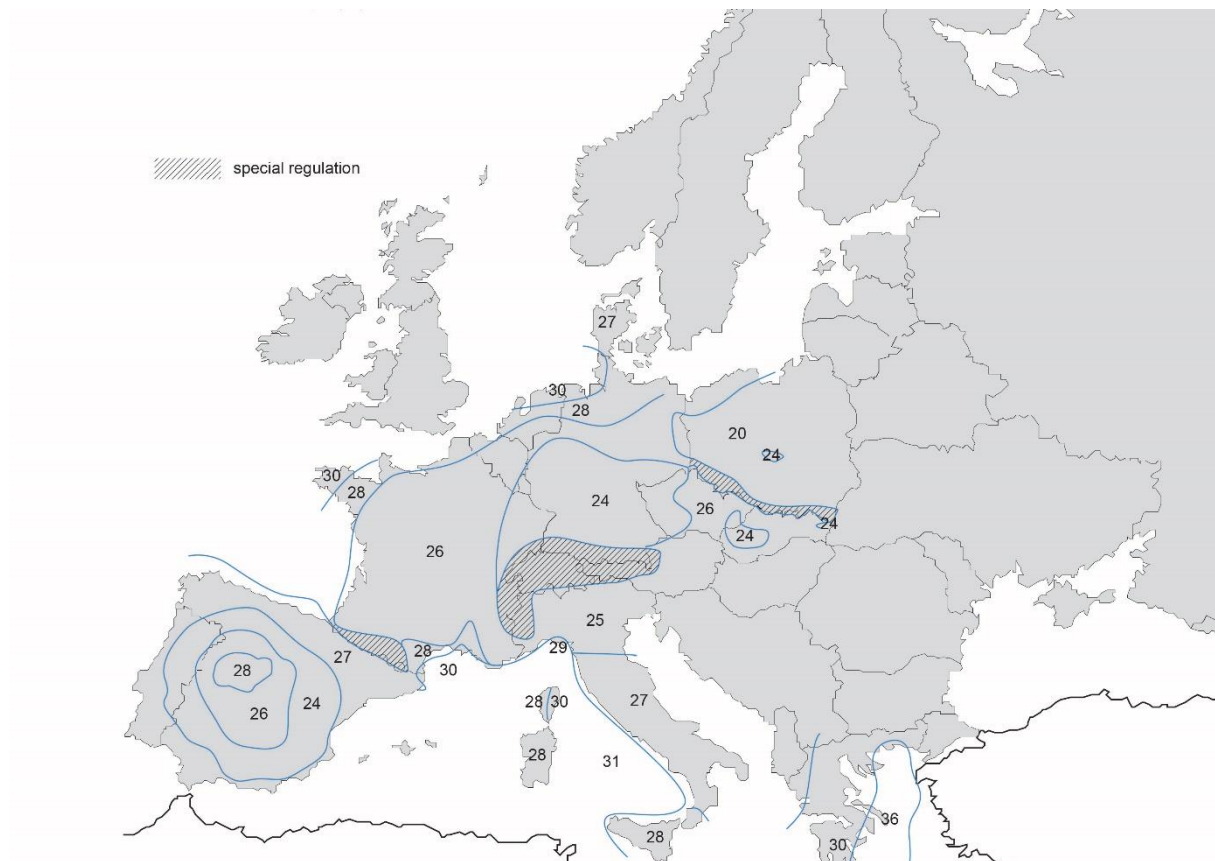


Fig. 1: Central and Mediterranean Europe wind map (map source [19])

## 2 Design approach

This paper aims to introduce a digital architectural design method based on the reciprocal interaction of architecture and the wind. The building form, global, as well as local, plays a fundamental role concerning wind-induced actions. The geometric features of the building, and, in the case of flexible building skins, the mechanical properties (aero-elastic effects) of such skin alter the wind load and the wind pattern around the buildings [5]. The ultimate wind effect on structures is, naturally, influenced by the approaching wind characteristics.

### 2.1 Wind-adaptive envelope

The wind on building envelopes acts as surface pressure; positive is compression, while

negative is suction. Depending on the direction and strength of the wind, buildings and their structures are subjected to variable pressure. This paper proposes a wind-adaptive building envelope that passively responds to the instant wind pressure in real-time. The geometry and material-based adaptive behavior consequently can contribute to the optimal utilization of the designed structure in various load conditions [20]. As contrary to the conventional inert structures which have to resist the external energy caused by the wind, adaptive structures can be designed as more lightweight because of their ability to comply with the external forces, transforming the wind energy into kinetic energy. The access kinetic energy could be used to generate electricity. The adaptive behavior can be particularly useful in case of unpredictable, swiftly altering events, such as wind storms.

## 2.2 Tensegrity-membrane adaptive element

The wind-adaptive envelope is developed digitally using the afore-mentioned software ergo Rhinoceros and Grasshopper. Translucency, as well as lightness, is the main criteria for the proposed adaptive skin. A tensegrity (tensional integrity) [21] structural configuration is employed to create the tensegrity-membrane adaptive module. The following reasons led to this choice: lightness, flexibility under the load (reversible passive deformation caused by the material-embedded properties), and structural stability ensured by the force equilibrium of tensioned and compressed elements. The principle of the shape adaptation of the adaptive module is depicted in Figure 2. The extent of the module's bending depends on the material properties, the direction of the acting wind, as well as the wind speed. The whole wind-adaptive envelope comprises of multiple adaptive modules, each fixed in 4 points to the supporting structural frame. One adaptive module consists of struts in compression, steel cables in tension, and two layers of translucent tensile fabric membranes in tension. A live physics engine Kangaroo 2, an add-on for Grasshopper, is used for finding the equilibrium state of the proposed tensegrity-membrane configuration. Depending on the speed of the acting wind, represented by the pressure, the adaptive module creating the adaptive envelope, bends and rotates adequately.

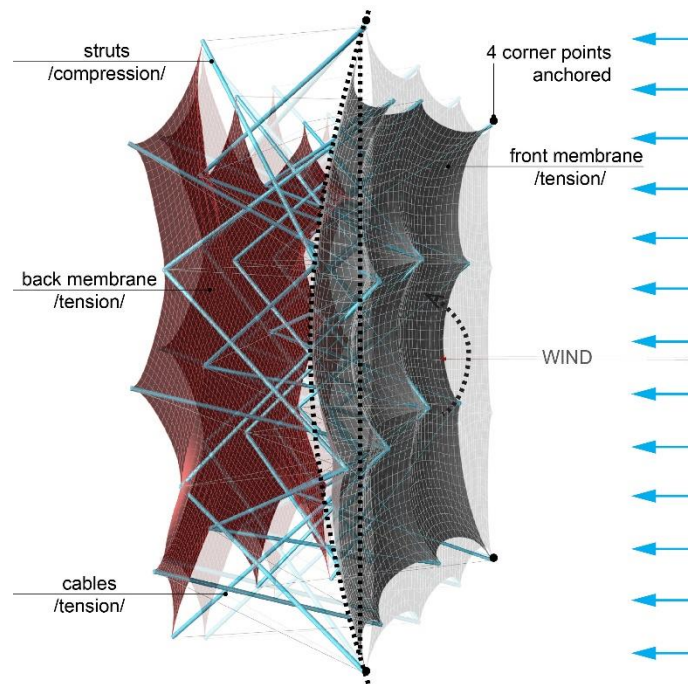


Fig. 2: One tensegrity-membrane module of the adaptive envelope (dotted is the bending and rotation under certain wind pressure)

Table 1 describes the material properties defined in the Kangaroo 2 simulation for examining the reconfiguration of the proposed adaptive element under the wind load.

Table 1. Material settings.

	Length $l$ [m]	Diameter $\Phi$ or thickness $h$ [m]	Stiffness $k$ [N/m]	Young's Modulus $E$ [Pa]	Pretension 0=max.; 1=min. [-]
<b>Struts</b>	1	$\Phi = 16e^{-3}$	2 110 080	$10.5e^9$	1
<b>Cables</b>	0.78	$\Phi = 2e^{-3}$	523 333	$130e^9$	0.99
<b>Membranes</b> (isotropic)	2.1 x 2.1	$h = 0.51e^{-3}$	20 000 or 84 000	$3.9 e^7$ or $16.5e^7$	0.90

### 2.3 Wind analysis of buildings of basic geometric shapes

CFD tests of basic-geometry building shapes are conducted to compare the influence of the wind-adaptive (morphing in the wind) building envelope versus the non-adaptive (steady) variant on the building aerodynamics. Swift, a plug-in for Grasshopper, running on the OpenFOAM® platform, is used to perform the simulations. The post-processing of the simulations' results is possible using stand-alone software, Paraview. The results are captured in the 2D top and side view. The finite volume method meshing is used to divide the virtual wind tunnel to 1x1x1 m cells. Closer to the tested geometry, the cells are refined to 0.125 x

0.125 x 0.125 m. The terrain roughness is set to 1, representing densely built-up areas. The convergence criteria are the following: velocity  $U$ , pressure  $p$ , turbulent model  $k/\varepsilon$ :  $1e^{-2}$ ,  $4e^{-2}$ ,  $1e^{-2}$ , respectively. It is suitable to set the relaxation factors for  $p = 0.3$  and  $U, k, \varepsilon = 0.7$  to achieve faster convergence. The pressure used in Swift is the kinematic pressure  $p_k$  [16]:

$$p_k = \frac{p}{\rho} \quad \#(1)$$

where  $p_k$  is the kinematic pressure used for incompressible flows [ $m^2/s^2$ ],  $p$  is the static pressure [Pa], and  $\rho$  is the air density [ $kg/m^3$ ].

The basic-shape objects will also be examined for their resistance to the wind flow, represented by the drag force,  $F_d$ :

$$F_d = -\frac{1}{2c_d A \rho v^2} \quad \#(2)$$

where  $F_d$  is the drag force [N],  $c_d$  is the drag coefficient [-],  $\rho$  is the air density [ $kg/m^3$ ],  $v$  is the wind speed [m/s].

### 3 Design experimentation

Creating an adaptive architecture able to react simultaneously with the changing wind conditions, requires a sequential analysis from the local (morphed) shape to the global building form, assessing their behavior in the wind. First, the live physics simulations have to be employed to obtain the shape change caused by the acting wind. Second, the changed geometry configuration is tested in Swift CFD plug-in.

#### 3.1 Digital simulations for creating a wind-adaptive shape-changing module

Nine 4-strut tensegrities create one shape-changing module, which is fixed in 4 corner points of the front membrane and morphs when loaded by the wind pressure (Fig. 2). The adaptive modules can be arrayed on any surface, covering or substituting building envelopes. This study deals with the latter. Two size versions of the adaptive module are examined in the paper, i.e., 2.1 x 2.1 m, and 4 x 4 m. The wind-responding envelope in two size variants is applied as a skin on each building surface, only on the windward side, or fully covering the building. The dimensions of the tested cube are 12x12x12 m, the cylinder is 12 m high, and 12 m in diameter. The interactive shape response of the whole building shape in the wind is achieved using Kangaroo 2 (Fig. 4), alike the simulation of one element. The bending in the wind, however, is simplified, as only the material characteristics of the front membrane are defined in the simulation, representing the building surface in contact with the wind flow. By changing the wind speed, the particle-spring system in Kangaroo 2 reconfigures to find another equilibrium state. Consequentially, the wind force acting on such an adaptive building envelope creates a dimpled, rough surface (Fig. 5). The value of the wind pressure in Pa is derived from Bernoulli's equation:

$$p = \frac{1}{2} \rho v^2 \quad \#(3)$$

where  $p$  is the wind pressure [Pa],  $\rho$  is the density of air [ $\text{kg/m}^3$ ], and  $v$  is the wind velocity [m/s]. Hence, in Kangaroo 2 simulations, the wind speed of 24 m/s is represented by the pressure of 360 Pa, acting on the windward side of buildings.

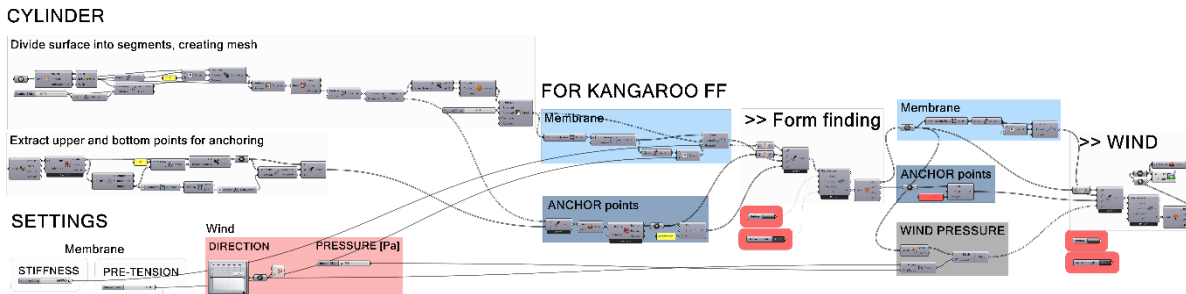


Fig. 4: The Grasshopper definition, employing Kangaroo 2. The membrane material properties, as well as the magnitude of the wind, influence the shape change

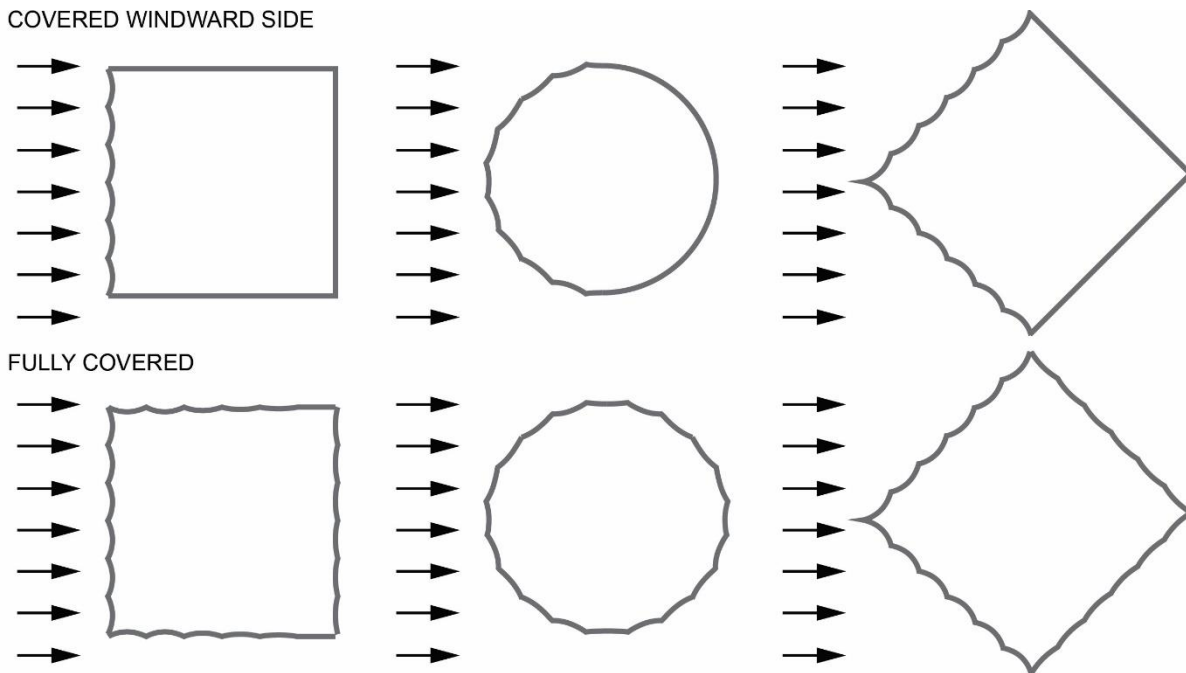


Fig. 5: The top view of the cube, cylinder, and 45-degree rotated cube with the wind-deformed skin

### 3.2 CFD simulations

After the wind-induced shape response of the adaptive envelope is found, the CFD analysis follows. Experiments with basic shapes (Fig. 6, 7, and 8) in the 24 m/s wind are performed to examine the surface wind pressure and drag force reduction, as well as the influence on the wind flow pattern. Three simulation cases are run for all three tested shapes. First, a smooth-surface building is tested, second, a shape with 2x2 m adaptive modules (fully or partially covering the object) is analyzed, and third, a variant with a 4x4 m adaptive module (fully or partially covering the object) is simulated using the CFD solver, Swift. Subsequently, the visualizations, as well as the calculations of the surface pressure  $p_k$ , as well as the drag force



$F_d$ , representing the resistance of the tested object to the wind flow, are performed using Paraview.

## 4 Results

The smooth variant is compared with four variants of adaptive façade for each basic shape. The results for the surface kinematic pressure  $p_k$  as well as for the shape's drag force  $F_d$  are described in Table 2.

**Table 2.** Numerical results of the CFD simulations.

Basic shape	maximum Negative pressure $p_k$ on the building surface [m <sup>2</sup> /s <sup>2</sup> ]	Maximum Positive pressure $p_k$ on the building surface [m <sup>2</sup> /s <sup>2</sup> ]	Drag force $F_d$ [N]
Smooth cube	<b>-375.37</b>	<b>+302.41</b>	<b>-44 088</b>
Cube with 2x2m dimples (windward adaptive façade)	-378.28 (↑ 0.8%)	+303.20	-44 614 (↑ 1.2%)
Cube with 2x2m dimples (whole façade is adaptive)	-917.57 (↑↑ 144%)	+303	-41 289 (↓ 6.3%)
Cube with 4x4m dimples (windward adaptive façade)	-368.49 (↓ 1.8%)	+303.91	-45 351 (↑ 2.9%)
Cube with 4x4m dimples (whole façade is adaptive)	-1075.74 (↑↑ 187%)	+301.66	-39 950 (↓ 9.4%)
Smooth cylinder	<b>-748.23</b>	<b>+296.36</b>	<b>-16 317</b>
Cylinder with 2x2m dimples (windward adaptive façade)	-886.34 (↑ 18.5%)	+295.99	-15 217 (↓ 6.7%)
Cylinder with 2x2m dimples (whole façade is adaptive)	-815.41 (↑ 8.9%)	+295.81	-14 979 (↓ 8.2%)
Cylinder with 4x4m dimples (windward adaptive façade)	-1015.87 (↑ 35.8%)	+295.82	-17 770 (↑ 8.9%)
Cylinder with 4x4m dimples (whole façade is adaptive)	-1005.24 (↑ 34.3%)	+296.43	-21 362 (↑ 31%)
Smooth 45° cube	<b>-908.75</b>	<b>+294.24</b>	<b>-57 785</b>

45° Cube with 2x2m dimples (windward adaptive façade)	-1182.39 (↑ 30.1%)	+298.20	-57 666 (↓ 0.2%)
45° Cube with 2x2m dimples (whole façade is adaptive)	-937.69 (↑ 3.2%)	+299.42	-41 373 (↓ 28.4%)
45° Cube with 4x4m dimples (windward adaptive façade)	-1033.61 (↑ 13.7%)	+299.00	-60 130 (↑ 4.3%)
45° Cube with 4x4m dimples (whole façade is adaptive)	-1011.76 (↑ 11.3%)	+299.25	-43 341 (↓ 25%)

#### 4.1 Numerical extremities

The actual values of the wind pressure, as well as drag force, are obtained in Paraview post-processing software. Although the results indicate that the suction is not reduced when the adaptive skin is applied, when every finite volume calculation cell was examined, it was observed, that there are some calculation extremities on the tested geometries. These extremities are caused by the spiky shape of the adaptive surface, combined with the size of the finite volume calculation cell. After the extremities are obviated, this can alter the actual values of the wind suction. This issue will be addressed in further research.

#### 4.2 The cube

The wind flow separation is induced on the front edges of the object, causing the fluid flow to change into turbulence. The smooth cube produces symmetrical swirls on the sides of the geometry, while the speed can reach 20 m/s. Downwind, the speed is around 15 m/s. The wind suction is visible on the sides, more to the back of the geometry.

After applying the wind-adaptive envelope on the front side of the cube, similar symmetrical swirls develop downwind, however, the speed is reduced to circa 12 m/s. The wind suction zones on the sides move closer to the front side of the geometry.

The adaptive surface with larger dimples (4x4 m), applied on the front side of the cube, behaves similarly as the 2x2 m variant. The symmetrical swirls on the leeward side develop closer to the geometry, while new areas of downwind suction are formed. In addition to the observations of the wind flow, the actual values of surface pressure, as well as drag force, are examined. In 24 m/s winds, the applied adaptive skin with the 2x2 m dimples does not contribute to reducing the surface wind suction. Nevertheless, the wind suction is slightly reduced when the 4x4 m variant is employed. The drag force increases after applying the adaptive envelope, due to the discernible spikes, caused by high wind speed.

The 2x2 m adaptive envelope covering the whole surface of the cube contributes to the reduction of the suction zones around the object, and the wind swirls on the sides of the cube. The extreme increase of the surface wind pressure acting on the object could be caused by the numerical extremities. The 4x4 m variant contributes to decreasing the drag force on the object. On the leeward side, a longer calm zone is formed, and the wind swirls on

the sides of the cube are eliminated. The wind pressure around the object is diffused, influencing the reduction of the wind suction zones. The reduced pressure zones around the cube suggest that the actual values of the surface wind pressure are probably influenced by the numerical extremities and consequently will be much lower.

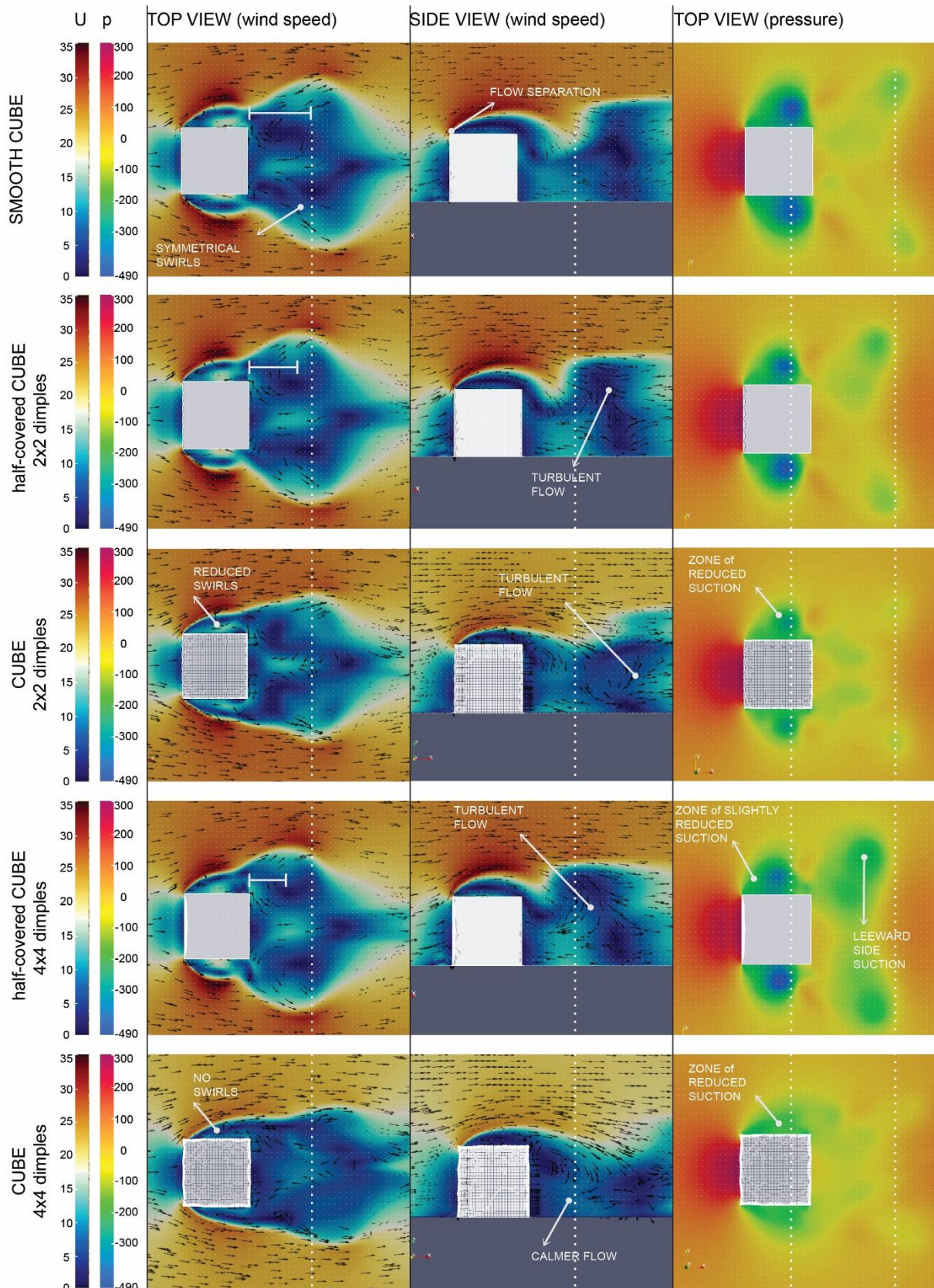


Fig. 5: The cube with and without the applied adaptive elements

SPS

### 4.3 The cylinder

The cylinder geometry with a smooth surface causes the wind to grow very turbulent in the downwind zone with high wind speeds, reaching 10-25 m/s. The cylinder, as an obstacle to the wind, does not provide a sheltered zone from the wind. The wind flow separates very early, which causes a strong suction after the flow separation, as well as high wind speeds on the sides of the geometry.

The cylinder half-covered in the 2x2 m dimples can slightly reduce the surface wind suction on the object. The separation of the wind flow moves towards the windward side of the cylinder, which consequently straightens the flow downwind, creating a wind-sheltered zone behind the object. The drag force is decreased by 6.7%. The 4x4 m windward side-variant induces the formation of downwind suction zones. The wind swirls with the speed of 5-20 m/s form on the leeward side of the object.

After the adaptive envelope with the dimensions of one adaptive element of 2x2 meters is applied on the whole surface of the cylinder, the influence on the wind flow pattern is very distinct. Although symmetrical wind swirls form on the leeward side, the wind speed is reduced to 0-5 m/s, rising again in the center of the swirl. The zone of wind suction on the sides is reduced. The drag force is decreased by 8.2%. After the application of 4x4 m dimples on the whole surface of the cylinder, the wind flow is straightened downwind. The zone of the strong suction (around  $-400 \text{ m}^2/\text{s}^2$ ), is further reduced.

Even though the surface suction and the drag force rise after the application of the dimpled adaptive envelope, the wind flow is undoubtedly calmer downwind.

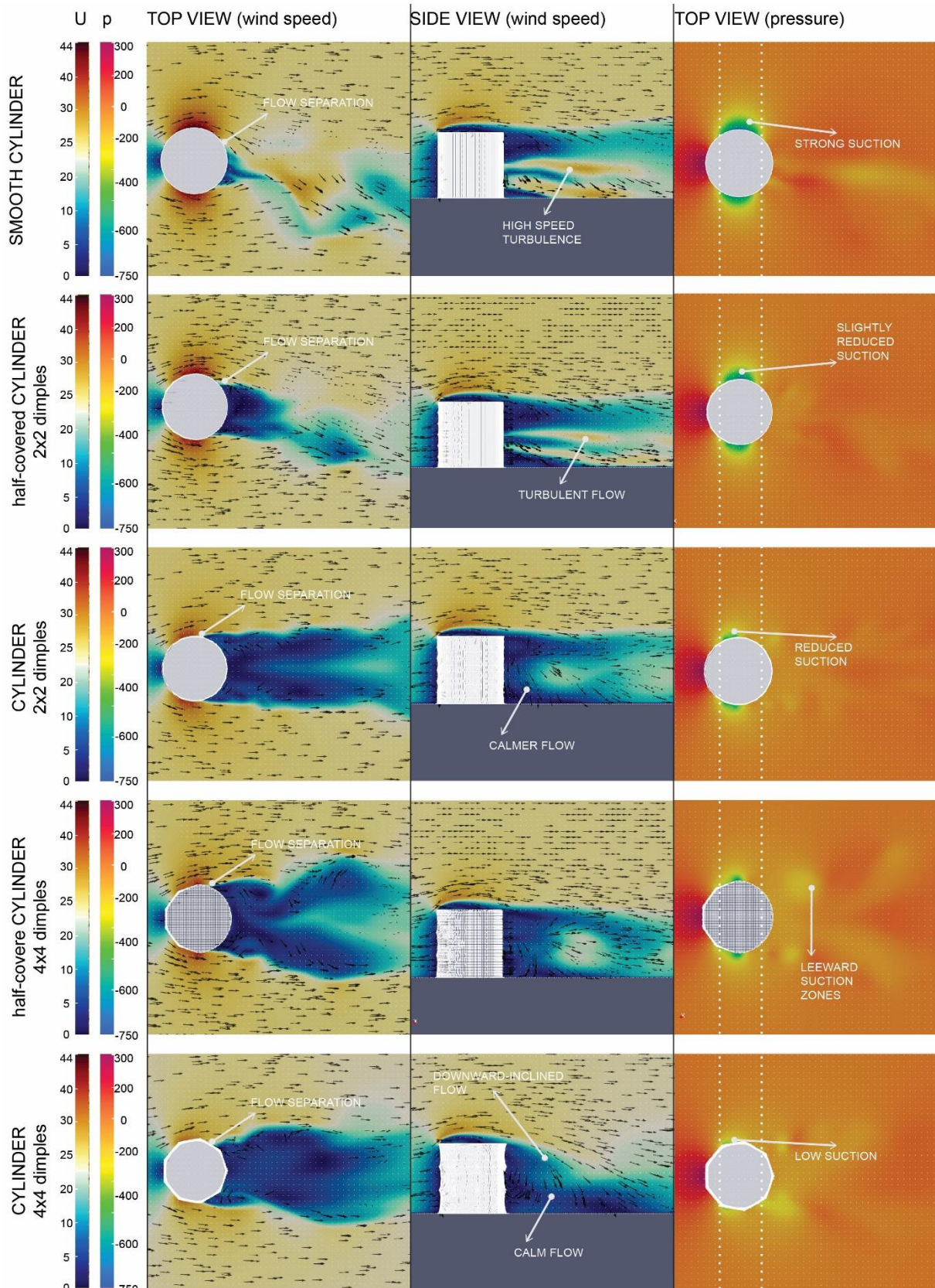


Fig. 6: The cylinder with and without the applied adaptive elements

SSP

#### 4.4 The cube rotated 45° towards the flow

The wind flow is due to the edgy geometry of the cube, separated on the side edges. The long downwind zone, with symmetrical swirls, is induced by the smooth-surface variant.

The cube with the 2x2 m dimpled surface, applied on the side of the wind approach, contributes to reducing the wind speed to 0-10 m/s. The wind suction on the leeward side is diffused and slightly reduced. The application of the adaptive envelope on the whole surface of the cube surprisingly causes a significant, 28.4% decrease of the drag force. The high-speed wind is downward-inclined early downwind. The width of the leeward-side wind-covered zone is reduced. Leeward side high-pressure zones form closer to the tested object.

With the 4x4 m dimples applied on the windward side, the symmetrical wind swirls are slightly calmer. The drag force increases with the more distinct spikes caused by the wind, acting on the adaptive envelope. The adaptive envelope fully covering the 45-degrees-rotated cube causes the wind flow to incline downward quite early downwind. The wind-shielded zone is narrow, compared to the half-covered variant. The 25% decrease of drag force can be achieved when the dimpled surface covers the whole cube, in spite of the spiky geometry.

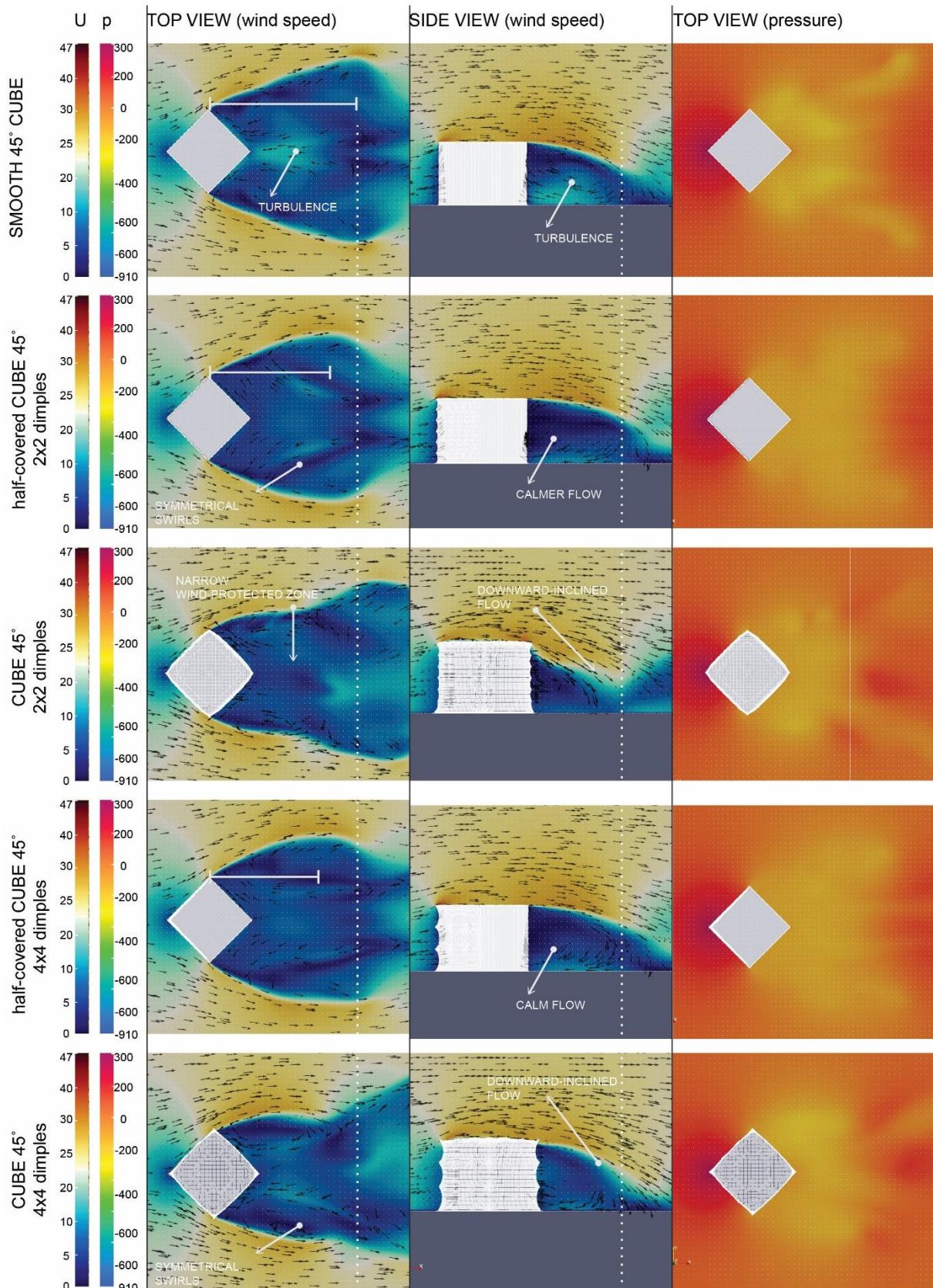


Fig. 7: The 45-degrees rotated cube with and without the applied adaptive elements

SSP



## 5 Conclusion

As was demonstrated by this research, the wind, through the local passive shape change of building envelopes, influences the flow pattern and suction zones around buildings, as well as the drag force and surface wind pressure. The designed adaptive module, exposed to the wind force, bends under this load, creating a dimpled building surface. The bending is directly dependent on the wind pressure magnitude and is reversible due to the tensegrity-membrane geometry. The simulations of the lightweight wind-adaptive building envelope in high, 24 m/s wind speed were performed for three building shape variants. Smooth building envelopes, as well as buildings fully covered or half-covered in adaptive envelopes, were reciprocally compared. Two sizes of adaptive modules were tested, and the results were evaluated from two aspects: the building's surface wind pressure and drag force reduction, as well as the character of the wind pressure and the wind flow pattern around the tested shapes.

The results show that the global shape of the building influences the ultimate effect the adaptive skin has on the wind. A reduction of drag force of 6.3% and 9.4% compared to the smooth variant can be achieved when a 2x2 m and 4x4 m (respectively) adaptive envelope covers the whole cube-shaped building. Juxtaposed to the smooth-surface cylinder, a 6.7% reduction of drag force can be achieved on a cylindrically-shaped building, half-covered with a 2x2 m adaptive envelope. The drag force can be decreased by 8.2% when the 2x2 m adaptive envelope fully covers the cylinder. A notable reduction of the drag force is observed when the 45-degrees rotated cube is fully covered in a 2x2 m adaptive envelope (28.4% reduction), as well as for the 4x4 m variant (25% reduction). Despite the decrease of the surface wind suction is not confirmed, it is assumed, that the extreme increase can be the result of the calculation extremities. This issue will be addressed in further research. The observations of the wind flow pattern confirm that the designed wind-adaptive envelope can have a strong influence on the downwind zone and create an area; shadowed from the wind (this is valid for all tested shapes).

## Acknowledgements

This research was funded by the Grant Agency of the Slovak Republic. The project numbers are VEGA 1/0674/18 and VEGA 1/0129/20.

## References

- [1] J. P. den Hartog, A. Koutamanis, and P. G. Luscuere, "Possibilities and limitations of CFD simulation for indoor climate analysis," in *Fifth Design and Decision Support Systems in Architecture and Urban Planning - Part one: Architecture Proceedings*, 2000, pp. 152–167.
- [2] J.-Y. Tsou, "Applying computational fluid dynamics to architectural design development," in *Proceedings of The Third Conference on Computer Aided Architectural Design Research in Asia*, 1998, pp. 133–142.
- [3] F. Moukalled, L. Mangani, and M. Darwish, *Fluid Mechanics and Its Applications*, vol. 113. Springer, 2016.
- [4] D. H. J. Chung and L. C. Malone-lee, "Computational Fluid Dynamics for urban design," in *New Frontiers: Proceedings of the 15th International Conference on Computer-Aided Architectural Design Research in Asia CAADRRIA 2010*, 2010, pp. 357–366.

- [5] A. Giacchetti, G. Bartoli, and C. Mannini, "Wind Effects on Permeable Tall Building Envelopes: Issues and Potentialities," *CTBUH Journal*, pp. 20–27, 2019.
- [6] T. J. Scanlon, "A NUMERICAL ANALYSIS OF FLOW AND DISPERSION AROUND A CUBE Thomas," *A Numer. Anal. FLOW Dispers. AROUND A CUBE Thomas*, no. 1977, 1991.
- [7] C. Yuan *et al.*, "Multilayer urban canopy modelling and mapping for traffic pollutant dispersion at high density urban areas," *Sci. Total Environ.*, vol. 647, pp. 255–267, Jan. 2019.
- [8] S. Sanquer, G. Caniot, and S. Bandhare, "Wind assessment in urban area with cfd tools application to natural ventilation potential and outdoor pedestrian comfort," *14th Int. Conf. IBPSA - Build. Simul. 2015, BS 2015, Conf. Proc.*, pp. 1684–1691, 2015.
- [9] L. Lignarolo, C. Lelieveld, and P. Teuffel, "Shape morphing wind-responsive facade systems realized with smart materials," in *Proceedings of the Adaptive Architecture Conference*, 2011, no. March, pp. 1–14.
- [10] L. Kabošová, "The search for an optimal architectural shape using wind performance analysis," *IOP Conf. Ser. Mater. Sci. Eng.*, vol. 566, no. 1, pp. 1–5, 2019.
- [11] K. Kuismanen, "Climate-conscious architecture: Design and wind testing method for climates in change," University of Oulu, 2008.
- [12] W. Janssen, B. Blocken, and T. Van Hooff, "Use of Cfd Simulations to Improve the Pedestrian Wind Comfort Around a High-Rise Building in a Complex Urban Area," in *13th Conference of International Building Performance Simulation Association, Chambéry, France, August 26-28, 2013*, pp. 1918–1925.
- [13] R. A. M. Castro, "Wind analysis in the early design stage: An empirical study of wind visualisation techniques for architects," 2015.
- [14] A. Chronis, A. Dubor, E. Cabay, and M. S. Roudsari, "Integration of CFD in computational design: An evaluation of the current state of the art," in *Proceedings of the 35th International Conference eCAADe: ShoCK! Sharing of Computable Knowledge!*, 2017, pp. 601–610.
- [15] S. Stankovic and A. Setrakian, "Air Flow Modelling - 1."
- [16] R. A. Moya Castro, D. Prohasky, S. Watkins, Y. Ding, J. Burry, and M. Burry, "Aerodynamic strategy applied in an urban shelter design - Simulation and analysis of aerodynamic phenomena in an urban context," *eCAADe 2014 Fusion - data Integr. its best*, vol. 1, pp. 137–144, 2014.
- [17] I. Olekšáková, O. Hubová, and L. Konečná, "Influence of nearby structure on the wind flow around the cube structure," *Rocz. Inz. Bud.*, vol. 15, pp. 29–36, 2015.
- [18] Eurocode 1, *Actions on structures, Part 1-4: general actions. Wind actions*. Brussels, 2010.
- [19] S. O. Hansen, "Wind loading design codes," in *Fifty years of wind engineering: Prestige lectures from the sixth European and African conferece on wind engineering*, 2012, pp. 35–68.
- [20] G. Senatore, P. Duffour, and P. Winslow, "Energy and Cost Assessment of Adaptive Structures: Case Studies," *J. Struct. Eng. (United States)*, vol. 144, no. 8, pp. 1–23, 2018.
- [21] R. Motro, *Tensegrity: Structural Systems for the Future*, 1st ed. Butterworth-Heinemann, 2003.

## Indoor and Outdoor Measurements of Particulate Matter Concentrations: A Case Study Košice-Sever, Slovakia

Eva Krídlová Burdová<sup>1</sup>, Silvia Vilčeková<sup>1</sup> and Peter Kapalo<sup>2</sup>

Technical University of Kosice

Civil Engineering Faculty, Institute of Building and Environmental Engineering

e-mail: eva.kridlova.burdova@tuke.sk, silvia.vilcekova@tuke.sk, peter.kapalo@tuke.sk

### Abstract

An occurrence of indoor particulate matters largely depends on outdoor pollution and its transportation indoors as well as on the presence of indoor pollution sources. Pollutants can flow from outdoor to indoor or indoor to outdoor under various conditions e.g. contribution of indoor pollutants to outdoor (in rural location with biomass fuel used for cooking) or outdoor to indoor in urban locations. This study aims to carry out an experimental investigation of particulate matter (PM) concentrations, temperature, humidity and air velocity during three days in winter season in Košice-Sever, Slovakia. Values of outdoor PM<sub>10</sub> concentrations ranged from 12.58 µg/m<sup>3</sup> to 6,627.51 µg/m<sup>3</sup>. Extremely high concentrations of PM<sub>10</sub> were found near the traffic. Outdoor mean value of PM<sub>2.5</sub> (21.82 µg/m<sup>3</sup>) did not exceed a permissible value of 25 µg/m<sup>3</sup>. Overloads by PM<sub>10</sub> concentrations denote almost 108% and 2,270%. The indoor/outdoor (I/O) ratio was <1 for all fractions of particulate matters.

**Key words:** outdoor environment, indoor environment, particulate matters, PM<sub>10</sub>, PM<sub>2.5</sub>, I/O ratio

## 1 Introduction

Outdoor air pollution is a complex mixture originating from different natural and anthropogenic sources and consists of particles, chemicals and biogenic substances with well-known health effects. Although outdoor air is an important source of indoor particulate matters (PM), additional sources must be considered, leading to quite different compositions of particle mass and particle size distributions in the indoor environment [1]. Concentrations of PM tend to exceed the limit values in many countries across the world [2]. Airborne PM is considered to be a main indicator of outdoor and indoor air quality [3]. Exposure to PM has been associated with negative health effects [4]. Health problems have been linked to long-term and short-term particle exposure. Long-term exposures, experienced by people living for many years in areas with high particle levels, have been associated with problems such as reduced lung function and the development of chronic bronchitis and even premature death. Short-term exposures to particles (hours or days) can aggravate lung disease, causing asthma

attacks and acute bronchitis, and may also increase susceptibility to respiratory infections. In people with heart disease, short-term exposures have been linked to heart attacks and arrhythmias [5]. The health and comfort of building users is an important aspect determining the quality of their life. Increase in air contamination by particulate matters and their negative impacts on human health have resulted in efforts to monitor and identify them [6]. According a European Environmental Agency report [7], PM belongs to major air pollutants and may originate from an outdoor environment or be generated in an indoor environment. Important sources of PM are fuels (power generation, heating, transport); industrial and agricultural processes; waste incineration; tyres, brakes, and road wear; other types of anthropogenic dust or natural sources, such as volcanic ash, sea salts, suspended crustal materials, spores, bacteria, pollen, etc. Results in this study [8] confirm that without other sources of particles, human activity is an important factor accounting for elevated indoor levels of coarse particles and those finer indoor fractions could be significantly influenced by concentrations of ambient particles, which originate in traffic-related combustion processes. Studies have shown a strong association between exposure to indoor PM and effect on children health [9]. In the assessment of indoor microclimate of heritage buildings, the general goal was to evaluate and improve users' comfort [10]. Nowadays, indoor environmental quality (IEQ) is growing as a new and very useful index of the building quality [11]. One of the key challenges noted in the sustainable development goals for good health and well-being is both ambient and household air pollution [12]. One study [13] states that over the last twenty years or so, considerable efforts have been made to clarify the relationship between airborne particulate matter (PM) and human health, and a number of excellent accounts of this relationship are now available. However, further long-term monitoring of air pollutant concentrations within cities is crucial for environmental management and public health policies in order to promote sustainable cities [14]. Even now, house heating and industry, as well as emissions from road traffic, are some of the primary sources of PM in the atmosphere in urban areas [15]. Exposure to PM<sub>2.5</sub> of outdoor origin, which leads to millions of global premature deaths annually, occurs mainly indoors [16]. To effectively control indoor PM<sub>2.5</sub> (particulate matter with diameter less than 2.5 µm) in residential buildings; it is essential to differentiate between the contributions of outdoor PM<sub>2.5</sub> infiltration and indoor PM<sub>2.5</sub> emissions to the total indoor exposure [17]. Air pollution is considered as the greatest environmental risk to health in 2019 according to the WHO [18]. Exposure to particulate matters has been associated with higher rate of morbidity and mortality in urban areas and the World Health Organization's International Agency for Research on Cancer (IARC) has classified PM component of air pollution as a carcinogen [19]. The health and comfort of building users is an important aspect in determining their quality of life [6]. If the Indoor/Outdoor (I/O) ratio is less than 1, the amount of particulate matter in the outdoor environment is greater. This means that outdoor air is predominantly the source of particulate matter indoors. The results of I/O ratios in many studies [20-22] demonstrated that the concentration of indoor air pollutants in different spaces was not necessarily influenced by outdoor air pollutants. The main contribution of this research is its pointing out differences in the occurrence of PM concentrations in the outdoor and indoor environment, confirming their most important sources, mapping out the selected location and pointing out the need to propose measures to reduce concentrations to the lowest possible level. This study also investigates the relationship between various fractions of particulate matter (PM<sub>0.5</sub>, PM<sub>1</sub>, PM<sub>2.5</sub>, PM<sub>5</sub> and PM<sub>10</sub>) in outdoor and indoor environments. The ratio of I/O particle

concentration is also presented.

## 2 Materials and Methods

The city part of Košice-Sever, Slovakia was selected for the measurement of particulate matter (PM) concentrations, temperature, relative humidity and air velocity. There are 16 measurement points shown on map (Fig. 1). Of the measurement points, 14 were located outdoors and two were located indoors. Košice-Sever is located in the north part of the city of Kosice. It is one of the more populous boroughs of the city as well as the largest of all 22 boroughs, which contributes to its low overall population density. Along with the neighbouring borough of Kavečany, Košice-Sever is the most popular recreational area in the city, frequented not only by locals but also visitors. Outdoor measurements were performed at 14 points to show the level and distribution of the PM occurrence in the selected location near traffic. Indoor measurements were carried out in a flat on the second floor of an eight floor residential building at Watsonova Street no. 55 (measurement point 15) and in office room at Letná Street no. 9 (measurement point 16). There is a four-lane road and a two-lane road with heavy traffic along Watsonova Street and Letná Street, respectively. For the investigation, a living room with floor area of 20.7 m<sup>2</sup> was selected. The floor was covered with laminate flooring. Walls were covered with plaster and paint. The living room was equipped with a sofa, small conference table, two chairs, a cabinet with a gramophone and bookshelves with books and vinyls. The office room was equipped with a table with four chairs, an office desk with a computer and two shelves. The floor was covered with carpet. Walls were covered with plaster and paint. The measurements of the mass concentrations of PM for fractions of 0.5, 1.0, 2.5, 5.0 and 10.0 micrometres were carried out using a HANDHELD 3016 Airborne Particle Counter, Lighthouse Worldwide Solutions, Inc., USA (Table 1). This instrument detects minimum particle size of 0.3 microns with a flow of 0.1 CFM and a touch-screen interface. The instrument uses a laser-diode light source and collection optics for particle detection. Particles scatter light from the laser diode, and the optics collect and focus the light onto a photo diode that converts the bursts of light into electrical pulses. Pulse height is a measure of particle size. Pulses are counted and their amplitude is measured for particle sizing. Results are displayed as particle counts in the specified size channel. Count data is displayed as a differential count. The airborne particle counter was located in the middle of the room, at the level of the breathing zone of a sitting person, which is 1.1 m above the floor. The ambient concentration of PM was measured at 14 measuring points with a three-minute measurement. Indoor PM concentrations were recorded every minute for one hour. An outdoor airborne particle counter was located on the balcony of a flat on the second floor. PM concentrations were recorded every minute for 24 hours. Physical parameters such as air temperature, relative humidity and air velocity were monitored using a multifunctional measuring device TESTO 435-4 with a probe intended for IAQ measurement, Testo, Inc., Germany. This device was located in the middle of the room at the level of the breathing zone of a sitting person (i.e., 1.1 m above the floor). These physical parameters in the outdoor air were recorded every ten minutes for 24 hours. The measurement device TESTO 435-4 was also located on the balcony of the flat of residential building in Watsonova Street. The measurements were carried out during three consecutive days in January 2020. On the first day, outdoor measurements in 14 points and indoor measurement in a flat at Watsonova Street

were carried out. On the second day, the measurement in an office room at Letná Street was carried out. On the third day, 24-hour measurement on the balcony of a flat at Watsonova Street was carried out. The measurement location is shown in the figure below (Figure 1).

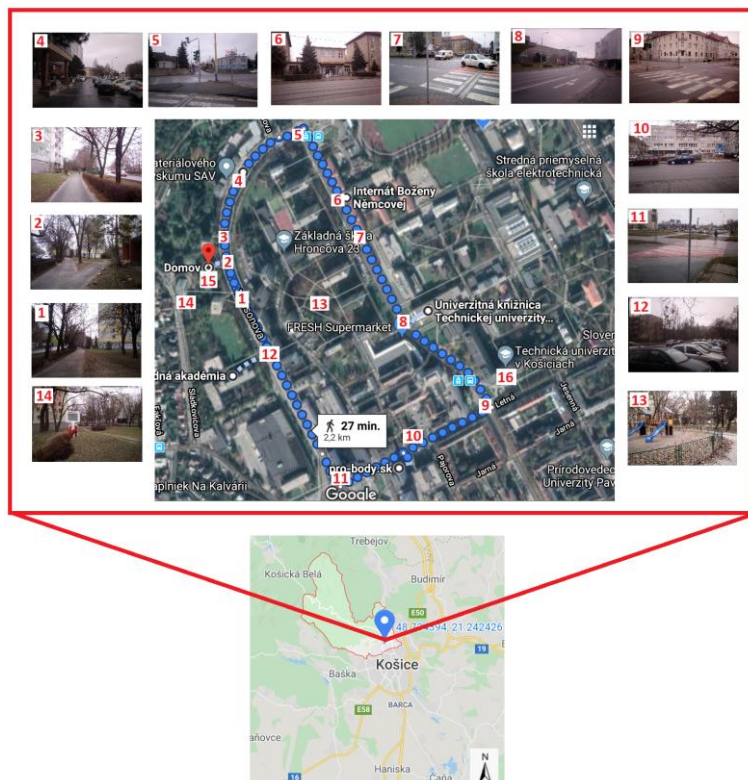


Figure 1: Locality of measurements in Košice-Sever

Table 1: Devices used for measurement of IEQ parameters

Instrument	Information
HANDHELD 3016 IAQ HANDHELD	Size range: 0.3–10 $\mu\text{m}$ , Counting efficiency: 50% at 0.3 $\mu\text{m}$ ;100% for particles > 0.45 $\mu\text{m}$ (per ISO 21501-4)
Multifunctional device Testo 435-4	Air temperature—accuracy: $\pm 0.3^\circ\text{C}$ , measurement range: 0 to $+50^\circ\text{C}$
	Relative humidity—accuracy: $\pm 2\%$ RH, measurement range: 0%–100% RH
	Air velocity—accuracy: $\pm(0.03 \text{ m/s} + 4\% \text{ of mv})$ , range: 0 to $+20 \text{ m/s}$

### 3 Results

Results of indoor and outdoor concentrations of particulate matters  $\text{PM}_{0.5-10}$  and indoor/outdoor ratio are presented in Table 2. The indoor-to-outdoor (I/O) ratios were calculated for  $\text{PM}_{0.5-10}$ .  $I/O_w$  are ratio between indoor concentration on Watsonova Street and outdoor concentration and  $I/O_L$  is ratio between indoor concentration on Letná Street and outdoor concentration.

Table 2: Result of measurements

		Indoor		Outdoor	I/O <sub>w</sub>	I/O <sub>L</sub>
		Watsonova Street	Letná Street			
PM <sub>0.5</sub> [ $\mu\text{g}/\text{m}^3$ ]	min	4.49	6.23	4.46	0.564	0.958
	mean	4.71	8.00	8.35		
	max	5.12	11.06	11.83		
	SD	0.14	1.24	1.17		
PM <sub>1.0</sub> [ $\mu\text{g}/\text{m}^3$ ]	min	7.37	10.99	7.20	0.536	0.978
	mean	7.82	14.26	14.58		
	max	8.75	20.34	20.72		
	SD	0.33	2.51	2.20		
PM <sub>2.5</sub> [ $\mu\text{g}/\text{m}^3$ ]	min	9.00	13.83	8.73	0.447	0.802
	mean	9.75	17.49	21.82		
	max	11.04	24.05	75.69		
	SD	0.53	2.73	10.38		
PM <sub>5.0</sub> [ $\mu\text{g}/\text{m}^3$ ]	min	13.59	19.21	12.58	0.158	0.301
	mean	15.45	29.45	97.80		
	max	18.15	76.34	1,141.67		
	SD	1.14	8.18	179.60		
PM <sub>10</sub> [ $\mu\text{g}/\text{m}^3$ ]	min	17.27	26.85	16.10	0.080	0.190
	mean	20.90	49.70	262.07		
	max	25.87	195.04	6,627.51		
	SD	2.40	27.28	781.61		

Indoor-outdoor ratios were below 1 for all fractions of particulate matters. Exceeded concentrations of PM in the outdoor environment were found near traffic in the investigated area. It can be stated that the main indoor source of PM concentrations is outdoor environment.

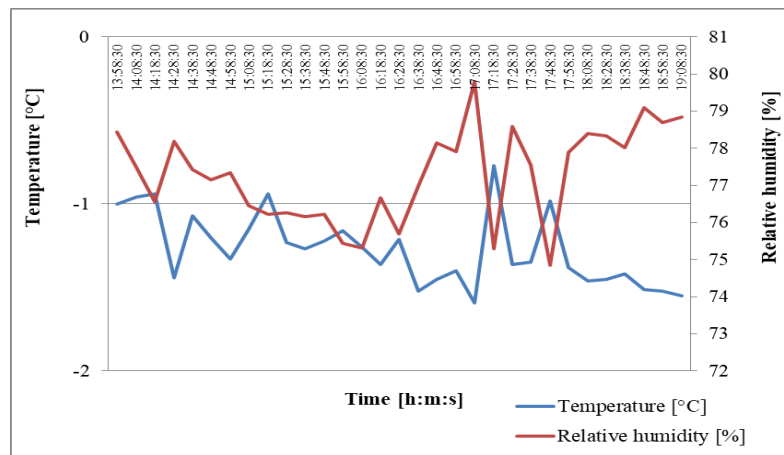


Figure 2: Courses of outdoor air temperature and relative humidity

The minimum outdoor air temperature was  $-1.6^{\circ}\text{C}$ , maximum was  $-0.8^{\circ}\text{C}$ , with a mean value of  $-1.3^{\circ}\text{C}$ . Outdoor air humidity ranged from 74.8% to 82.1%, with a mean value of 77.4%.

The outdoor air velocity ranged from 0 m/s to 1.37 m/s, with a mean value of 0.32 m/s. In the figure Fig. 2, there are illustrated courses of outdoor air temperature and relative humidity.

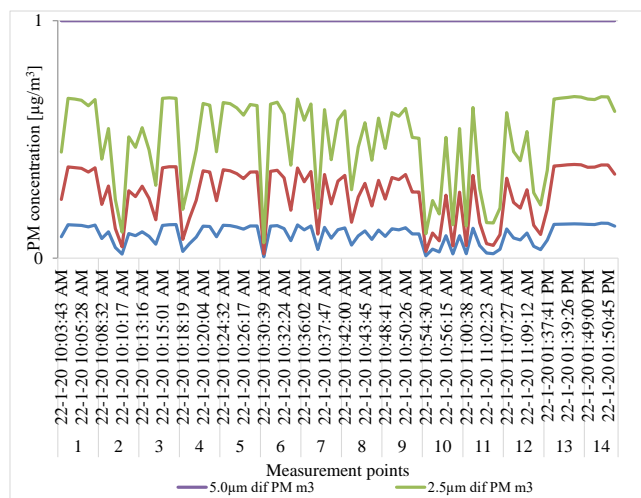


Figure 3: Courses of outdoor PM concentrations in the measured area

Fig. 3 depicts courses of outdoor PM concentrations for fractions from 0.5 to 10 micrometres for all outdoor measurement points. Values of outdoor PM<sub>10</sub> concentrations ranged from 12.58 µg/m<sup>3</sup> to 6,627 µg/m<sup>3</sup>. Mean values of PM<sub>10</sub> and PM<sub>2.5</sub> were compared with the permissible values of 50 µg/m<sup>3</sup> and 25 µg/m<sup>3</sup> according to Decree of the Ministry of Environment of the Slovak Republic No. 244/2016 [24]. The mean value of PM<sub>10</sub> (262.07 µg/m<sup>3</sup>) was compared with the permissible value of 50 µg/m<sup>3</sup>. This permissible value was exceeded in 11 of the 14 external measurement points (1, 2, 4, 6-11, 13, 14). Only in measurement points 2, 5 and 12 the mean values of PM<sub>10</sub> were not exceeded. The mean value of PM<sub>2.5</sub> (21.82 µg/m<sup>3</sup>) compared with the permissible value of 25 µg/m<sup>3</sup> was not exceeded. The minimum indoor air temperature in flat at Watsonova Street was 22°C, maximum was 23.7°C, with a mean value of 23.2°C. Indoor air humidity ranged from 32.9% to 36.1%, with a mean value of 33.7%. Fig. 4 illustrates courses of indoor air temperature and relative humidity. Indoor air velocity ranged from 0 m/s to 0.01 m/s, with a mean value of 0.01 m/s.

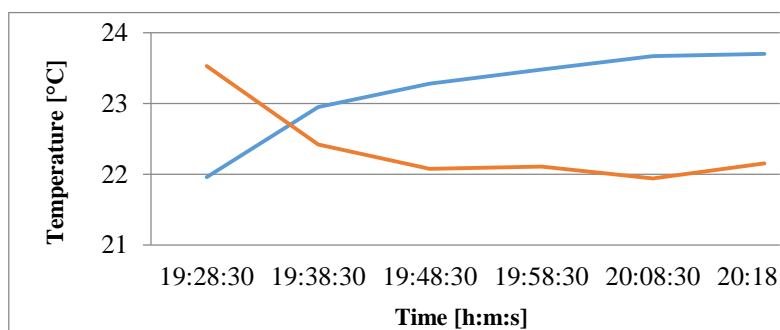


Figure 4: Courses of indoor air temperature and relative humidity in flat at Watsonova Street  
 Fig. 5 depicts courses of indoor PM concentrations for fractions from 0.5 to 10 micrometres.



Values of indoor PM<sub>10</sub> concentrations ranged from 17.27 to 25.87  $\mu\text{g}/\text{m}^3$ . The mean value of PM<sub>10</sub> (20.9  $\mu\text{g}/\text{m}^3$ ) was compared with the permissible value of 50  $\mu\text{g}/\text{m}^3$  according to Decree of the Ministry of Health of the Slovak Republic No. 210/2016 [24]. This mean value was not exceeded.

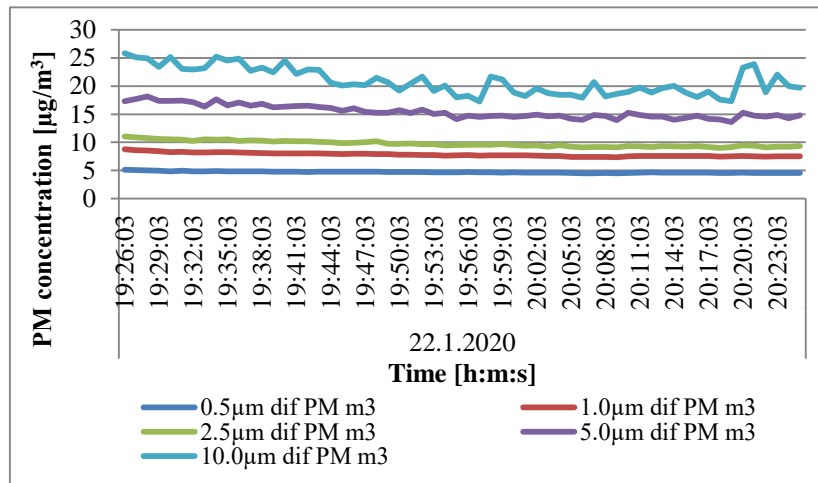


Figure 5: Courses of indoor PM concentrations in flat at Watsonova Street

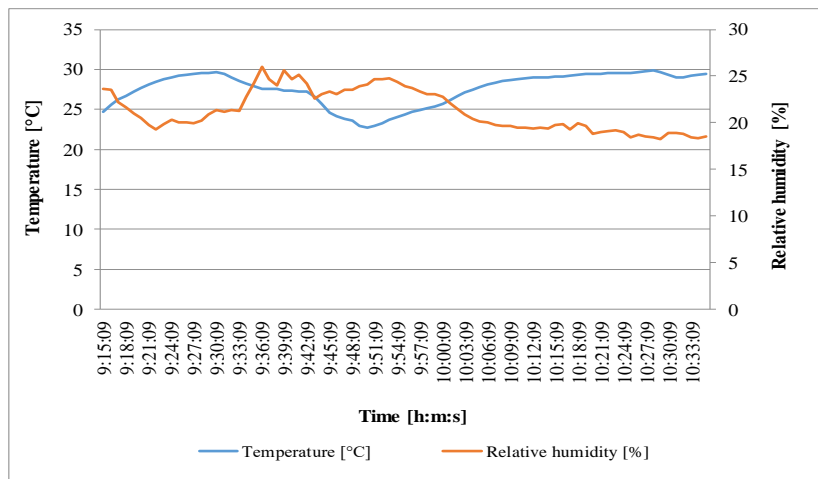


Figure 6: Courses of indoor air temperature and relative humidity in office room at Letná Street

The minimum indoor air temperature in an office room at Letná 9 street was 22.8°C, maximum was 29.8°C, with a mean value of 27.6°C. Indoor air humidity ranged from 18.3% to 26.0%, with a mean value of 21.3%. Fig. 6 illustrates courses of indoor air temperature and relative humidity. The indoor air velocity ranged from 0 m/s to 0.23 m/s, with a mean value 0.03 m/s. Fig. 7 depicts courses of indoor PM concentrations for fractions from 0.5 to 10 micrometres. Values of indoor PM<sub>10</sub> concentrations ranged from 13.83 to 24.05  $\mu\text{g}/\text{m}^3$ . The mean value of PM<sub>2.5</sub> (17.49  $\mu\text{g}/\text{m}^3$ ) compared with the permissible value of 25  $\mu\text{g}/\text{m}^3$  according to the WHO standard was not exceeded. Values of indoor PM<sub>10</sub> concentrations ranged from 26.85 to 195.04  $\mu\text{g}/\text{m}^3$ . The mean value of PM<sub>10</sub> (49.7  $\mu\text{g}/\text{m}^3$ ) compared with

permissible value of  $50 \mu\text{g}/\text{m}^3$  according to Decree [24] was not exceeded.

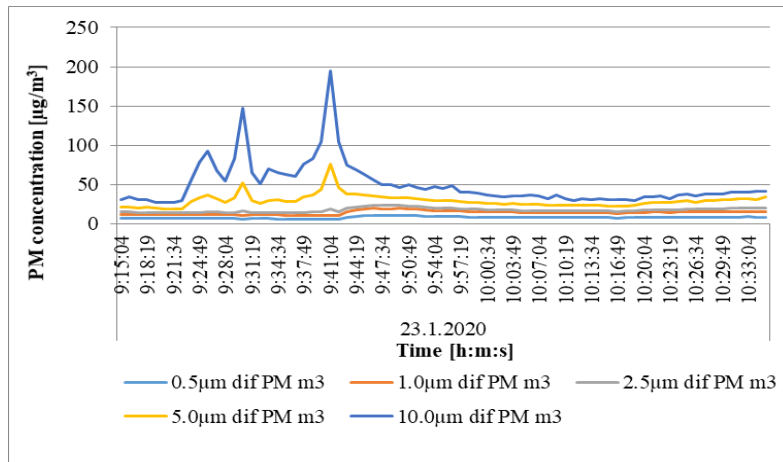


Figure 7: Courses of indoor PM concentrations in office room at Letná Street

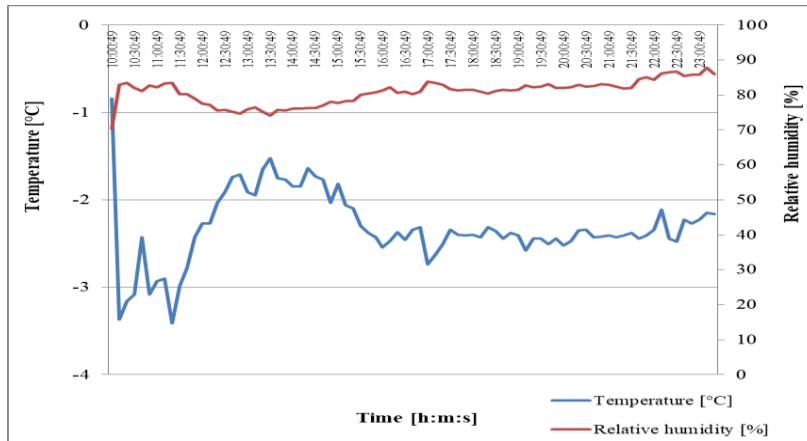


Figure 8: Courses of outdoor air temperature and relative humidity

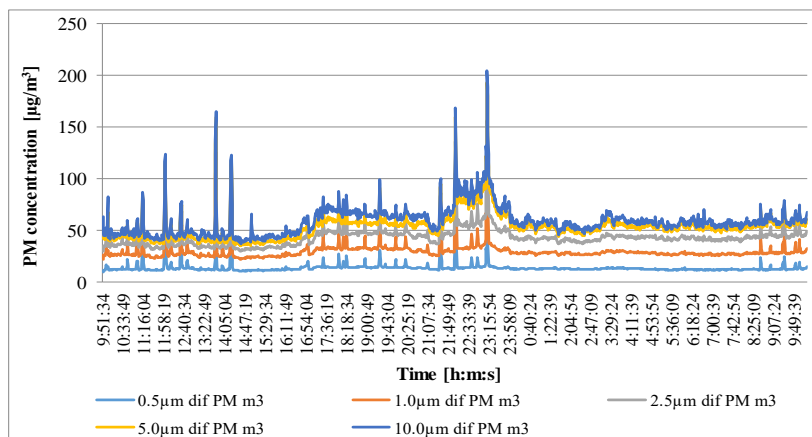


Figure 9: Courses of outdoor PM concentrations at Watsonova Street

Minimum outdoor air temperature was  $-2.5^{\circ}\text{C}$ , maximum was  $-2.1^{\circ}\text{C}$ , with a mean value of -

1.6°C. Outdoor air humidity ranged from 79.9% to 87.7%, with a mean value of 83.6%. The outdoor air velocity ranged from 0 m/s to 0.38 m/s, with a mean value of 0.04 m/s. Fig. 8 illustrates courses of outdoor air temperature and relative humidity. Fig. 9 depicts courses of outdoor  $PM_{0.5-10}$  for all outdoor measurement points. Values of outdoor  $PM_{10}$  concentrations ranged from 37.26 to 204.9  $\mu\text{g}/\text{m}^3$ . The mean values of  $PM_{10}$  and  $PM_{2.5}$  were compared with the permissible values according to Decree No. 244/2016 [23]. The mean value of  $PM_{10}$  (56.02  $\mu\text{g}/\text{m}^3$ ) exceeded the permissible value of 50  $\mu\text{g}/\text{m}^3$ . Values of outdoor  $PM_{2.5}$  concentrations ranged from 30.1 to 156.02  $\mu\text{g}/\text{m}^3$ . The Mean value of  $PM_{2.5}$  (43.76  $\mu\text{g}/\text{m}^3$ ) did not exceed permissible value of 25  $\mu\text{g}/\text{m}^3$ . Fig. 10 depicts particulate matter distributions of  $PM_{0.5-10}$  concentrations in the measured area. The bubble size on the graph represents the size of  $PM_{0.5-10}$  concentration. The highest concentrations of PM were measured mainly at large intersections and also in the vicinity of car parks.

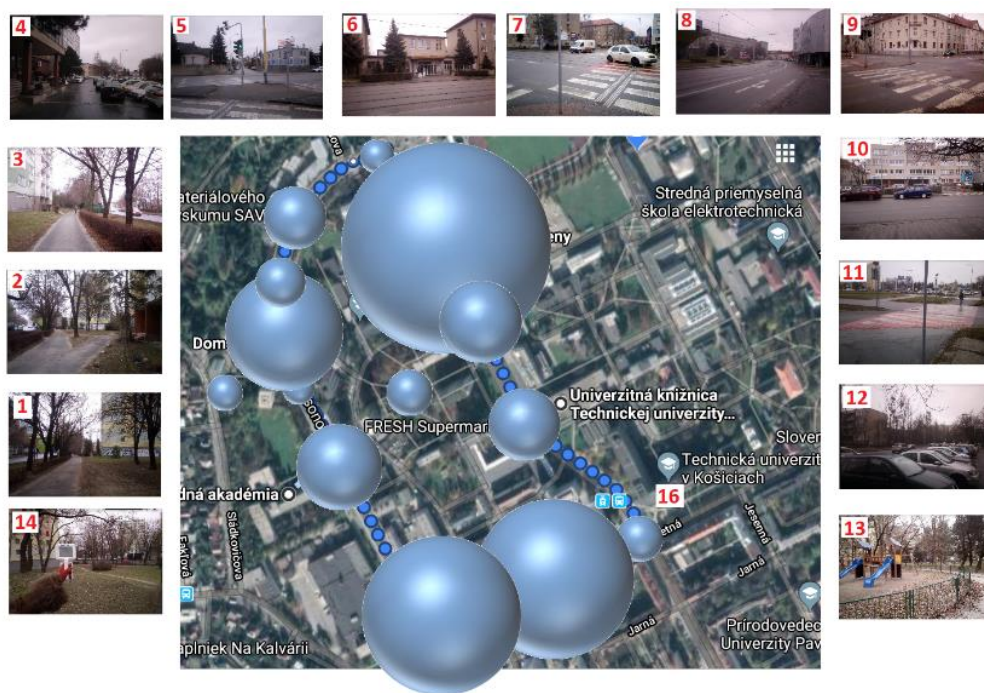


Figure 10: Distributions of  $PM_{0.5-10}$  concentrations in the measured area

## 4 Discussion

Winter air conditions and conditions in other seasons can be drastically different from each other, with sources of particulates differing significantly, as well as air movements differing, air humidity, quality as well. The degree of photochemical and vegetation contributions is also minimal. Winter season was specially to eliminate contributions that the vegetation would give, or photochemical reactions, or other summer or seasonal sources. Winter is season when residences do not have open windows as frequently than in other season, which drastically minimizes air circulation and particulate movements as well. In the literature, there exist many studies concerning the relationship between concentrations of particulate matters

in outdoor and indoor air of buildings expressed through ratio of indoor-to-outdoor (I/O) particle concentration. The results of a study [25] that monitored indoor and outdoor concentrations in passive low energy consumption residential buildings confirmed that the indoor  $PM_{2.5}$  and  $PM_{10}$  mass concentrations were decreased with a decreasing of outdoor PM concentrations. Study [26] that measured mass concentration of particulate matters and the I/O ratios of  $PM_{2.5}$  showed that keeping windows closed provides partial protection to traffic-related  $PM_{2.5}$ . In study [4], the high indoor-to outdoor concentration (I/O) ratios calculated in schools for  $PM_{2.5}$  (1.8) and  $PM_{10}$  (2.1) suggest that a substantial fraction of particles was generated by indoor sources. Another study [27] aimed to investigate the variation in the transportation of PM from outdoor to indoor space under mechanical ventilation in two similar residential buildings. Reductions of PM concentration from external values were 56% ( $PM_{10}$ ), 49% ( $PM_{2.5}$ ) and 37% ( $PM_1$ ). PM levels were also determined in 15 households in Colorado. Measured indoor  $PM_{2.5}$  and  $PM_{10}$  levels were 8.1 and 15.4  $\mu\text{g}/\text{m}^3$ . The I/O ratio of  $PM_{2.5}$  was 1.6 and was not statistically, significantly different across the seasons [28]. Relationship between indoor and outdoor levels for particulate matter in naturally ventilated homes in study [29] showed that in homes without any indoor sources and where human activity is low,  $PM_{10}$  ratios amount to approximately 0.7. In our study, measurement of outdoor PM points out that the occurrence of PM significantly depends on the measuring points as it ranged from 12.58  $\mu\text{g}/\text{m}^3$  (measurement point 14) to 6,627.51  $\mu\text{g}/\text{m}^3$  (measurement point 6). The I/O ratio was  $<1$  for all fractions of particulate matters. It is obvious that outdoor air is a significant source of pollution by particulate matters.

## 5 Conclusion

The excessive occurrence of  $PM_{2.5}$  and  $PM_{10}$  concentrations was not observed in the indoor environment of the flat as well as the office building. The permissible value for indoor  $PM_{10}$  concentration (50  $\mu\text{g}/\text{m}^3$ ) was not exceeded. According to the measurement of particulate matters in an outdoor environment, we can state that the occurrence significantly depends on the pollution sources. Excessive concentrations of  $PM_{10}$  were found mainly near traffic. Mean values were exceeded in 11 of the 14 external measurement points. Overloads of  $PM_{10}$  concentrations denote almost 108% and 2,270%. Mean value of  $PM_{2.5}$  (21.82  $\mu\text{g}/\text{m}^3$ ) did not exceed the permissible value of 25  $\mu\text{g}/\text{m}^3$ . Our future research work will focus on monitoring of PM concentrations in a residential area during each period of the year, in-depth investigation of the occurrence of indoor PM depending on the surrounding environment and indoor sources, and assessing the sustainability of the buildings.

## Acknowledgements

This study was financially supported by Grant Agency of Slovak Republic to support of project No. 1/0512/20.

## References

- [1] Fromme, H., Diemer, J., Dietrich, S., Cyrys, J., Heinrich, J., Lang, W., Kiranoglu, M. & Twardella, D. (2008) Chemical and morphological properties of particulate matter ( $PM_{10}$ ,  $PM_{2.5}$ ) in school classrooms and outdoor air, *Atmos Environ.* vol. 42, pp. 6597–6605.

- [2] Dedele, A. & Miskinyte, (2019) A. Seasonal and site-specific variation in particulate matter pollution in Lithuania. *Atmos Pollut Res.* vol. 10, pp. 768–775.
- [3] Karri, R.R., Heibati, B., Yusup, Y., Rafatullah, M., Mohammadyan, M. & Sahu, J.N. (2018) Modeling airborne indoor and outdoor particulate matter using genetic programming. *Sustain. Cities Soc.* vol. 43, pp. 395–405.
- [4] Faria, T., Martins, V., Correira, C., Canha, N., Diaouli, E., Manousakas, M., Eleftheriadis, K. & Almeida, S.M. (2020) Children's exposure and dose assessment to particulate matter in Lisbon. *Build Environ*, 106666.
- [5] The EPA document. Available online: <https://nepis.epa.gov/Exec/ZyPDF.cgi/P100RQ5N.PDF?Dockey=P100RQ5N.PDF> (accessed on 06 May 2020).
- [6] Vilcekova, S., Estokova, A, Kridlova Burdova, E. & Budaiova, Z. (2017) Investigation of particulate matter concentration in offices, *Fresen Environ Bull.* vol., 26(2), pp. 1225–1233.
- [7] EEA Report No 13/2017 "Air quality in Europe—2017 report" presents an updated analysis of air quality and its impacts, based on official data from more than 2,500 monitoring stations across Europe in 2015. Available online: <https://www.eea.europa.eu/publications/air-quality-in-europe-2017> (accessed on 20 January 2020).
- [8] Branis, M., Rezacova, P. & Domasova, M. (2005) The effect of outdoor air and indoor human activity on mass concentrations of PM<sub>10</sub>, PM<sub>2.5</sub>, and PM<sub>1</sub> in classroom; *Environ Res.* vol. 99, pp. 143–149.
- [9] Nunes, R.A.O., Branco, P.T.B.S., Alvim-Ferraz, M.C.M., Martings, F.G. & Sousa, S.I.V. (2015) Particulate matter in rural and urban nursery school in Portugal. *Environ Pollut.* vol. 202, pp. 7–16.
- [10] Fabbri, K. & Pretelli, M. (2014) Heritage buildings and historic microclimate without HVAC technology: Malatestiana Library in Cesene, Italy, UNESCO Memory of the World. *Energ Buildings.* vol. 76, pp. 15–31.
- [11] Catalina, T. & Iordache, V. (2012) IEQ assessment on school in the design stage. *Build Environ.* vol. 49, 2012, pp. 129–140.
- [12] Adesina, J.A., Piketh, S.J., Ohekwana, M., Burger, R., Language, B. & Mkhathswa, G. (2020) Contrasting indoor and ambient particulate matter concentrations and thermal comfort in coal and non-coal burning households at South Africa Highveld. *Sci. Total Environ.* vol. 699, pp. 134403.
- [13] Sangiorgi, G., Ferrero, L., Ferrini B.S., Lo Porto C., Perrone, M.G., Zangrando, R., Gambaro, A., Lazzati, Z. & Borzacchini, E. (2014) Indoor airborne particle sources and semi-volatile partitioning effect of outdoor fine PM in offices. *Atmos Environ.* vol. 65, pp. 205–214.
- [14] Cesar I.A., Teodoro, A.C., Torres, N. & Vivanco, V. (2019) Assessment of remote sensing data to model PM<sub>10</sub> estimation in cities with a low number of air quality stations: a case of study in Quito, Ecuador. *Environments*, vol. 6(85), pp. 1–15.
- [15] Penkała, M., Ogródnik, P. & Rogula-Kozłowska, W. (2018) Particulate matter from the road surface abrasion as a problem of non-exhaust emission control, *Environments*, vol. 5(9), pp. 1–13.
- [16] Sun, Z., Liu, C. & Zhang, Y. (2019) Evaluation of a steady-state method to estimate indoor PM<sub>2.5</sub> concentration of outdoor origin, *Build Environ.* vol. 161, 106243.
- [17] Xia, T. & Chen, C. (2019) Differentiating between indoor exposure to PM<sub>2.5</sub> of indoor and

- outdoor origin using time-resolved monitoring data. *Build Environ.* vol. 147, pp. 528–539.
- [18] WHO. Available online: <https://www.who.int/emergencies/ten-threats-to-global-health-in-2019> (accessed on 20 January 2020).
- [19] Li, H., Fang, C.H.Y., Shi, W., Gurusamy, S., Li, S., Krishnan, M.N. & George, S. (2015) Size and site dependent biological hazard potential of particulate matters collected from different heights at the vicinity of a building construction. *Toxicol Lett.* vol. 238, pp. 20–29.
- [20] Razalia, N.Y.Y., Latifb, M.T., Dominick, D., Mohamad, N., Sulaimand, F. R. & Srithawirate, T. (2015) Concentration of particulate matter, CO and CO<sub>2</sub> in selected schools in Malaysia Author links open overlay panel. *Build Environ.* vol. 87, pp. 108–116.
- [21] Braniš, M. & Šafránek, J. (2011) Characterization of coarse particulate matter in school gyms. *Environ Res.* vol. 111(4), pp. 485–491.
- [22] Goyal, D.R. & Kumar, P. (2013) Indoor–outdoor concentrations of particulate matter in nine microenvironments of a mix-use commercial building in megacity. *Air Qual Atmos Helth.* vol. 6, pp. 747–757.
- [23] Decree of the Ministry of Health of the Slovak Republic No. 259/2008 about details of the requirements for the indoor environment of buildings and the minimum requirements for lower-standard apartments and accommodation
- [24] Decree of the Ministry of Environment of the Slovak Republic No. 244/2016 of the Slovak Republic on air quality <https://www.noveaspi.sk/products/lawText/1/86985/1/2>
- [25] Wang, Z. & Yu, Z. (2017) PM<sub>2.5</sub> and ventilation in a passive residential building, *Procedia Eng.* vol. 205, pp. 2646–3653.
- [26] Sharma, R. & Balasubramanian, R. (2019) Assessment and mitigation of indoor human exposure to fine particulate matter (PM<sub>2.5</sub>) of outdoor origin in naturally ventilated residential apartments: a case study. *Atmos Environ.* vol. 212, pp. 163–171.
- [27] Wallis, S.L., Hernandey, G., Pozner, D., Birchmore, R. & Berry, T. (2019) Particulate matter in residential buildings in New Zealand: part I. Variability of particle transport into unoccupied spaces with mechanical ventilation. *Atmos Environ.* vol. X2, pp. 1–9.
- [28] Clements, N., Keady, P., Emerson, J.B., Fierer, N. & Miller, S.L. (2018) Seasonal variability of airborne particulate matter and bacterial concentrations in Colorado homes. *Atmosphere.* vol. 9(4), p. 133.
- [29] Monn, Ch., Fuchs, A., Högger, D., Junker, D., Kogelschatz, D., Roth, N. & Wanner, H.-U. (1997) Particulate matter less than 10 µm (PM<sub>10</sub>) and fine particles less than 2.5 µm (PM<sub>2.5</sub>): relationships between indoor, outdoor and personal concentrations. *Sci Total Environ.* vol. 208 (1–2), pp. 15–21.

## Effect of the Roof Slope on the Cost Variation of Residential Houses

Leopold Mbereyaho<sup>1a\*</sup>, Doris Daniella Dusabe Minani<sup>1b</sup>, Alain Niyonshuti<sup>1c</sup>, Yvan Coppens Nsenga<sup>1d</sup>

<sup>1</sup>University of Rwanda, College of Science and Technology. Department of Civil, Environmental and Geomatics Engineering. P.O Box: 3900 Kigali, Rwanda

<sup>a\*</sup> [imbereyaho2015@gmail.com](mailto:imbereyaho2015@gmail.com); <sup>b</sup> [dorisdaniella19@gmail.com](mailto:dorisdaniella19@gmail.com); <sup>c</sup> [alainniyo@gmail.com](mailto:alainniyo@gmail.com); <sup>d</sup> [nyvan90@gmail.com](mailto:nyvan90@gmail.com)

<sup>a\*</sup> Corresponding email

### Abstract

The building industry has been one of the fast-growing sectors in Rwanda, and multiple residential houses with amazing pitched roofs are being implemented in different cities. As the country is very hilly, the influence of wind loads on the buildings is high and therefore the selection step of roof slopes needs to be carefully undertaken, in order to ensure not only the structure safety, but also the economy. Available international and national guidelines give details about safety and functionality requirements, but don't talk much about economic aspect, and this was the purpose of the given study. Using a well elaborated methodology, the influence of the roof slope on its cost was checked, and it was established that the slope's increase of one degree would raise the roof cost by 3.6%. Therefore, during the roof slope selection and design process, economic requirements need more attention.

**Key words:** Aesthetics, hipped roof, roofing, roofing material, roofing cost, roof sheet, roof slope.

## 1 Introduction

Sloped roofs have been in use for many years, especially for a big number of domestic roofs. With the rapid growth of building industry sector in the world, the construction of residential buildings, including both apartments and detached houses has also developed. In Rwanda, multiple houses with remarkable pitched roofs are being constructed, especially in the six secondary cities (cities selected to supplement the main country city of Kigali). The country, being called a "country of thousand hills" is characterized by hilly sites and the influence of wind loads on the buildings is high. Therefore the selection of roof slopes needs a special attention in order to ensure the whole building structure safety. Nevertheless, one cannot distinguish any difference between the roof for houses built in the valley and those built on

hills, and this gives impression that people either pay more attention to aesthetics than to the safety, or those roofs were achieved at higher cost while providing their security. It would appear that information offered currently by the International and National guidelines in terms of the selection of roof slope was sufficient even if not quite exhaustive. For example, guidelines about minimum roof slope in function of roof covering materials and location have been in place from 2012 [1]. Also, the National Land Use Planning Guidelines in relation to Rwanda Green Growth and Climate Resilience Strategy in place from 2017 sets out different guidance, among others, guiding principles for sustainable land use planning, which include the consideration of the natural sloping conditions [2]. Moreover, according to the Rwanda Building code, the roof of any building should be so constructed that it would be durable, fire resistant, and waterproof, and it should not allow the accumulation of any rainwater upon its surface. The same code provide the requirements in accordance to which the designed and constructed roof should meet with regards to roof slope in function of the roof structure and covering materials in order to ensure its weather-proof [3]. However, the majority of people, when building their houses were still having tendency to select the steep pitched roof disregarding the preferable slope for the given site location. As the time goes on and with the building cost only going higher, there was a need to establish factors which should contribute on the decrease of that cost, and one of them could be the selected roof structure slope.

The purpose of this study was to assess the influence of the roof structure slope on the cost of a residential house, with purpose of designing not only strong but also economically efficient roofs. Among others, the specific objectives were to establish types of roof most used in the country, to identify the individual reasons behind the selection of roof slopes for their houses, to assess awareness level on available guidance and policies related to the roof slope selection, to design a house with four proposed roof slopes as a case study, and analyse their influences on the roof cost variation.

As for limitation, during the cost estimation stage, it was assumed that the parameters representing the labour cost, the roof trusses structure and other non structural elements, like bolts or nails, etc. were constant for all selected four sloped roofs. Therefore those parameters were not considered during the cost estimation. However, authors suggest that this may be considered as a good scope for another study.

## 2 Literature review

The analysis and design of building roof structure has always been important step to ensure the structure safety and its functionality. Some key elements of the roof include its structure, the slope, purlins, covering materials, among others. National guidance and previous studies describe the importance of the roof, roof slop and its selection, while others talk about roof materials.

The selection of a roof type for low-rise buildings is an important step as it may influence on the shielding effect, with regards to the wind pressures action [4], and on natural ventilation and air circulation [5]. The roof pitch has also a big effect on air flow and heating load of sealed and vented attics for a Gable-Roof Residential Building [6]. While for the factors considered during selection of the roofing system, aesthetics, minimum slope, and maintenance requirements were consistent, aesthetics might be the most significant aspect [7], even if for some situations, the set of requirements was economy, drainage, durability, wind resistance, service, safety, and aesthetics, among others [8]. Regarding the roof materials, the preference and influence look to depend on materials manufacturing industry level of each



country. As example, the comparison between reinforced concrete flat roofs (RCFR) and free standing wooden roofs (FSWR) determined the later as the most used roof in housing projects, but the RCFR was found to be clearly a more cost-effective and advantageous roof type than FSWR [9], while a comparative study with five different roofing materials established that the tile roofing was the best in Polish [10]. The energy efficiency of the building may be another aspect for selection of the roof, as the roof slope has a certain influence on the internal temperature of building, along with the exposure and roofing materials [11]. In relation to that energy saving, the optimum slope was found to be between 30 and 60° [4, 12]. Looking at the same influence of roof types on the energy efficiency, different roof types concerning daylight in industrial buildings were evaluated during the initial design phase, in function of a geographic location and some relevant results were established [13]. The effect of the roof slope on the wind pressure needs to be considered as important even if the distribution is not proportional to the slope [14]. Lastly, the reduction of the use of resources and unnecessary costs was achieved by [15] while working on the maintenance planning of pitched roofs in existing buildings.

From the above overview, it can be realized that the economic aspect in selection of roof slope is fairly or not discussed adequately, and therefore the scope of this study.

### 3 Materials and Methods

In this study, the literature review, site or industry visit and observations, interview and discussions, the roof structure design and cost estimation were used. Materials and tools used including Software, ruler, and others were either as office or laboratory materials. For roof structure analysis, the King Post truss was used.

#### 3.1 Materials

During the investigation of the houses, only the roof was considered. The used roof covering materials as presented below were all locally available. They were obtained from the local manufacturing industry, Safintra Rwanda Ltd, a member of the SAFAL Group. Among other roofing sheet materials, the versatile type was selected for the study. It is a premium steel tile roofing sheet with the look of a classic roof tile but with a much longer life span. Below the Fig.1 shows the Safintra's Versatiles.



Figure 1: Versatile roofing material

Other used tools like papers, rulers, software, etc. were available at researchers' institution.

### 3.2 Research Methods

#### 3.2.1 The Slope Measuring

The slope was measured using a ruler and following the steps presented below in Fig. 2



Figure 2: Measuring of the roof span (a), and roof rise (b)

The measurement consisted of reading the rise and the run as key parameters of the slope. These parameters were used to calculate the slope using the formula (1) and obtained slopes are presented in section 4, table 1.

$$Slope, h(\%) = \frac{Rise}{Run} \times 100 \quad (1)$$

#### 3.2.2 Interview and Discussion

The objective of this interview was to collect views from stakeholders about the roof slope selection criteria. It was conducted using a well designed questionnaire, and the targeted audience was citizens, site or practicing engineers, authority officers as well as technicians in the field of civil engineering. In total 50 respondents participated in the interview. This questionnaire comprised of questions concerning every aspect regarding the building roof slope and its selection. The considered factors were the following: type of roof used in Rwanda, requirements for roof slope selection, awareness of applied standards related to roof selection, approximated cost for a roof structure, and advantages of sloped roofs.

#### 3.2.3 Site Visit and Observation

The purpose of the visit was to observe and identify the most used roof slope, in order to establish either or not any strategic guidance was behind such selection. Different detached houses were observed and respective records were done.

### 3.2.4 Design and Cost Estimation

This exercise aimed at establishing the influence of the roof slope on the building/its overall cost. The collected information about the most applied roof slopes was used in designing a house model with a sloped roof, the area of the roof was calculated and the cost of roof covering materials was estimated using unit cost method. In order for the above to be achieved, a plan of single-family detached house was selected, and then its roof with different slopes was proposed. The roof analysis and cost estimation was finally performed for those sloped roofs. Results are presented in section 4.

## 4 Results and Discussion

### 4.1 Results

#### 4.1.1 Site Visit & Observation

During the site visit, it was observed that the pitched roofs covered with Iron sheets of various styles were the most used. During this activity the slope of the roof for some of local detached houses was identified, where most of them had a slope visibly high but with an aesthetically pleasant appearance. The Fig. 3 presented below shows some those residential houses with different slopes, as examples of today roofs in Rwanda.



Figure 3: Residential Houses with different roof slopes

#### 4.1.2 The results from Slope Measurement

The results obtained using the formula (1), presented in section 3 established four slope categories as given in table 1 below:

Table 1: Slope used by respondents

S/N	Slope (%)	Number of residential houses	
		In figures	In %
1	Below 50%	6	12%
2	Between 50% and 75%	9	18%
3	Between 75% and 100%	21	42%
4	Above 100%	14	28%
5	Total	50	100%

### 4.1.3 Interview activity

The distribution of all 50 participants in the interview is given below in table 2.

Table 2: Respondents classes

S/N	Types of respondents	Numbers	
		In Figure	In %
1	Ordinary citizens	15	30%
2	Practicing/site engineers	12	24%
3	Authority officers	2	4%
4	Technicians in the field	21	42%
5	Total	50	100%

Results from the interview activity are presented below.

- (1) Feedback about the type of roof used in Rwanda: all 50 respondents confirmed that the pitched roof was used and preferred.
- (2) Views about the roof slope selection requirements: According to 26 respondents (around 52%), and who included all engineers, all authority officers and quite the half of technicians, the requirements for roof slopes were clear. The remaining 24 people (48%) were not familiar with any requirement for roof slope selection and these included the half of field technicians and all the citizens interviewed. The table 3 below shows the distribution of respondents' views.

Table 3: Awareness of requirements for roof slope selection

S/N	Types of respondents	Aware of roof slopes selection requirements		NOT Aware of roof slopes selection requirements	
		In Figure	In %	In figure	In %
1	Citizens	0	0%	15	30%
2	Practicing/site engineers	12	24%	0	0%
3	Authority officers	2	4%	0	0%
4	Technicians in the field	12	24%	9	18%

5	Total	26	52%	24	48%
---	-------	----	-----	----	-----

- (3) About the requirements for roof slope selection: For the majority of respondents that were aware of the roof slopes selection requirements, the application of available standards especially regarding the minimum slope in function of used materials was the most important guidance. Also, the architectural view (aesthetics) was one of the leading factors, while other factors included the wall height, altitude on which the house was located compared to other neighboring houses. For those respondents who were not aware of any requirement for roof slope selection, the replication or recommendations from friends or neighbors were being used.
- (4) About the awareness of available standards related to roof selection: With reference to respondents' feedback, for only 34% and mostly engineers and authority officers confirmed the applied standards related to roof selection were known. The table 4 below shows the distribution of respective respondents' views.

Table 4: Awareness of applied standards related to roof selection in Rwanda

S/N	Types of respondents	Aware of any applied standard related to roof selection in Rwanda		NOT Aware of any applied standard related to roof selection in Rwanda	
		In Figure	In %	In figure	In %
1	Citizens	0	0%	15	30%
2	Practicing/site engineers	12	24%	0	0%
3	Authority officers	2	4%	0	0%
4	Technicians in the field	3	6%	18	36%
	Total	17	34%	33	66%

These respondents underlined the awareness of the Rwandan Code, EAC Code and International Standards among others.

- (5) Regarding the cost of the roof structure in function of selected slope selected, results are presented in table 5 below. For respondents, the following were reasons which influenced on the cost of their house roof structure: cost of materials used, roof type and size, and manpower.

Table 5: The approximated cost range of the roof structure

S/N	Cost of the roof structure	Number of residential houses	
		In figures	In %
1	2 – 3 million Rwf	4	8%
2	3 – 4 million Rwf	18	36%

3	Above 4 million Rwf	28	56%
4	Total	50	100%

Note: 1 USD was equivalent to 790 Rwandan francs (Rwf)

(6) About the advantages of pitched roof: For all the respondents the advantages of sloped roofs were the very good drainage and the aesthetical expression, in addition to the dwelling safety.

#### 4.1.4 Design and Cost Estimation

**Roof area calculation:** the design phase was performed using classic method where manually the amount of the roof structure elements and sheet coverage were established. The selected building general characteristics are given below:

- The area of the floor plan was 136m<sup>2</sup>
- An overhang of 0.5m provided for all the sides
- The height of the wall was 4m
- The King Post truss was used for the roof structure.

The figure 4 below shows the sample of the residential house with a sloped roof.

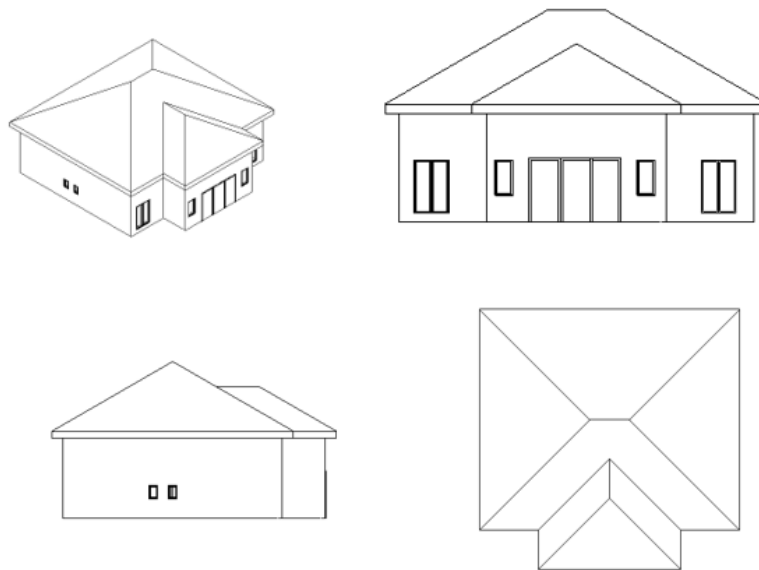


Figure 4: Sample of a residential house from different views

The five roof slopes selected, with respective calculated area of roof sheets are given in table 6 below.

Table 6: Roof slopes and roof areas

S/N	Type of roof	Slope (in degree)	Max. ridge height, h	Area of roof sheets
1	Roof slope of	26.57°	6.886m.	181.398m <sup>2</sup>

	50%				
2	Roof slope of 75%	36.87°	8.20m.	202.800m <sup>2</sup>	
3	Roof slope of 100%	45°	9.523m	229.442m <sup>2</sup>	
4	Roof slope of 125%	51.34°	10.855m	259.710m <sup>2</sup>	
5	Roof slope of 150%	56.31°	12.191m	292.483m <sup>2</sup>	

For verification, one of the design software **AutoCAD Revit** was used. Referencing to the table 6, the respective graph under Fig. 5 shows the variation of roof area in function of the roof slop. This graph shows how the roof area was increasing as the slope increases.

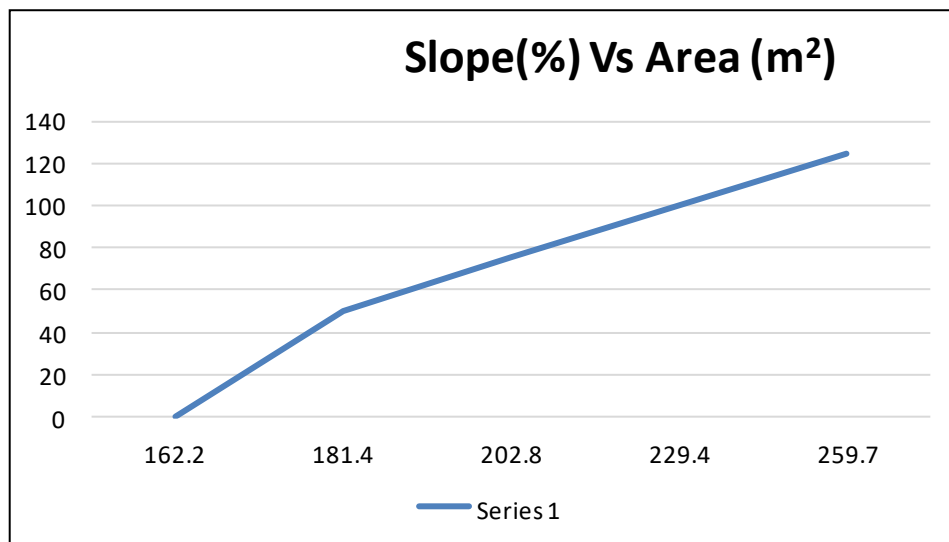


Figure 5: simple curve showing Area (Horizontal axis) in function of Slope (Vertical axis)

**The roof cost estimation:** As it was stated in the introduction, the cost estimation solely focused on the cost of the roofing materials. In order to achieve successfully this phase four essential parameters were considered. They included area of roofing sheets, unit price of one roofing sheet, total area of roof (for each slope), and safety factor (to compensate for any loss/damage or change that might occur). The cross sectional profile of the used roofing material as found on the market is presented below in Fig. 6.

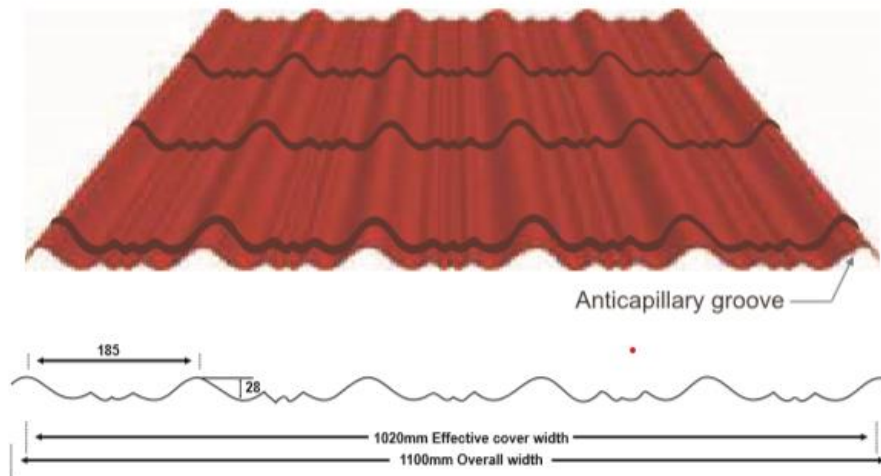


Figure 6: Roofing sheet section

The net effective cover width is approximately 1m, the net effective length is approximately 0.9m. The results of the cost estimation for all four selected roof types are given in table 7 below.

Table 7: Cost estimation Results for the sloped roof analysis

S/N	Type of roof	Slope (in degree)	Area of roof sheets	Unit cost, with safety factor (Rwf)	Total cost (Rwf)
1	Roof slope of 50%	26.57°	181.398m <sup>2</sup>	4900	974,000
2	Roof slope of 75%	36.87°	202.800m <sup>2</sup>	4900	1,089,000
3	Roof slope of 100%	45°	229.442m <sup>2</sup>	4900	1,232,000
4	Roof slope of 125%	51.34°	259.710m <sup>2</sup>	4900	1,394,000

The Fig.7 gives a graph representing the cost variation for the roofing material. It can be seen that the cost of the roofing material increases as the slope increases.



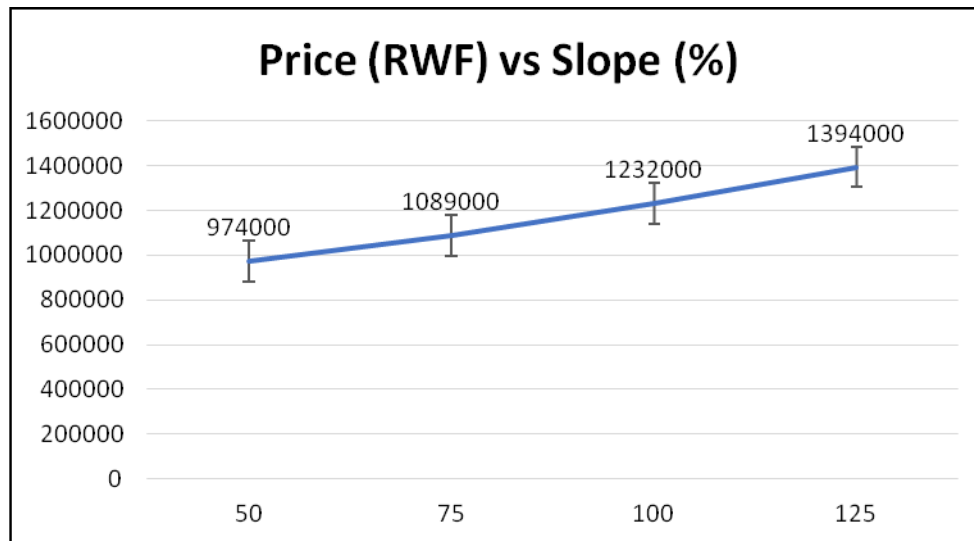


Figure 7: simple curve showing Price (Vertical axis) in function of Slope (Horizontal axis)

## 4.2 Discussion of Results

Results from the analysis of the collected data, especially those that are relative to the set objectives are discussed below with reference to the available references.

- (1) The established most used type of roof in Rwanda: It was established that the pitched roof was most used type in researched city area, Gasabo district. This choice is reasonable as it is normally recommended for use where the rain and snowy seasons are aggressive [15], and the rainy period takes long in Rwanda.
- (2) Identified reasons behind the selection of roof slopes: More than 52% of respondents confirmed that they were aware of requirements for roof slope selection, such as architectural view, wall height, etc. and used them while selecting the roof type. However 42% stated that for them the most important reasons behind that selection were replication or recommendations from friends or neighbors. Normally, the roof is selected basing on climate, economy, aesthetics, function and standards [16]. Therefore until currently in Rwanda the majority was still not considering those guidelines, except the aesthetics.
- (3) Assess available guidance and policies related to the roof slope selection: in this study, only 34% confirmed that they were aware of standards related to the roof selection. This uncomfortable tendency was in line with previous study showing that the available standards were not only incomplete, but also rarely consulted [17]. The international Building code (2006) and the Rwanda Building Code have provided the minimum slopes values depending on the materials used, but were not giving details regarding the impact of roof slopes on the overall building cost.
- (4) Results from respondents established that reasons which influenced on the cost of their house roof structure were the cost of materials used, roof type and size, and manpower. It is therefore noted that the influence of the slope its self was not well known. However, from the results given in table 5, and comparing with those in table 7, the influence of the roof slope was clear and should be estimated.

- (5) From table 6 and its respective fig.5, it is established that a steeper roof would require a larger roof area, and therefore more covering materials would be needed. This is also in line with some previous studies [6].
- (6) About the cost estimation, from the results presented in Fig.7, it is easily noted that as the slope increases the cost of the roofing materials increases as the slope of the roof increases. The slope increase of 25% (from 50% to 75% or from 75% to 100%) results in the cost increase by 115,000Rwf, or by 143,000Rwf respectively. In average, these results would mean that the slope increase of one degree should result in cost increase of 3.6%. This was certainly due to the increment in the quantity of roof materials used for the its covering, as stated under (4). Therefore the roof slope should not be neglected during roof design process.

## 5 Conclusion and recommendation

This study aimed at assessing the influence of the roof structure slope on the overall building cost, or more precisely on the roofing cost. The understanding level of stakeholders, including managers, Engineers and habitants, was checked with regards to the roof slope selection criteria. Around 52% of participants confirmed their own awareness of requirements for roof slopes, while only 34%, mostly engineers and authority officers confirmed that they were aware of the applied standards related to roof selection. Furthermore, while the available international and country codes and standards clearly state guidance about roof slope design, they don't go deeper to insist on economic aspect related that design. This situation would explain why a good number of citizens were still copying the roof slope from colleagues, neighbors or other sources. While focusing solely on the roof covering materials, the roof of a detached house, with four different slopes was designed and its cost was estimated. It was established that the slope increase of one degree would result in cost increase of 3.6%. As long as climate conditions allows, and without going against the aesthetical and strength requirements, it is recommended that during the roof slope selection process, not only strength and functional standards requirements are considered, but also economic factors should be checked.

## Acknowledgements

The authors sincerely acknowledge the support from Safintra Rwanda Ltd for detailed information about manufactured roof covering materials. The participation in the interview and discussions, of some site or practicing engineers, authority officers as well as technicians in the field of engineering working in Kigali City is also recognized. Authors are finally thankful to the leadership of University of Rwanda, College of Science and Technology for moral and technical support provided during the research process.

## References

- [1] Ministry of Infrastructures (2012). Basic Housing Construction Instructions for Protection against Natural and Manmade Disasters in Rural Areas, Rwanda Housing Authority, Kigali, Rwanda
- [2] Ministry of Natural Resources (2017). *Rwanda National Land Use Planning Guidelines*, Kigali, Rwanda
- [3] Ministry of Infrastructures (2015). *Rwanda Building Code, 1<sup>st</sup> edition*. Kigali, Rwanda
- [4] Jwo-Hua Chen (2012). A Study on the Selection of Optimal Roof Type for Low-rise buildings group in a View of Wind Pressures Action. International Conference on Advances in Computational Modeling and Simulation. *Procedia Engineering*, 31, 1149 – 1154. DOI:10.1016/j.proeng.2012.01.1155
- [5] Siti Halipah Ibrahim,S.H., Roslan, Q., Affandi, R., Razali, A.W., Samat,Y.S., Nawi Mohd N.M.(2018). Study On The Optimum Roof Type With 30° Roof Angle To Enhance Natural Ventilation And Air Circulation Of A Passive Design, *International Journal of Technology*, 8, 1692-1701. DOI: <https://doi.org/10.14716/ijtech.v9i8.2759>
- [6] Shen, S. W. A. Z.(2012). Effects of Roof Pitch on Air Flow and Heating Load of Sealed and Vented Attics for Gable-Roof Residential Building. *Sustainability*, 4, 1999-2021.
- [7] Guyer, J.P. (2009). *Introduction to Roofing Systems, Continuing Education and Development*, Inc. 9. Greyridge Farm Court Stony Point, NY 10980
- [8] Stramit Corporation Pty limited (2017). *Stramit-Roof-Slope. Design-Guide*
- [9] Ulubeylia, S., Kazazb, A., Er, B., Birgonul M.T. (2014). Comparison of Different Roof Types in Housing Projects in Turkey: Cost Analysis. *Procedia - Social and Behavioral Sciences*, 119, 20 – 29.
- [10] Radziszewska-Zielina, E.(2014). A comparative analysis of selected parameters of roofing used in the Polish construction industry. *SSP - Journal of Civil Engineering*, 9(1), 41-50. DOI: 10.2478/sspjce-2014-0005
- [11] Melo V. T., Renato L. F., Adhemar P. M., Marcos E. B., Diego A. M.(2014). Evaluation of roof slope and exposure with different roofing materials in reduced models of animal production facilities in spring and summer. *Eng. Agric., Jaboticabal*, 34(6), 1030-1038.
- [12] Ghaedi, A., Ghaedi, H., Ghaedi, H.(2012) The role of roof shapes in design of green building, systems (case study: Iran, Bandar Abbas). *ICESD 2012*, 5-7. DOI: 10.1016/j.apcbee.2012.03.055
- [13] Mavridou, T., Doulos, L.T. (2017). Evaluation of Different Roof Types Concerning Daylight in Industrial Buildings during the Initial Design Phase: Methodology and Case Study. *Buildings*, 9 (7). DOI: 10.3390/buildings9070170.

- [14] Singh, J., Roy, A.K.(2019). Effects of roof slope and wind direction on wind pressure distribution on the roof of a square plan pyramidal low- rise building using CFD simulation. *International Journal of Advanced Structural Engineering*. <https://doi.org/10.1007/s40091-019-0227-3>
- [15] Morgado, J., Flores-Colen, I., De Brito, J. , Silva, A. (2017). Maintenance Planning of Pitched Roofs in Current Buildings. *Journal of Construction Engineering and Management*, 143 (7). doi: 10.1061/(ASCE)CO.1943-7862.0001316
- [16] Syazili, F., (2005). *Chapter 8 roof lecturer notes*. Universiti Teknologi Malaysia
- [17] Mbereyaho Leopold, Abaho G. Gershome, Mutabaruka Jean de Dieu, Ndayisenga Jean Claude, Niyomwungeri Evariste, and Nsabimana Jacques (2019). Investigation on Application of Rwanda Building Standards in Local Construction Industry. *Rwanda Journal of Engineering, Science, Technology and Environment, Volume 2(I),1-17*. <https://dx.doi.org/10.4314/rjeste.v2i1.3>

# Numerical Modeling of Hole Under Opposite Biaxial Loadings

**Meriem Fakhreddine Bouali**

University of Mohamed Cherif Messaadia, Souk Ahras, Algeria  
Department of Civil Engineering, Faculty of Sciences & Technology  
e-mail: [m.bouali@univ-soukahrass.dz](mailto:m.bouali@univ-soukahrass.dz) [b.meriemfakhreddine@gmail.com](mailto:b.meriemfakhreddine@gmail.com)

## Abstract

The exact concentration of the stress generated by the presence of a cavity is a problem of great significance in Mining and Civil Engineering. An interesting stress concentration problem is the biaxial one. A numerical analysis of stress around a cylindrical hole in an infinite elastic medium under opposite biaxial loading was investigated. This far-field loading is equivalent to a pure shear loading on planes rotated  $45^\circ$ . Analysis consisted of two-dimensional finite-difference computations carried out with the Fast Lagrangian of Continua (FLAC) code. The Stress Concentration Factor (SCF) is evaluated numerically and compared with the existing solution. Predicted results of stress distribution around the hole were found in good agreement with the analytic theory.

**Key words:** numerical modeling, hole, biaxial opposite loading, shear, Stress Concentration Factor

## 1 Introduction

Holes appear with various shapes in many types of engineering, such as : aerospace, mechanical, and tunneling [1]. The determination of displacements and stresses around the cavities, tunnels and mining excavations is a problem of great magnitudes in Mining and Civil engineering. The exact concentration of the stress generated by the presence of a cavity is a problem of great significance [1]. Several works studied the distribution of stress around the hole [2, 3]. An interesting stress concentration problem is the biaxial one. If the far-field stress is biaxial with a tensile stress in the horizontal direction and compressive stress in the vertical direction; the loading, in this case, corresponds to a pure shear loading on planes rotated  $45^\circ$  [4].

In this purpose, a numerical analysis of stress distribution around a cylindrical hole in an infinite elastic medium under a biaxial opposite loading using FLAC code [5] is investigated. The usefulness of proposed results for the stress distribution is highlighted, and then the Stress Concentration Factor (SCF) is evaluated numerically and compared with the analytic existing result.

## 2 Analytic solution

### 2.1 Kirsch solution

The determination of displacements and stresses around a cylindrical cavity with a radius 'a' belonging to an infinite medium, isotropic, homogeneous with a linear elastic behavior was discussed firstly by Kirsch in 1898 [6].

Considering a point in polar coordinate  $(r, \theta)$  near an opening radius  $a$  (Fig. 1) has stresses given by expressions [7] (Eq.1):

$$\begin{cases} \sigma_r = \frac{P_1 + P_2}{2} \left[ 1 - \frac{a^2}{r^2} \right] + \frac{P_1 - P_2}{2} \left[ 1 - \frac{4a^2}{r^2} + \frac{3a^4}{r^4} \right] \cos 2\theta \\ \sigma_\theta = \frac{P_1 + P_2}{2} \left[ 1 + \frac{a^2}{r^2} \right] - \frac{P_1 - P_2}{2} \left[ 1 + \frac{3a^4}{r^4} \right] \cos 2\theta \\ \tau_{r\theta} = -\frac{P_1 - P_2}{2} \left[ 1 + \frac{2a^2}{r^2} - \frac{3a^4}{r^4} \right] \sin 2\theta \end{cases} \quad (1)$$

Where:

$\sigma_r$ ,  $\sigma_\theta$  and  $\tau_{r\theta}$  are respectively the radial, hoop and tangential stresses.

$P_1$ ,  $P_2$  the applied stress field respectively in the horizontal and vertical directions.

$a$ : radius of the hole.

$r$ ,  $\theta$ : the polar coordinates.

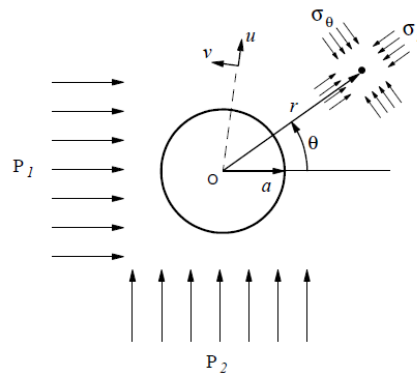


Figure 1: Stress around a cylindrical hole in an infinite elastic medium.

### 2.2 Hole under biaxial opposite loading

Considering a cylindrical hole subjected to a tensile and compressive stress in an infinite medium. Two cases of opposite loading can be obtained: the first one a tensile stress in the horizontal direction equal to  $T$  and compressive stress in the vertical direction equal to  $-T$  (Fig. 2a); and the second case corresponds to a compressive stress in the horizontal direction and a tensile stress in the vertical one (Fig. 2b). Stresses at the limits in both directions based on Eq. (1) are therefore equal to Eq. (2) and Eq. (3) for the first and the second cases respectively:

$$P_1 = +T \quad P_2 = -T \quad (2)$$

$$P_1 = -T \quad P_2 = +T \quad (3)$$

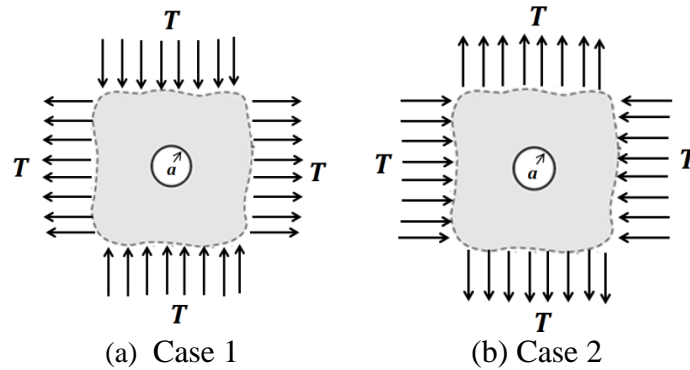


Figure 2: Cylindrical hole subjected to opposite biaxial loading

We obtain the stress field around the hole for the two cases by substituting the Eq. (2) and Eq. (3) into Eq. (1). So the expressions of stresses are given by Eq. (4) and Eq. (5) respectively:

$$\begin{cases} \sigma_r = +T \left[ 1 - \frac{4a^2}{r^2} + \frac{3a^4}{r^4} \right] \cos 2\theta \\ \sigma_\theta = -T \left[ 1 + \frac{3a^4}{r^4} \right] \cos 2\theta \\ \tau_{r\theta} = -T \left[ 1 + \frac{2a^2}{r^2} - \frac{3a^4}{r^4} \right] \sin 2\theta \end{cases} \quad (4)$$

$$\begin{cases} \sigma_r = -T \left[ 1 - \frac{4a^2}{r^2} + \frac{3a^4}{r^4} \right] \cos 2\theta \\ \sigma_\theta = +T \left[ 1 + \frac{3a^4}{r^4} \right] \cos 2\theta \\ \tau_{r\theta} = +T \left[ 1 + \frac{2a^2}{r^2} - \frac{3a^4}{r^4} \right] \sin 2\theta \end{cases} \quad (5)$$

The uniform field is disturbed by the presence of the hole. It is assumed that this disturbance is local, therefore the disturbing field will decay to zero as we move far away from the hole [4, 6].

### 2.3 Stress Concentration Factor

The influence of the presence of the hole is very local character, if the radius increases stress approaching very rapidly from the value imposed at the limits. The high concentration of stress observed near the hole is of great practical importance. As a practical example we can cite the case of holes in the decks of ships [7]. It is mentioned that deterioration of the resistance and premature failure of the structures due to fatigue cracking and plastic

deformation that occurs is caused by high concentration of stress at points having the highest Stress Concentration Factor [8].

The ratio between the maximum and the minimum stress is defined as Stress Concentration Factor. It only depends on the geometry, loading mode and the type of material chosen. It appears that the equal biaxial loadings enhance the local stress field, but the opposite biaxial one gives the highest concentration effect [4]. In order to confirm this high effect, the Stress Concentration Factor will be estimated by the numerical model and the value will be compared with the analytical one.

### 3 Numerical analysis

The main objective of this part is a numerical modeling of the cases shown in Fig. 2 using the finite-difference element code  $FLAC^{2D}$  version 2007.

**Fast Lagrangian Analysis of Continua  $FLAC^{2D}$**  is a two dimensional explicit finite difference code for engineering mechanics computations which discretizes the behavior of structures built of soil, rock or other materials. A grid which is adjusted by the user is forming by elements or zones. The shape of the discretized material can be fitted by the user. Several stress/strain laws can be prescribed linear or nonlinear in response to the applied forces or boundary restraints [5].

Considering plane strain condition, this problem can be reduced to a bi-dimensional analysis. By reason for existing symmetry in the geometry view model and loading, only a quarter of the problem needs to be analyzed as shown in Fig. 3 which indicates the boundary conditions applied in our numerical model. The mesh must be refined near the hole for better precision in the area where the stresses and strains varied rapidly from one point to another [9].

A cylindrical hole with a radius  $a=1m$  exists in an infinite medium, isotropic, homogeneous and with elastic behavior. It is well noted as seen in Eq. (4) and Eq. (5) that the stresses around the hole does not depend on material's elastic properties. For this reason, the following material properties as example are assumed for the two cases: density  $\rho=2500kg/m^3$ , shear modulus  $G=2.8GPa$  and Bulk modulus  $K=3.9GPa$  [5].

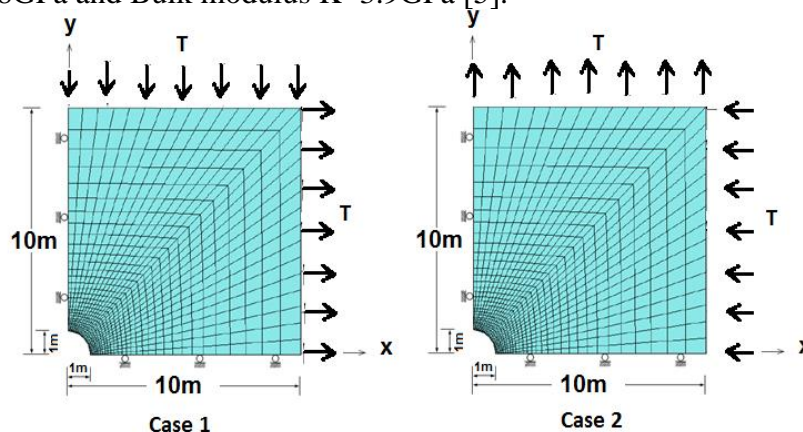


Figure 3: Cylindrical hole under opposite loading (boundary conditions)

The limits of this medium are subjected to a biaxial opposite loading, a tensile stress in the horizontal direction equal to  $T=30 \cdot 10^6$  MPa and a compressive stress in the vertical direction



equal to  $-T$  in the case 1.

But in the second case, we take a compressive stress in the horizontal direction equal to  $-T$  and tensile stress in the vertical direction equal to  $+T$ . The two cases of opposite biaxial loading considered in this analysis are shown in Fig. 4 and Fig. 5 respectively.

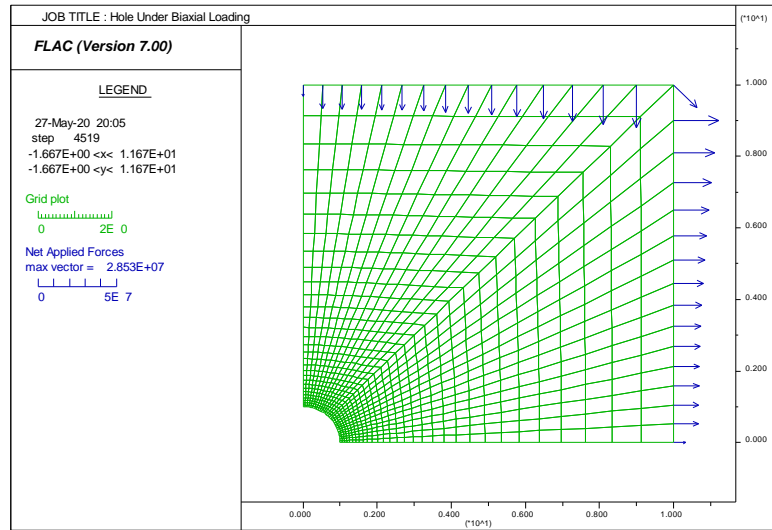


Figure 4: Applied loading, biaxial opposite loading: Case 1

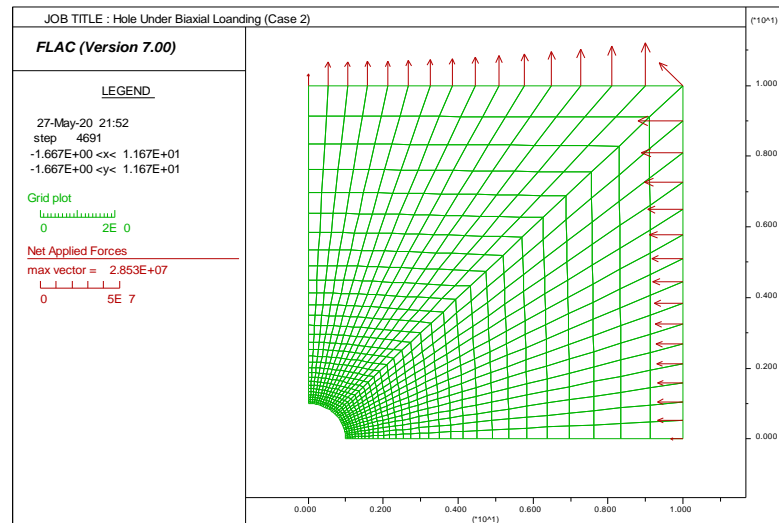
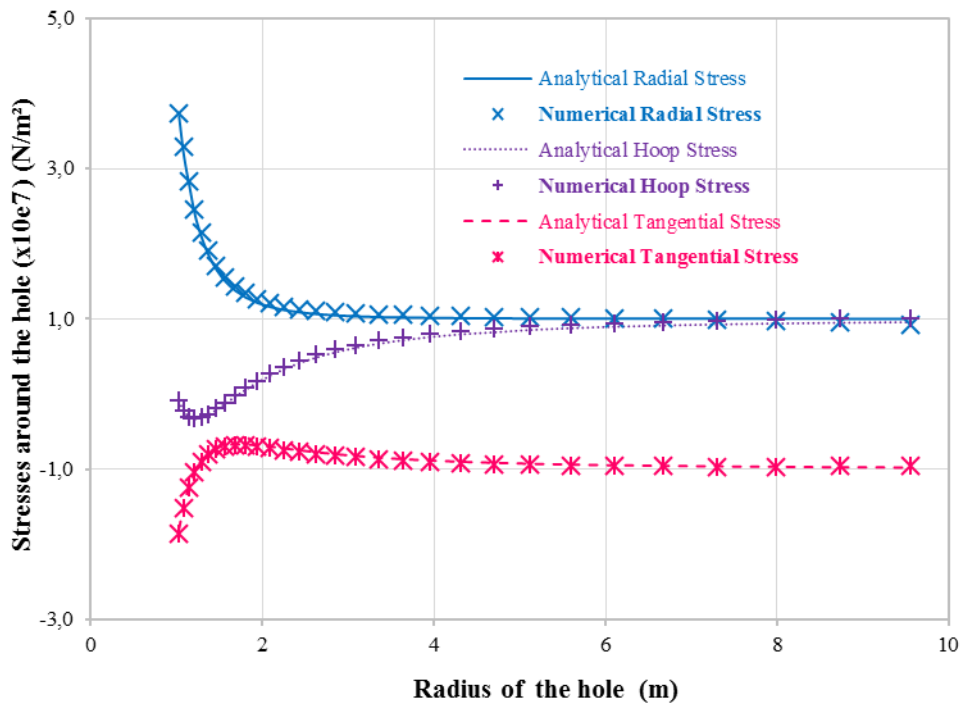


Figure 5: Applied loading, biaxial opposite loading: Case 2

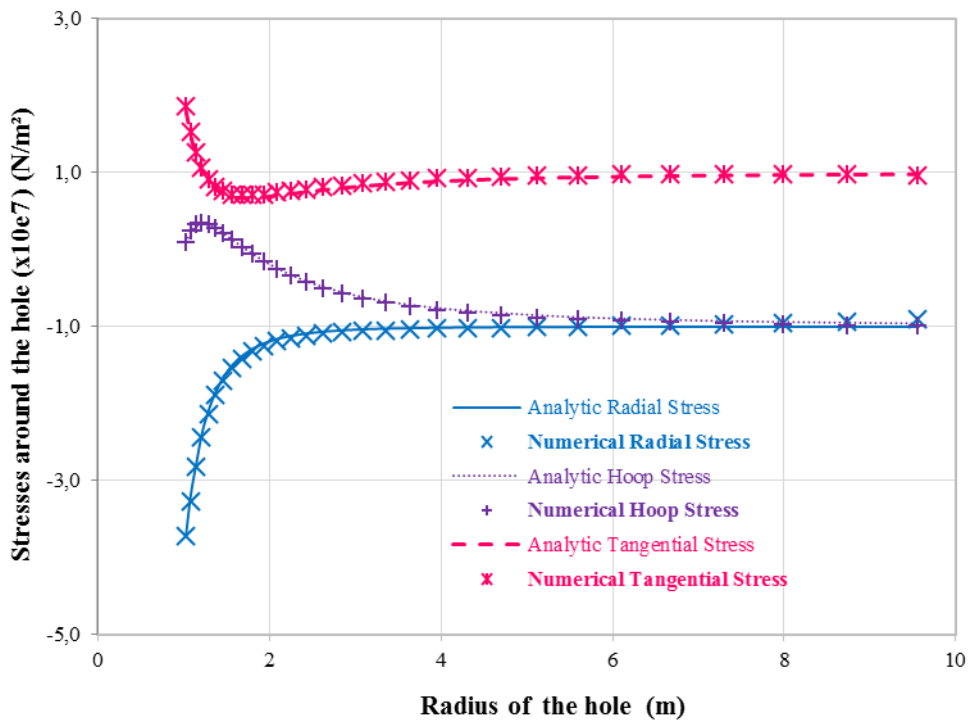
## 4 Results and discussions

Stresses around the hole are evaluated numerically for the two cases in this study.

If  $\theta=0$  and  $r$  varies from  $a=1m$  to  $r$  equal to  $10a$ , the radial stress  $\sigma_r$ , Hoop stress  $\sigma_\theta$  and maximum tangential stress  $\tau_{r\theta}$  are calculated numerically for the two cases of opposite biaxial loading (Fig. 6) and then compared to those obtained analytically by the Eq. (4) and Eq. (5) respectively.



(a) Case 1



(b) Case 2

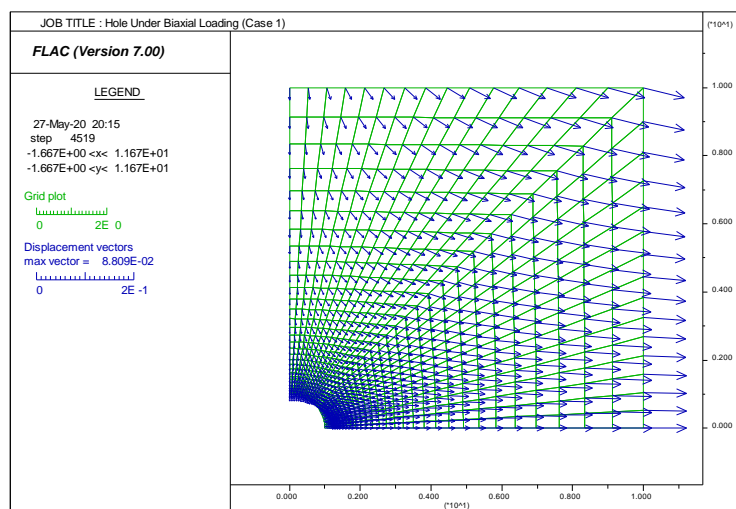
Figure 6: Numerical stresses around the cylindrical hole compared to analytic solution

As shown in Fig. 6, the stresses obtained numerically for the two cases (showed by cross points) are in very good agreement with those obtained analytically (showed by continuous line) by the formulas of Kirsch which confirm the reliability of the numerical model.

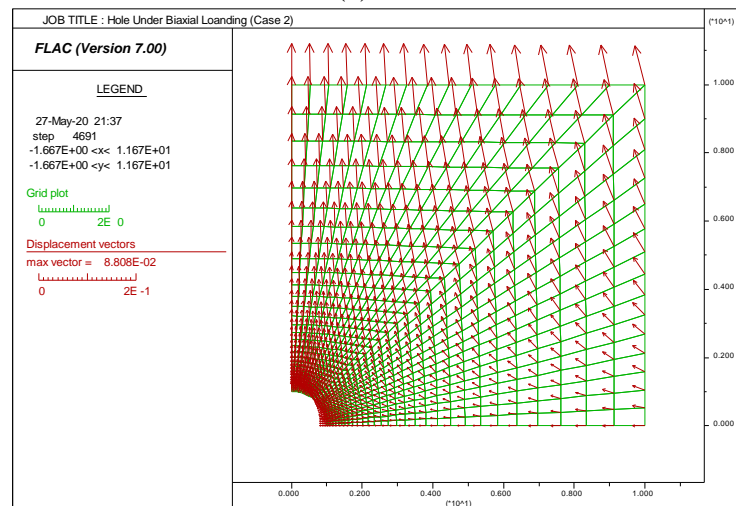
The stresses to the inner edge of the hole ( $r=a=1m$ ) are very large, they vary very quickly if we are moving away from the hole to stabilize at the end.

It is very clear from Fig. 6 that the two cases converge towards the same loading mode which will be confirmed and discussed in what follows.

The generated displacement field vectors during the application of the opposite biaxial loading imposed on the boundaries of the model obtained by FLAC for the two cases is shown in Fig. 7.



(a) Case 1



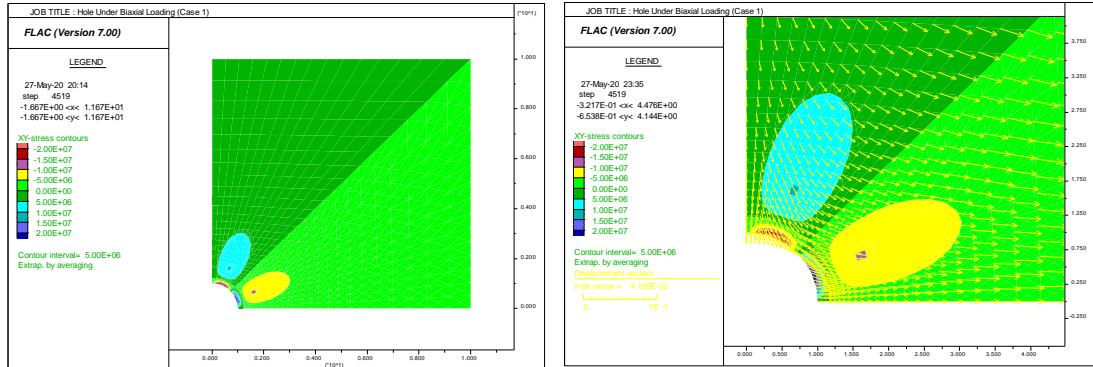
(b) Case 2

Figure 7: Displacement fields around the hole

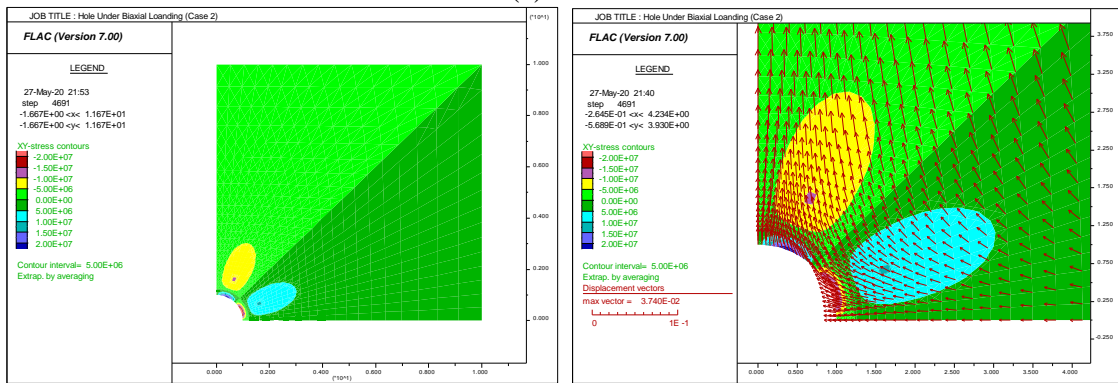
As shown in Fig. 7 the medium tends to move from an angle equal to 45 degrees. This result obtained numerically confirms that these opposite biaxial loadings are equivalent to a pure

shear loading on planes rotated 45°.

The tangential stress and volumetric strain concentration are shown respectively in Fig. 8 and Fig. 9. We can observe easily the pure shear loading in the two cases.

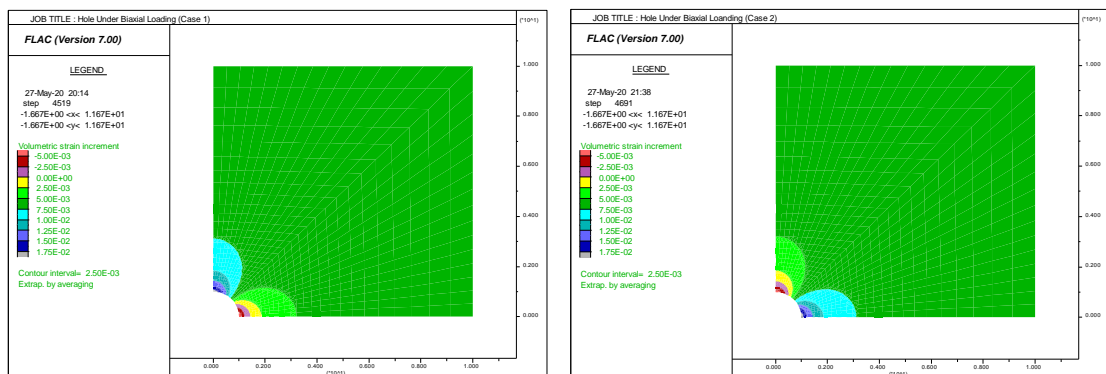


(a) Case 1



(b) Case 2

Figure 8: Tangential stress and displacement vectors around the hole



(a) Case 1

(b) Case 2

Figure 9: Volumetric strain around the hole

The Stress Concentration Factor (SCF) is calculated numerically for the two cases. This Stress Concentration Factor as a function of radius if the angle  $\theta$  equal to 90° is shown in Fig. 10. The numerical result for Stress Concentration Factor (SCF) corresponding to this case is equal

to 3.696.

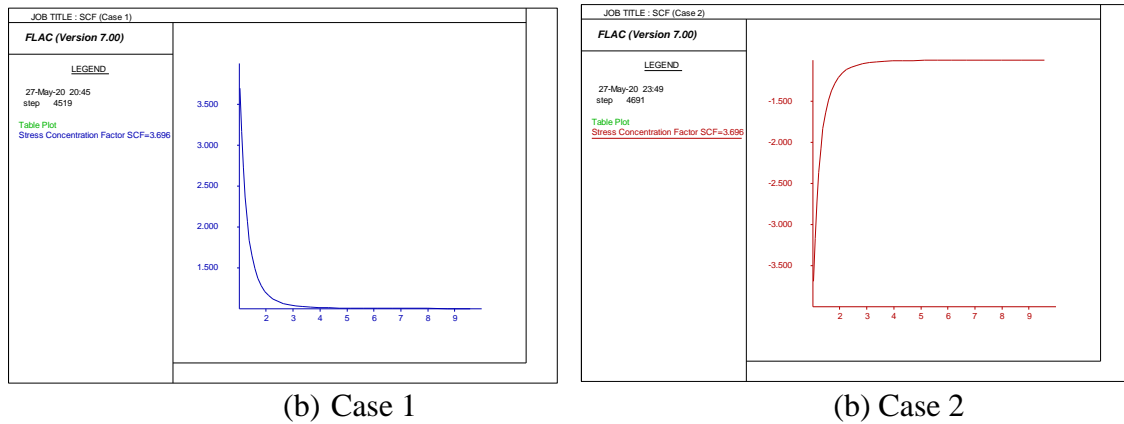


Figure 10: Stress Concentration Factor (SCF) around the hole

Looking at Figs. 10a-b, we can observe if  $(r/a=1)$ , the SCF is equal to 3.696 and then declines slowly with  $(r/a)$  to be stable at the end (equal to 1).

The analytic SCF is equal to 4 [4], so the error percentage between the numerical and analytical results is about 7.60%. This numerical result confirms the theory, thus giving the highest concentration effect (the analytic SCF is equal to 4).

## 5 Conclusion

A numerical evaluation of stresses, displacement and Stress Concentration Factor (SCF) has been confronted with the analytic solution.

Predicted numerical results of stress distribution and Stress Concentration Factor around the hole were found in good agreement with the analytic solution. From the obtained numerical predictions, the main findings are summarized below:

The biaxial opposite loading is equivalent to a pure shear around the hole.

The Stress Concentration Factor (SCF) for this case is equal to 3,696 which confirm the phenomenon of stress concentration around the hole.

This factor is higher than that obtained in the case of compression biaxial (1,948) and that obtained in the case of traction uniaxial traction (2,822) [10].

This numerical investigation is an intuitive appeal to the negative impact of the phenomena of stress concentration caused by discontinuities.

## References

- [1] Zeng XT, Lu AZ. (2019). Stress solution for an infinite elastic plate containing two arbitrarily shaped holes. *AIAA Journal*. 57(4), 1691-1701. Doi :10.2514/1.J057578.
- [2] Mallikarjun B, Dinesh P & Parashivamurthy K I. (2012). Finite element analysis of elastic stresses around holes in plate subjected to uniform tensile loading. *Bonfring International*

- Journal of Industrial Engineering and Management Science*. 2(4), 136-142. Doi: 10.1.1.404.1756.
- [3] Mekalke G C, Kavade M V & Deshpande S S. (2012). Analysis of a plate with a circular hole by FEM. *Journal of Mechanical and Civil Engineering*, 25-30.
- [4] Sadd M H. (2009). *Elasticity: theory, applications, and numerics*. Academic Press.
- [5] Itasca F LAC. (2007). *FLAC-Fast Lagrangian Analysis of Continua*. Version. 7.0.
- [6] Jaeger JC, Cook NGW & Zimmerman RW. (2007). *Fundamentals of Rock Mechanics*. Blackwell Publishing.
- [7] Timošenko SP & Goodier JN. (1951). *Theory of elasticity*. McGraw-Hill.
- [8] Wilson T L & Leviathan SS. (1930). Damage, Repairs and Strength Analysis, presented at a meeting of the American Society of Naval Architects and Marine Engineers. November.
- [9] Mestat P. (1997). Maillages d'éléments finis pour les ouvrages de géotechnique. Conseils et recommandations. *Bulletin-Laboratoires des Ponts et Chaussées*, 39-64.
- [10] Bouali M F, Hamaidia A & Kouaoucha H. (2014). Numerical Modelling of Cylindrical Hole Under Equal Biaxial and Uniaxial Tension Loadings at the Infinity. *International Review on Modeling and Simulations*. 7(5), 893-899. Doi: 10.15866/iremos.v7i5.3487.

## An experimental study on damaged cementitious mortars repaired by glass/epoxy composite materials

Chouaib Aribi<sup>1</sup>, Aissa Bouaissi<sup>2</sup>, Brahim Safi<sup>1\*</sup>, Mohammed Saidi<sup>1</sup>

<sup>1</sup> Research Unit; Materials Process and Environment, Faculty of Technology, M'hamed Bougara University of Boumerdes, 35000, Algeria

<sup>2</sup> School of Engineering, University of Plymouth, Plymouth PL4 8AA, United Kingdom

\*corresponding authors: [safi\\_b73@univ-boumerdes.dz](mailto:safi_b73@univ-boumerdes.dz)  
[mgmchouaib@gmail.com](mailto:mgmchouaib@gmail.com), [issam3009@gmail.com](mailto:issam3009@gmail.com), [safi\\_b73@univ-boumerdes.dz](mailto:safi_b73@univ-boumerdes.dz), [mo.saidi@univ-boumerdes.dz](mailto:mo.saidi@univ-boumerdes.dz)

### Abstract

This paper presents an experimental investigation on the post-repair flexural response of mortars with and without damage. In order to improve the mechanical properties of the damaged mortars, which were subjected to different loads ranging between 40 % and 90 %, the mortars specimens were reinforced and repaired using two different composite materials, the first with only epoxy resin, while the second consisted of a mixture of epoxy resin and glass fiber. The results show a significant improvement in the stiffness damaged. Therefore, the reinforced specimens by a layer of resin on the lower side surface increased the bending strength by 58 %, when compared to those control samples. The reinforcement using composite resin-fiber of glass exhibited considerable increases in the safety of constructions. The SEM images of damaged samples with and without repair, revealed the impact of reinforced glass fibers-mortar on the matrix-mortar by improving their mechanical performances.

**Key words:** Cement mortar; Glass Fiber; damaged cementitious materials, Composite materials; Epoxy Resin; Mechanical Properties; SEM

## 1 Introduction

In civil engineering, the technique of joining is mainly used for concrete repair or reinforcement of elements in constructions, where rigid external reinforcements can be fixed on the defective structures in order to restore or increase their mechanical capacities. These reinforcements were initially introduced using steel plates in 1970, afterwards were replaced using much lighter and more sustainable composite materials [1]. Further, the process of reinforcement using fiber fabrics stuck was developed in Japan by the earlier of the 1990s, which shown a success growing in France a decade later [1,2]. These techniques showed remarkable performance by prolonging the lifespan of the defective structures with lower costs. In civil engineering, the concept of adhesive-bonded joint refers to the join applied on a cementing substrate (concrete, mortar or paste of cement) through a polymeric adhesive. This

bibliographical section briefly describes the components of the assembly (adhesive and cementing substrate), and clearly provides a state of knowledge on the physicochemical interactions which could be occurred with both organic /inorganic interfaces. It is well known that many structures suffer from continuous deterioration. It has been reported that reliable systems can maintain structural integrity and extend the life of constructed facilities, which in turn lead to saving a huge amount of money from repair costs. It was stated that a high strength can be achieved on repair concrete members when external bonded fiber-reinforced plastic sheets used. Experimental studies showed an effective technique when both virgin and damaged beams were strengthened using externally bonded FRP plates [3-5]. The increase in strength exhibited by beams strengthened with FRP plates can be three times higher than their original capacity, which is believed, it depends on the steel ratio, concrete strength, FRP ratio, FRP mechanical properties and properties of the bonding agent and the level of pre-existing damage on the beams. P. A. Ritchie investigated fourteen reinforced concrete beams using steel plates, glass and carbon FRP laminates [6]. The results showed a significant increase in beam stiffnesses and the ultimate flexural capacity with approximately 116 % and 97 %, respectively, the beams made up with externally bonded plates, also exhibited other desirable features where the cracking patterns changed from several widely spaced cracks with relatively large widths to many more closely spaced cracks with much narrower widths. In 1992, Ghaleb studied the use of externally bonded fiber glass plates to increase both the flexural and shear capacity of damaged reinforced concrete beams [7-8]. The study was conducted using three repair techniques for shear damaged beams, including, FRP side plates, FRP side strips and FRP U-jackets. The results showed an observable improvement of shear capacity of those shear damaged beams repaired by FRP side strips and FRP side strips and FRP side plates by 26 and 32 %, respectively. Whereas, the beams repaired with FRP U-jackets reached the ultimate flexural capacity without experiencing a shear failure.

Much research has been done on the investigations of fiber-reinforced mortar or concrete. Numerous studies were conducted on the mechanical behavior of cement mortars reinforced with naturel fibers, steel fibers and polypropylene fibers [9-12]. Further, it was found that the ductility of fiber-reinforced composites based cementitious materials have been improved, because the fibers clogged the cracked surfaces, hence delay the onset of the extension of cracks [13]. Shah and Naaman investigated the tensile strength, the flexural strength and the compressive strength of mortar samples reinforced with steel and glass fibers [14]. The results exhibited that the tensile or flexural strengths of steel fiber-reinforced mortar were at least two to three times higher than those plain mortar samples. Nataraja, et al. observed that the variation of compressive strength of concrete reinforced with steel fibers ranges between 0 to 25 % [15]. However, the addition of steel fibers significantly increased the strain capacity and elastic deformation toughness of concrete matrix around 75 % [15].

Some authors stated that modern concretes can be designed to have a great degree of flowbility, which allows it to flow in congested reinforcement areas and fill the complicated formwork segregating [16-17]. Domone & Jin stated [18] that the evaluation of mortar flowbility is a substantial property in determining concretes' flowbility on the other hand, it is difficult to obtain well-compacted repair mortar, when applied to concrete from this side, a high fluid repair mortar may drive considerable advantages when used in narrow mould systems [19]. The main concern with high- strength mortar is increasing the brittleness when the strength increased; this becomes a serious problem in improving the ductility of High-



Strength Fluid Mortar (HSFM) (Zhou et al., 1994) [20].

Based on the literature survey described above, there is a lack of investigations on the use of resin/fibres as reinforcements and repair materials for mortar and concrete. This experimental study aims to improve the mechanical properties of the damaged mortars when subjected to different loads ranging between 40 % and 90 %., The main objective was focused to reinforce and repair the latter with composite materials using at first only epoxy resin then used a composite epoxy resin /glass fiber.

## 2 Materials and methodology of experiment

### 2.1 Materials used

**Cement and mortar ordinary:** In order to see the influence of epoxy resin and glass fibres on the mechanical behaviours of the damaged mortars, a total of 30 prismatic specimens with the dimensions of 40 mm x 40 mm x 160 mm were prepared and cast. The mortars specimens were prepared in accordance with the EN 196-1 standard (Table 1). The cement used during the mortar mixtures preparation was Ordinary Portland Cement (OPC) (CEM II/A 42.5).

Table 1 Composition of control mortar

Component	Cement	Sand	Water	E/C
Quantity in (g)	450	1350	225	0.5

**Glass fibres:** Ordinary long glass fibers of E type were used in this investigation. Their chemical composition and mechanical properties are displayed in Tables 2 and 3.

Table 2 Chemical composition of glass fibers

Elements	%
SiO <sub>2</sub>	53
Al <sub>2</sub> O <sub>3</sub>	15
CaO	22
MgO	22
B <sub>2</sub> O <sub>3</sub>	8
F	0.7
Fe <sub>2</sub> O <sub>3</sub>	< 1
TiO <sub>2</sub>	< 1
Na <sub>2</sub> O	< 1
K <sub>2</sub> O	< 1

Table 3 Mechanic properties of glass fibers

Tensile strength (MPa)	217.8
Elastic Modulus (GPa)	12.9
Strain at tensile fracture (%)	2.9

**Resin:** According to previous research, the most used adhesive resin in construction sectors is of type thermohardening epoxide systems (with 90 % of tonnage) [21]. For this reason, the conducted studies were primarily focused on the assemblies adhesives occurred through these adhesives. In civil engineering, the adhesives epoxide intended are bi--components systems, which consisted of one base epoxy (pre-polymer comprising reactive functions oxyranes) and of a hardener which is a mixture of aliphatic or cyclic amines or polyamides. Groupings functional calculate of the resin and the hardener is able to react by polycondensation at room temperature and leads to form a reticule polymeric network. A reaction enters the biphenyl diglycidylether A or DGEBA and an aliphatic diamine.

The mechanical properties of the epoxy adhesives can be rather variable according to their Formulation [22-24]. It is worth noting that that resistance in traction of the epoxy resins is definitely higher than that of cementing materials. The resin used was an epoxy resin (STR), obtained from MEDAPOXY STR EA for the resin, and EB for the hardener (Table 4).

Table 4 Characteristics of the resin

Characteristics	Résultats
Density (ISO758)	1,1 ± 0.05
Viscosity (NF T76-102) Pa.S at 25°C	0,011
Duration practices use (NFP18 810) h	1 h15mn à 20°C and 65 % Humidity
Compressive strength (NA 427) Mpa	> 70
Bending strength (NA 234) Mpa	> 25
Adherence to concrete Mpa	> 3

**Characterization of the composite resin-fiber:** The results of the tensile tests on the composite resin-long fibers are displayed in Table 5.

Table 5 Results of the mechanical tests on the composite resin- long fibers

Samples	Tensile strength breaking (MPa)	Elastic Modulus in traction (MPa)	Lengthening with rupture in traction (%)
average of 4 tests	133	8985	1.6

## 2.2 Test methods

The objective of the present work mainly focuses on the investigation of mortars damaged of the final material, which was reinforced using: s:

- Epoxy resin on a side face and the two side faces
- The composite epoxy glass/resin fiber on one face and the two side faces.

A total of 30 prismatic specimens with 40 mm x 40 mm x 160 mm were prepared then kept as control samples. Fiber-resin and glass fibers and various stackings were used as reinforcement to manufacture other 15 specimens and cured in laboratory conditions before the specimens were tested. . The samples were made in accordance to the EN standard 196-1, which explains the preparation procedures of normal mortar, also provides the measurement details of the mechanical resistance to compression and the inflection. This experimental work is divided into four stages as:

- Step 1: Studying of the mechanical behavior of three control specimens.
- Step 2: For each serial specimens, starting from the maximum values of the load to the inflection, it was applied a damage of various levels, going from 40 % of the maximum loading up to 90 %, with a step of 10 %.
- Step 3: consists of reinforcement of the damaged specimens using the following methods:
  - Coating both sides faces (higher and lower) with a layer of the epoxy resin of thickness 1 to 2 mm.
  - Coating the lower side face (against the third pressure point) with a layer of the resin. Applying the composites glass fiber-resin a fold on both side faces.
  - Applying the composites glass fiber-resin folds on the lower side face (against the third pressure point).
- Step 4: morphological investigation using Scanning Electron Microscope analysis technique (SEM), to examine the microstructural interface zones (Interface composite-mortar).

### *a) Failure mode:*

Typically, the rupture corresponds to the separation of two initial cracking of interdependent bodies, starts from a notch or of a preexistent defect. Its aspect and propagation speed depend on the properties of the materials used, the internal stresses to the system and other external factors (temperatures, forces applied, etc.), of the geometry of the solids.

### *b) Interactions cementitious materials polymers matrices*

- A complex adhesion mechanism occurs, when a polymer adhesive contacts a porous cementing substrate, and resulting in Damping the surface which allows the resin to penetrate into the substrate porosities, this induce a mechanical phenomenon so-called 'the anchoring'.
- The creation of physical and chemical cross-links to the interfaces, due to the penetration of the resin into the cementitious matrix.
- Therefore, the penetration depth depends on the properties of the porous substrate

and the resin.

- The roughness and the porosity of the cementing support contribute to increase the contact area and support the mechanical anchoring. It is believed that the treatment of the support surface make it possible to optimize the roughness of its surface [25].
- The water presents in the substrata is harmful and has a substantial influence on the penetration of the resin. This affects the drainage by capillarity, due to the saturated pores by water molecules.
- The viscosity of resin is an essential parameter in controlling the capillary flow in the porous concretes [26].

The prepared specimens were subjected to loading ranges between 40 and 90 % of the maximum loading to the inflection with a step of 10 % (Table 6). Afterwards, only those specimens were damaged under 90 % were repaired, using the epoxy resin and by a composite resin-fiber glass of type E.

### 3 Results and Discussions

#### 3.1 Creating damage

To create damage, loading series ranged between 40 and 90 % were applied as shown in (Table 6).

Table 6 Various forces of damage applied to the specimen

Charge max applied (%)	90	80	70	60	50	40
Reference (N)	2653	2358	2063	1769	1474	1180

Table 7 Maximum force and lengthening of the specimen reinforced after the damage

Method of reinforcement	Max. force with the inflection (N)	Lengthening (mm)
Lay down resin on the lower side face	4660	0.62
Lay down resin on the two side faces	5250	0.71
Composite 1 pli on the lower side face	5100	1.75
Composite 1 pli on the two side faces	6400	1.85

According to the results obtained, the deterioration values after repair of the specimens damaged at 90 % ultimate force (Fig. 2) are much higher than the reference values (Fig. 1)

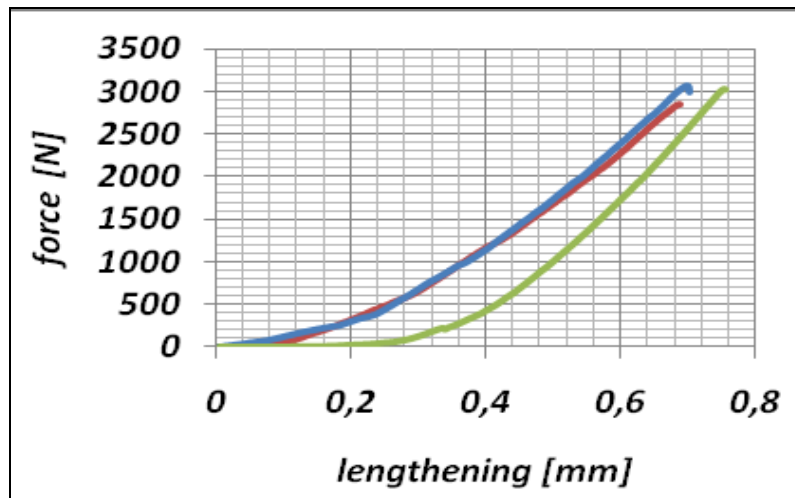


Figure 1 Curve of pilot three point bending (not damaged)

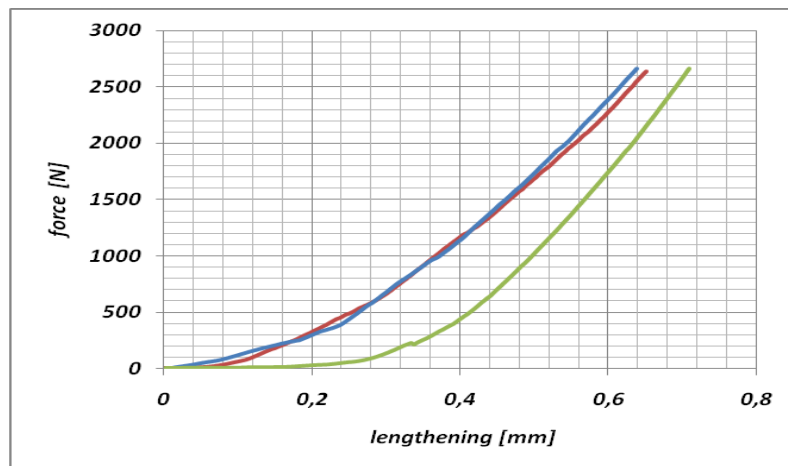


Figure 2 Curve of flexural strength third point indicating the damage of 90 % on the references

### 3.2 Reinforcement of the damaged specimens

To apply the reinforcement, the following steps should be followed:

**Preparation of glass fiber:** The glass fibers were cut carefully with dimensions of 40 x 160 mm, and then left in the flat position without folding to prevent any damages.

**Preparation of the resin:** Two-thirds of the resin B (2/3) and one-third of hardener A (1/3) were mixed for (3 to 5 minutes) at room temperature using an electric mixer at low mixing speed.

**Application of reinforcement:** to apply a layer of the resin on the surface of the specimens, a roller has been used (Fig. 3). For composite resin-glass fiber was positioned and plated manually on the support, then, one strongly pressed using the roller. Lastly, the same method was followed to apply another layer of resin with a slight of pressing to ensure that the air

bubbles would not remain inside (Fig. 4). The specimens were left to cure at room temperature and relative humidity until being tested.

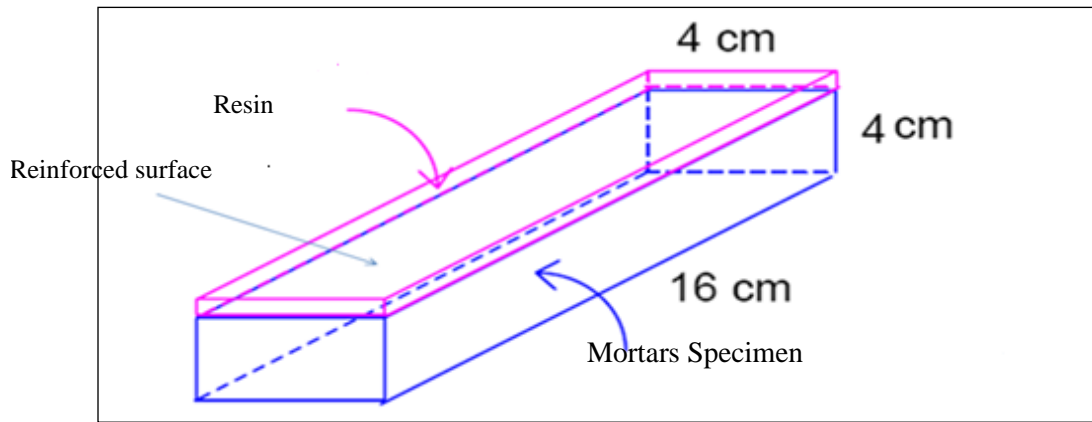


Figure 3 Reinforcement by the resin on lower surface

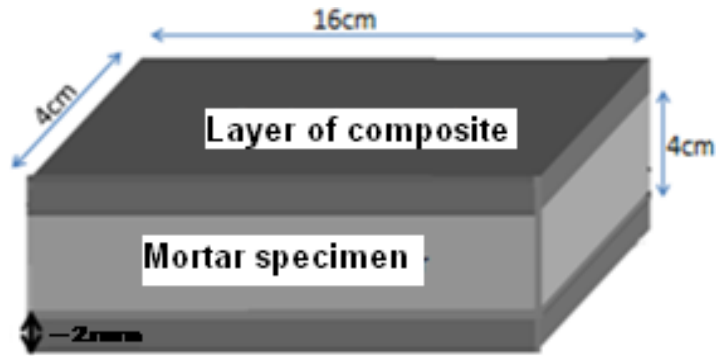


Figure 4 Reinforcement by a layer of composite on two surfaces

The results obtained do not depend on initial stacking, they are directly dependent on the method of reinforcement after the damage, with a margin of error lower than 100N (Fig. 5 to Fig. 8).

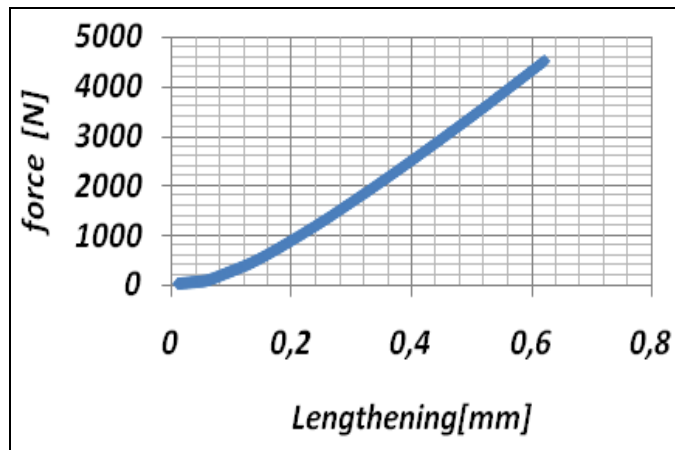


Figure 5 Curve of flexural strength third point of the specimen reinforced by the resin on lower surface

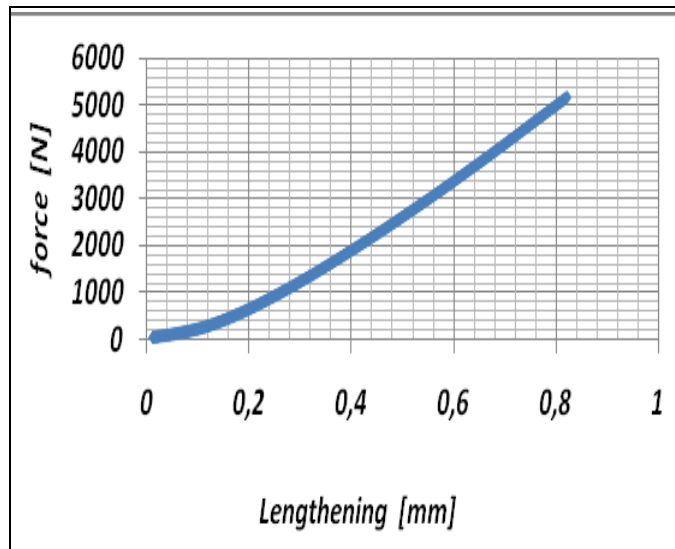


Figure 6 Curve of flexural strength third point of the specimen reinforced by the resin on two side surfaces

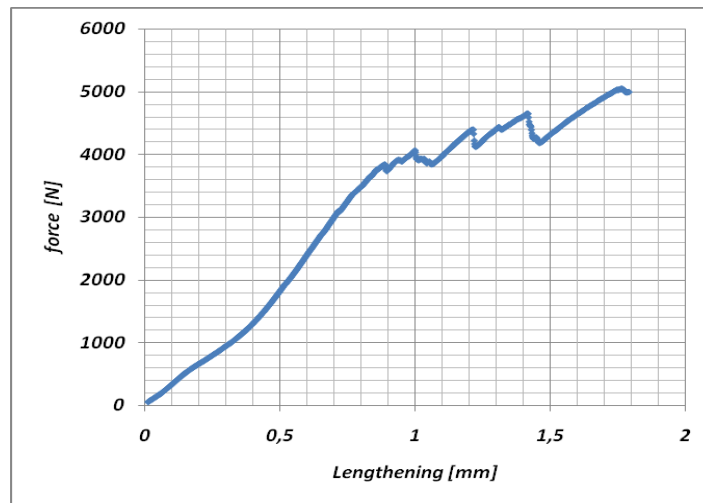


Figure 7 Curve of flexural strength third point of the specimen reinforced by the composites on side surfaces lower

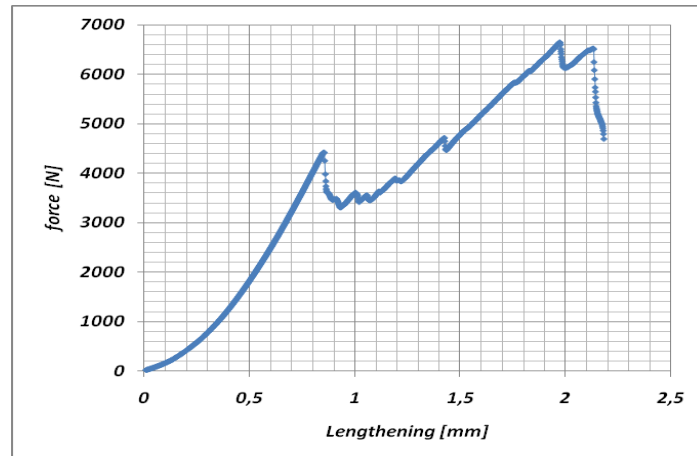


Figure 8 Curve of flexural strength third point of the specimen reinforced by the composites on two side surfaces.

The results show that the reinforced materials present more reliable mechanical properties to those of the mortar alone within the meaning of the inflection strength 3 points. However, from the mechanical behavior, each type gives a specific behavior.

For the reinforcement by a layer of the resin on a lower side surface, the force applied at the time of the inflection creates constraints which will be transmitted towards the three following zones:

- Interfacial zone resin mortar;
- The layer of the resin;
- Interior of the specimen.

The force was transferred initially towards the specimen in accordance to its length, which can also be seen by its lengthening. This last, resists thanks to the layer of resin which him confer rigidity higher than that of mortar without repair.



Continuously, this opposition will transmit the force towards the interfacial zone resin-mortar, knowing that the force of adherence of the resin is of an order of 3 MPa.

As the force applied increases, these constraints will be localized on the level of the weakest zone (the vertical plan which passes through the higher support). At the moment where the force is higher than that of cohesion of the resin on the level of the axis of intersection between the latter and the plan of the weak zone, there will be a bursting of the test-tube in two separate parts starting from the zone of plan specified already.

The addition of another layer of resin on the higher side face eliminates the effect against lengthening, due to this material, The weak increase in maximum force to the inflection (12.66 %) is a clear reason showing that the resin plays its typical role, especially, when its opposed to the bending strain [27]. (see Fig. 9 and Fig. 10)

The addition of a composite a fold on lower surface provides a maximum loading of 5100 N, which corresponds to the total wrenching of this layer starting from 4200 N with a lengthening of 10 mm. Wrenching starts without having a shearing of composite and characterized by a bending strength about the order 133,21 MPa. (Fig. 10)

The addition of another layer of composite on the upper surface eliminates these influences on lengthening and wrenching starts from 4300 N. This latter is clearly appeared on the road base and increased the total biting force up to 6400 N. (Fig. 9)

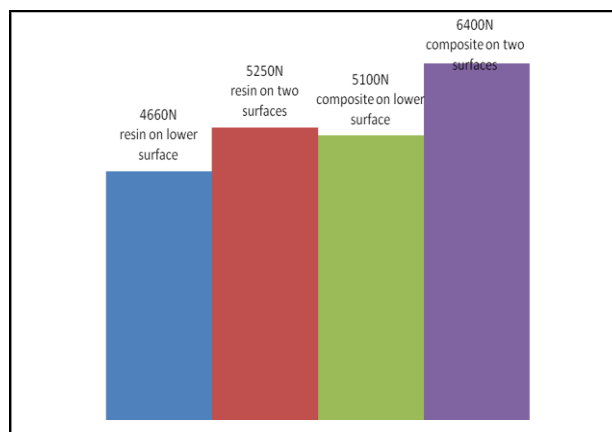


Figure 9 Histogram showing the maximum load of specimen reinforced after damage 90 %

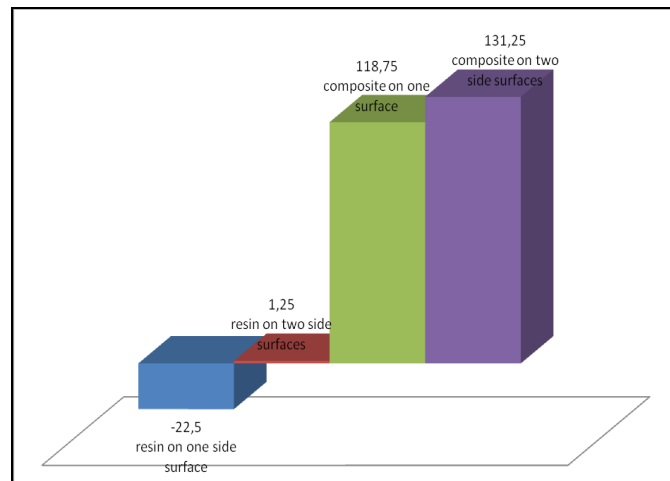


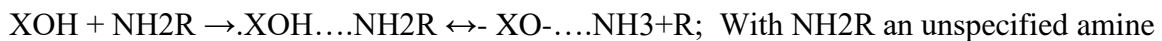
Figure 10 Histogram showing the elongation in % of the specimen reinforced after damage

### 3.3 Microstructural study of the interfacial zones (resin-cementitious matrix)

According to the literature, many types of interactions are likely to be established on the interface between the epoxy adhesive and the cementing substrate: specific interactions of acid-base type or hydrogen. Indeed, cementing surfaces can be considered as oxidized surfaces, due to the presence of silicates. The oxides on the surface could then interact with polar organic compounds by an acidic or basic mechanism [28-29].



With X = structure silicates subjacent, HOR an acid



The most probable reaction which can occur between an epoxy adhesive and the cementing medium is the attack of the epoxy cycles by OH<sup>-</sup> ions generated from the hydration process of cement [29]. Recently, many studies have been conducted on the durability and alkali resistance of glass fibers of reinforced concrete [30, 31]. However, the long-term decline of the properties of these composites has been reported later [30]. The chemical attack on glass by the alkaline cement environment and the growth of hydration products such as calcium hydroxides, in between the filaments in the strand have been pointed out as the main reason in evaluating durability of the GFRC mechanical properties [32-36].

The following images of interface resin-mortar under the electron microscope with sweeping (SEM) are shown in (Fig.11 and Fig.12)

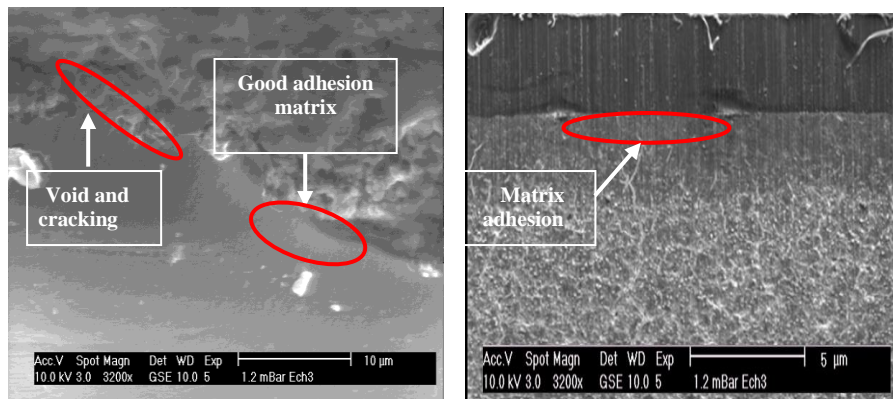


Figure 11 Te images of the resin-mortar interface by the SEM

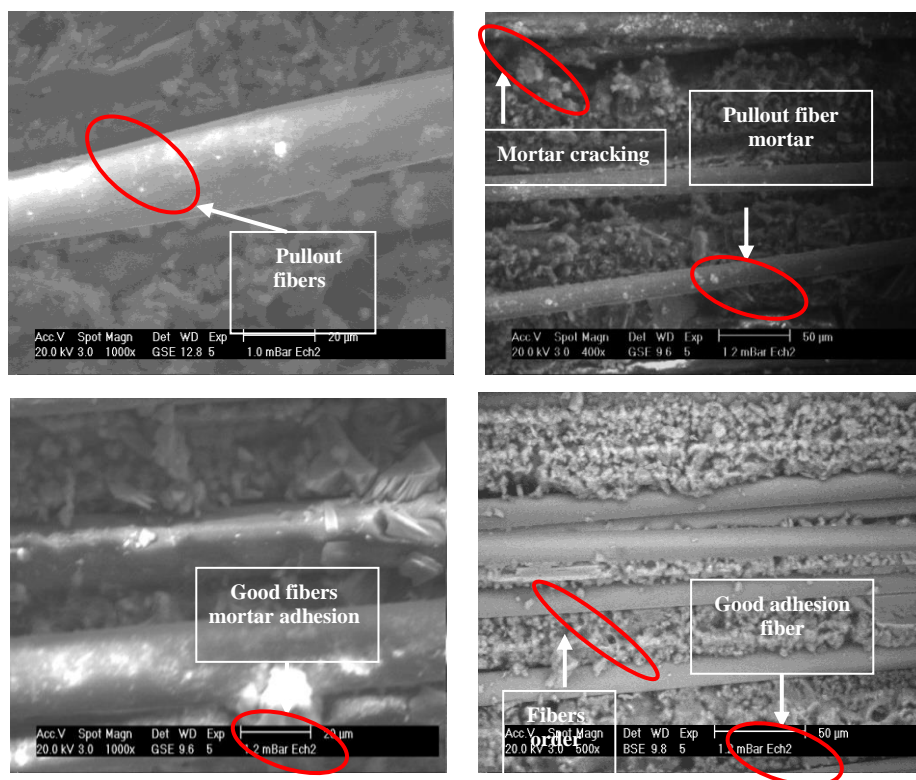


Figure 12 Series of the images of the Glass fiber-mortar by the SEM

The images present a zone of interference between the both materials resin-mortar, this accouchement can return to the one of the following causes [36-40]:

- Mechanical interaction (mechanical of materials put in contact).
- Chemical interaction by the formation of covalent or ionic chemical bonds between the resin and the cement.
- Electrostatic interaction.
- Thermodynamic interaction (the phenomenon of damping): translated by the aptitude of the adhesive to create cross-links of Vander Waals or of the type acid-bases (“hydrogen” bridges) with the mortar.

## 4 Conclusion

This investigative study mainly provides a clear experimental data on the influence of reinforcement cementitious material using the resin or composite resin- glass fiber, watch that, and its mechanical behaviors after subjecting to loading up to 90 %. The following conclusion can be drawn from the obtained results as follows:

1- Reinforcement by a layer of resin on lower side surface, an Increase in rigidity and the bending strength of 58 % compared to those of control specimens (not damaged), has been noted. Also, more smooth and impermeable surface has been obtained.

2- Reinforcement by a layer of resin on two side surfaces can be favourite the elimination the influence from the resin on rigidity and have improved the strength by increasing the bending strength of 73 %. Also, this method can be making two surfaces smooth impermeable thus resistant.

3- Reinforcement by composite resin-fiber, it can be reported:

a). The behavior with respect to the action of inflection translates by the wrenching of the layer of composite as the load increases until takeoff total around 5100 N for a layer and 6400 N for the two layers. That makes it possible to increase considerably the safety of our constructions, by eliminating the brutal effect at the intrinsic time of destruction (seism, explosion... etc.).

b). On the external level, these composites give an esthetic aspect par excellence, and give impermeability which is very wished for a construction of quality within the meaning of resistance to the chemical attacks.

This study makes it possible to quote qualitatively and quantitatively the influence of various stackings on the mechanical behaviors, primarily with the inflection, which will have an application on the reinforcement of the walls, and on their esthetic aspects.

In the seismic areas, it is essential to isolate the intrinsic effect of the headings from the ground on the walls in order to avoid the accidents, which can occur in a very short time, in particular, in the public buildings (schools, hospital, quote them university,... etc), the use of glass fibers and of resin is a good and recommended solution to reinforce the walls of buildings.

## 5 Reference

- [1]. Jain S., Chellapandian M., Prakash S. S. (2017). Emergency repair of severely damaged reinforced concrete column elements under axial compression: An experimental study, *Construction and Building Materials*, 155 751–761.
- [2]. P. Azarsa, R. Gupta. (2018). Specimen preparation for nano-scale investigation of cementitious repair material, *Construction and Building Materials*, *Micron*, 107 43–54.
- [3]. A. Irene Ortega, Teresa M. Pellicer, Jose M. Adam, Pedro A. Calderón. (2018). An experimental study on RC columns repaired on all four sides with cementitious mortars, *Construction and Building Materials*, 161 53–62.

- [4]. M. Elghazy, A. El Refai, U. Ebead, A. Nanni. (2018). Post-repair flexural performance of corrosion-damaged beams rehabilitated with fabric-reinforced cementitious matrix (FRCM), *Construction and Building Materials* 166 732–744
- [5]. American Concrete Institute (ACI). (1995), *Building Code Requirements for Reinforced Concrete*. Detroit, MI.
- [6]. J. Castro and A. E. Naaman, (1981) *Cement Mortar Reinforced with Natural Fibers*, *ACI Journal*, January
- [7]. Saadatmanesh, H. & Ehsani, M.R. (1990). *Fiber Composite Plates Can Strengthen Beams*, *Concrete International*, March, pp. 65-7 1.
- [8]. Meir, U. and Kaiser, H. (1991). *Strengthening Structures with CFRP Laminate*, *Proceedings of Advanced Composite Materials in Civil Engineering; Structures*, ASCE, Las Vegas, Nevada, pp. 224- 232.
- [9]. Ross, C.A., Jerome, D.M. and Hughes, M.L. (1994). *Hardening and Rehabilitation of Concrete Structures Using Carbon Fiber Reinforced Plastics (CFRPL Final Report, Wright Laboratory Armament Directorate) Eglin Air Force Base, Florida*.
- [10]. Ritchie, P.A. (1988). *External Reinforcement of Concrete Beams Using Fiber Reinforced Plastic*, Thesis, Leigh University.
- [11]. Ghaleb, B.M. (1992). *Strengthening of Damaged Reinforced Concrete Beams by External Fiber Glass Plates*, Thesis, King Fahd University of Petroleum and Minerals, Saudi Arabia.
- [12]. PCI committee on glass fiber reinforced concrete panels. (1981). *Recommended practice for glass fiber reinforced concrete panels*. *PCI J.*, 26(1):25-93.
- [13]. Gonilho-Pereira C., Faria P., Figueiro R., Vinagre P., Martins A., (2011). *Cement based fiber-reinforced mortar: the fiber influence on the mortar performance*, 6th Congresso Luso-Moçambicano de Engenharia CLME'2011, Maputo, 29 August - 2 September.
- [14]. Puertas, F., Amat, T., Fernandez-Jimenez A., and Vazquez, T., (2003). *Mechanical and durable behaviour of alkaline cement mortars reinforced with polypropylene fibres*, *Cement and Concrete Research* 33 pp. 2031–2036.
- [15]. Toledo, R.D., and Sanjuan, M.A., (1999). *Effect of low modulus sisal and polypropylene fibers on the free and restrained shrinkage of mortars at early age*, *Cem. Concr Res* 29 pp. 1597– 1604.
- [16]. ACI 544.1R-96, (1996) *State-of-the-art report on fiber reinforced concrete*, Farmington Hills, Michigan: American Concrete Institute
- [17]. Aydin, A.C.( 2007). *Self compactability of high volume hybrid fiber reinforced concrete*. *Const. Build. Material*;21, 1149-1154.
- [18]. Shah, S. P. and Naaman, A. E. (1976). *Mechanical properties of glass and steel fiber reinforced mortar*. *ACI Journal*; 73(1), 50-53.
- [19]. Nataraja, M. C, Dhang, N. & Gupta, A. P. (1999). *Stress-strain curves for steel fiber reinforced concrete under compression*. *Cement & Concrete Composite*; 21, 383-390.
- [20]. Okamura, H. & Ouchi, M. (2003). *Self-compacting concrete*. *J. Adv. Concr Technol*,1(1), 1-15.
- [21]. Gang, L. Wang, K & Rudolphi, T.J. (2008). *Modeling rheological behavior of highly flowable mortar using concepts of particle and fluid mechanics*. *Cem. & Conc. Comp.* 30, 1-12.
- [22]. Domene, P. L. & Jine, J. (1999). *Properties of mortar for self-compacting concrete*. *Proceedings of the 1st international RILEM symposium on self-compacting concrete*, 109-20.

- [23]. Khayat, KH , Morin, R. (2002). Performance of self-consolidating concrete used to repair parapet wall in Montreal. Proceedings of the first North American conference on the design and use of self-consolidating concrete, 475-481.
- [24]. Zhou, F. P., Barr, B. I. G. & Lydon, F. D. (1994) Fracture mechanical properties of high strength concrete with varying silica fume content and aggregates. *Cement & Concrete Research*, 25(3), 543-52.
- [25]. Carlach D., Hemery Y. (2002). Etude prospective sur le collage en France, Digitp/Simap, décembre, 237 pages <http://www.industrie.gouv.fr/pdf/collage.pdf>
- [26]. A. Finley. (1999). Notice technique, Les résines époxydes EPONAL (sols industriels, étanchéité, réparations, collages), éditions mars.
- [27]. Bardonnat P. (1992). Résines époxydes: composants et propriétés. *Techniques de l'ingénieur, traité de Plastique et Composites*,
- [28]. Mays G., Hutchinson A.R. (1992). *Adhesives in Civil Engineering*, Cambridge University Press. Cambridge (UK),.
- [29]. Toutanji H., Ortiz G. (2001). The effect of surface preparation on the bond interface between FRP sheets and concrete members, *Composite Structures* (53), 457-462.
- [30]. Maugis D., Barquins M. (1986). Adhésion, collage et mécanique de la rupture, Colloque RILEM Adhesion between polymers and concrete – bonding, protection, repair, 16-19 Septembre Aix en Provence, 41-54.
- [31]. Pang M., Yang S., Zhang Y.. (2011). Experimental study of cement mortar-steel fiber reinforced rammed earth wall, *International Symposium on Innovation & Sustainability of Structures in Civil Engineering*, Xiamen University, China.
- [32]. Mc. N. Shaw I. (1989). Interactions between organic polymers and cement hydration products,, PhD thesis of Birmingham University.
- [33]. Neves M.I., Chabut M., Perruchot C., Chehimi M.M., Benzarti K. (2004). Interfacial interactions of structural adhesive components with cement pastes: studies by inverse gas chromatography (IGC), *Journal of Applied Surface Science* (238),523-529..
- [34]. Majumdar, A. J. (1975) Properties of fibre cement composites, *Fibre Reinforced Cement and Concrete*, RILEM Symposium, 279-313.
- [35]. Lerner, L. J., Speakman, K. and Majumdar, A. J. (1976), Chemical interaction between glass-fibres and cement, *J. of Non-Crystalline Solids*, 20, 43-74.
- [36]. Bijen, J. (1983). Durability of some glass fiber reinforced cement composites. *ACI journal*, July-August 305-311.
- [37]. Leonard, S. and Bentur, A. (1984) Improvement of the durability of glass fiber reinforced cement using blended cement matrix. *Cement and concrete research* 14:717-728.
- [38]. Bentur, A. (1986). Aging process of glass fibre reinforced cements with different cementitious matrices. *RILEM symposium FRC 86*, vol. 2, paper 7.3.
- [39]. Shah, S.P., Ludirdja, D., Daniel, J.I., Mobasher, B. (1988). Toughness-durability of glass fiber reinforced concrete systems. *ACI materials journal*, September-October 352- 360.
- [40]. Li, Z. and Mobasher, B. & Shah, S.P. (1991). Evaluation of interfacial properties in fiber reinforced cementitious composites. *Fracture processe in concrete, rock and ceramics*, J.G.M. Van Mier, J.G. Rots, A. Bakker, RILEM, E. an F.N. Spon. Pp. 317-326,

## Effect of Fiber Distribution on the Mechanical Behavior in Bending of Self-Compacting Mortars

Lynda Kheddache <sup>1</sup>, Kahina Chahour <sup>1,2</sup> and Brahim Safi <sup>1,\*</sup>

<sup>1</sup> Research Unit; Materials Process and Environment, Faculty of Technology, University M'Hamed Bougara of Boumerdes, 35000, Algeria

<sup>2</sup> Université Mouloud Mammeri de Tizi Ouzou, Algeria,  
Department of Civil Engineering

e-mail: l.kheddache@univ-boumerdes.dz, kahina.chahour@umt.dz, safi\_b73@univ-boumerdes.dz

### Abstract

The purpose of this work is to assess the steel fiber distribution effect on physical and mechanical properties of self-compacting mortar. An experimental study was conducted to see the fiber distribution during the implementation of self-compacting mortars that are fluid and on mechanical behavior in bending tensile strength. A method of placing self-compacting mortar in the molds has been developed to highlight the distribution of fibers in the cementitious matrix. The mortars are placed in prismatic molds in three layers. The amount of steel fibers differs from one layer to another. A total quantity of 90 kg /m<sup>3</sup> was distributed in prismatic molds of dimensions 40x40x160 mm<sup>3</sup>. Straight and hooked ends steel fibers were used. The characteristics of mortars containing both types of fibers in the fresh and hardened state were measured and compared to those of self-compacting mortar without fibers. The pouring by layer allowed us to deduce that the distribution of metallic fibers has a significant effect on the hardened properties of the mortar. Indeed, the mechanical strength of the fiber-reinforced mortar depends on the nature and distribution of fibers in the cementitious matrix (mortar). A gain in bending tensile strength of 71.83% was recorded for self-compacting mortars elaborated with hooked end fibers and 52.11% for those containing straight steel fibers. Indeed, mortars containing entirely the same dosage of steel fibers (90 kg/m<sup>3</sup>) have a bending tensile strength that varies according to the fibers dosage by layers. Mortar samples with higher fiber content in the lower layer have a higher bending tensile strength than other samples with a higher fiber layer in the middle or layer above. However, it should be noted that steel fibers with hooks are much more effective than those without hooks. Indeed, the effect of fiber distribution is more significant for fibers without hooks because the hooks can slow down the movement of the fibers during the pouring of the mortar. The variation of the dosages per layer generated a difference in the deflection values for the mortars. The deflection is much higher for fiber-reinforced mortars (with hooks) compared to fiber-reinforced mortars without hooks.

**Keywords:** Self-compacting mortar, steel fiber, distribution, fluidity, bending tensile strength, strength gain

## 1 Introduction

In recent years, several researches have been devoted to the development of the characteristics of ultra-high performance fiber concrete (UHPFC). This material allowed the construction of

several structures with complex architecture around the world [1-3]. Due to its durability over time, it is often used in the manufacture of prefabricated elements for use in the repair or replacement of bridges in countries with severe climatic conditions [4-7]. It is characterized by exceptional mechanical properties [8-10]. These properties are noted on the weak cracks recorded when the material is subjected to shrinkage stresses [11-12], its behavior to the phenomenon of creep [13-14] and the resistance which it can present in the event of impact [15]. They are developed according to the chosen composition. In general, the optimization of its granular structure favors the increase in compressive strength which sometimes reaches 150 MPa [16-18]. The use of steel fibers brings ductility, increases the tensile strength and reduces the size of cracks during the solicitation [19]. The nature, size and content of steel fibers are factors which have a great influence on the mechanical behavior of UHPC. Huy Hoang et al. [20] have experimentally examined the effect of six types of steel fibers incorporated in a UHPC with different volume fractions. Three types of straight fibers had a length / diameter (L / D: 13mm / 0.2mm; 20mm / 0.2mm and 25mm / 0.3mm). Two wavy types were of (L / D: 9 mm / 0.12 mm; 12 mm / 0.18 mm). The last type has a hooked end and dimension (L / D: 30mm / 0.55mm). The results of the pullout strength test indicate that the recorded pullout stresses were high for the wavy and hooked fibers. The use of six types of fibers enables to have different resistances from one type to another. The authors concluded that the use of 1.75% hooked ends fibers makes to obtain higher flexural and direct tensile strength which are respectively of 22.09 MPa and 10.31 MPa. In the same context, Haber et al. [21] also prepared six variants of UHPC containing six types of fibers of different geometries and dosages. The results obtained during the pullout test, resistance to compression, bending and traction varied according to the type and size of the fibers used. Gangwar et al. [22] conducted an experimental study on the influence of the dosage and size of fibers in a UHPC. Two sizes of different short and long straight steel fibers of dimensions (L / D = 6mm / 0.20mm and 13mm / 0.2mm) were mixed to manufacture a UHPC with a percentage of fibers ranging from 0 to 4%. The results indicated that the more the fiber content increases the more the compressive, bending and tensile strengths increase.

The orientation and distribution of these steel fibers in the cement matrix is another very important parameter to take into account to obtain a material with better mechanical performance. Several studies have been presented to determine the exact parameters that influence the orientation and distribution of fibers in a UHPC. Duque and Graybeal [23] investigated the influence of fiber orientation on the mechanical tensile response of UHPC. The authors used an image analysis technique that provided them with strong evidence of the impact of the flow pattern and the casting process on the actual distribution of fiber orientation within a structural element. They resulted in a strong influence of the orientation of the fibers not only on the post-cracking response of UHPC but also on the first crack stress. Huang et al. [24] also looked at the effect of fiber orientation on the mechanical properties of UHPC. Mixtures containing different water / binder ratios and three volume fractions of steel fibers were formed. The authors developed an L-shaped device with a narrow horizontal channel to control the flow of the fresh mixture. This mixture was poured into this device placed on one side of the prismatic mold. This method of placing concrete in molds has improved the orientation coefficient and the flexural strength of concrete shaped. These authors recently also studied the wall effect on the orientation of fibers and the flexural strength of a UHPC [25]. Using the same device, they prepared prismatic molds with 2% of steel fibers. Once cured, samples of equal size were cutted from various locations on the test



pieces. For each sample, the flexural strength and orientation of the fibers were measured and observed using image processing technique. The results obtained show that a better orientation of the fibers and higher bending performance were obtained near the limits of the formwork due to the restriction effect on the rotation of the fibers. The authors concluded that the wall effect has a great influence on the orientation of the fibers in the cement matrix of UHPC. Wang et al. [26] studied the influence of rheological properties on the distribution of steel fibers in a UHPC. They concluded that the distribution of the fibers along the depth of the test pieces depends mainly on the rheological parameters of the fresh mixture, in particular on the flowability which varies according to the variation of the volume fraction in steel fibers of the mixtures. Lu et al. [27] studied the theoretical effect of the thickness of the elements on the behavior of cement composites compared to laboratory data obtained from small samples. Their conclusion is that a reduction factor dependent on the thickness of elements influencing the mechanical properties (mainly the tensile strength and ductility) must be taken into account in the design of real structural elements.

Some authors have mentioned the effect of placing concrete in the mold on the orientation and distribution of the fibers. Kang et al. [28] have led research on the influence of concrete placement in molds on flexural strength using the image processing technique. The concrete was placed in prismatic molds in two different methods. The first method is to put it parallel to the longitudinal direction of the mold and the second was to place it transversely to the longitudinal direction. It has been found that implementation of concrete parallel to the longitudinal direction of the mold, has a benefic effect on the distribution of the fibers during flow concrete. The latter strongly affect the ultimate flexural strength.

Song et al. [29] in their research used fresh concrete flow parameters to describe the effect of steel fiber distribution and orientation on the mechanical properties of UHPFRC. Two methods of placing concrete in prismatic molds were tested. The first is to pour the concrete on one side of the mold and let it flow; the second is to place it randomly in the mold. They demonstrate that the flow parameters of fresh concrete when placing concrete through one side of the mold significantly influences the distribution and orientation of the fibers in the cement matrix, such as the direction of flow, the flow distance, fiber content and wall effects. They explain that the flow process for fresh UHPC can be divided into three periods: a period of disorder, a period of stability and a new period of disorder. During the stable period, all fibers tend to line up along the flow direction of fresh UHPC and simultaneously improve the flexural strength of UHPC.

Although several works carried out on the fiber-reinforced concretes, however it is necessary to make more research to deal the implementation of fiber concrete in the mold of structural elements. This parameter is essential given its direct influence on the tensile strength and bending of fiber-reinforced concrete. Indeed, it is important to spread the steel fibers well in the cementitious matrix (concrete) in order to allow them to act effectively in the face of external stresses. These fibers are most effective when used in self-compacting concrete fluids, in particular mortars [30-34]. According to the literature, there is little work dealing the problem of the fibers distribution within the concrete during the Implementation of the latter. From a practical point of view, a poor distribution of fibers can have an important effect on the mechanical behavior of fiber-reinforced concrete; this is the main objective of this study.

This article aims to expose a method of placing self-compacting mortars in prismatic molds, which allows to efficiently distribute the steel fibers in the cement matrix and to avoid the effects of walls. This method aims to highlight the effect of the distribution of steel fibers on

the mechanical behaviour of self-compacting mortars, in particular the bending tensile strength.

## 2 Experimental Program

### 2.1 Raw materials

The materials used in this study purposes are described in this section. Portland cement (CEM II/B 42.5 N) and marble powder were used as a binder. The powder marble is obtained from crushed wastes of the white marble quarry of north-east of Algeria. The used sand is natural river sand with a maximum aggregate size of 4 mm. The sand was first screened to remove large grains, then washed and dried in an oven at 105°C during 24 hours. Chemical characteristics of binder mixture and physical characteristics of sand are given in Table 1.

A polycarboxylate based superplasticizer was necessary to obtain a self-compacting mortar with a low water / binder ratio. The amount of superplasticizer used was set at 9.4 kg /m<sup>3</sup> and kept constant for all mixtures.

Steel fibers with hooks at the ends were cutted into straight fibers T1 and hooked at one end T2. The initial length of these fibers is 30 mm. Straight T1 and hooked T2 steel fibers (Figure 1) were chosen and used in this study. The physical characteristics of the steel fibers are shown in Table 2.

Table 1 characteristics of Portland cement, marble powder and natural sand

	Portland Cement	Marble Powder	Natural sand
<i>Chemical composition [%]</i>			
CaCO <sub>3</sub>	-	99.05	-
CaO	62.9	54.86	-
P.C	-	44.26	-
MgO	1.90	1.03	-
SiO <sub>2</sub>	20.7	0.15	-
Al <sub>2</sub> O <sub>3</sub>	4.75	0.08	-
Fe <sub>2</sub> O <sub>3</sub>	3.75	0.04	-
SO <sub>3</sub>	1.98	-	-
Na <sub>2</sub> O	0.90	-	-
<i>Mineralogical composition [%]</i>			
C <sub>3</sub> S	55	-	-
C <sub>2</sub> S	21	-	-
C <sub>3</sub> A	06	-	-
C <sub>4</sub> AF	12	-	-
<i>Physical properties</i>			
True density	3.10	-	2.47
apparent density	-	-	2.68
Specific surface (cm <sup>2</sup> /g)	3720	3890	-
Fineness modulus	-	-	3.21
Sand equivalent (%)	-	-	83
Absorption (by weight) (%)	-	-	0.79

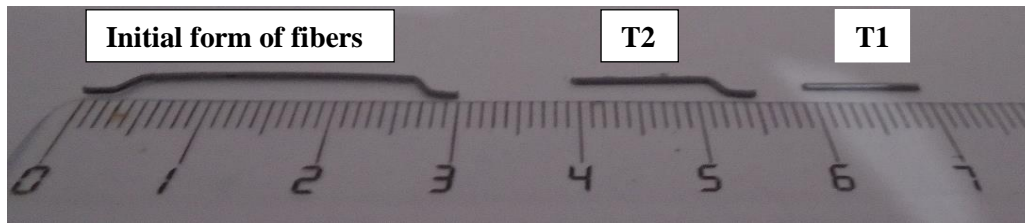


Figure 1: Shape and size of used fibers (T1: Straight; T2: With hooked ends)

Table 2: Physical characteristic of steel fibers

Type	Length (mm)	Diameter (mm)	Young's module (GPa)	Tensile Strength (MPa)
T1 : Straight	10	0.55	200	1 345
T2 : Hook at one end	15	0.55	200	1 345

## 2.2 Mix proportions of self-compacting mortars

The self compacting mortar composition studied retained in this work is that obtained by the method of concrete equivalent mortar (CEM) developed by Schwartzentruber [35]. Table 3 shows the mixes details of control mortar (M0) with ratio (F/C = 0.10) is kept constant. The mixing protocol was kept constant for all mortar mixtures.

Ten variants of fiber-reinforced mortars for each type of fiber were prepared. Three specimens of dimension  $40 \times 40 \times 160 \text{ mm}^3$  were made for each mixture by varying the quantity and distribution of the steel fibers. The mixture details of the variants elaborate is illustrated in Table 4. Initially, three mixtures M20, M30 and M40 containing 20, 30 and 40  $\text{kg/m}^3$  of steel fibers respectively were prepared.

Table 3: Details of self-compacting mortar mixtures

Component	M0
Cement [ $\text{Kg/m}^3$ ]	663
Marble Powder [ $\text{Kg/m}^3$ ]	66
Natural Sand [ $\text{Kg/m}^3$ ]	1371.4
Water [ $\text{L/m}^3$ ]	252
Superplasticizer [ $\text{L/m}^3$ ]	9.4

Table 4: Mixture details of all studied mortars (%)

Variants	Cement	Sand	MP	SP	Steel fiber	Water
M0	28.07	58.07	2.79	0.40	-	10.67
M20	27.83	57.58	2.77	0.40	0.84	10.58
M30	27.71	57.34	2.76	0.40	1.25	10.54
M40	27.60	57.10	2.75	0.40	1.66	10.49
M234	27.04	55.94	2.69	0.38	3.67	10.28
M243	27.04	55.94	2.69	0.38	3.67	10.28
M324	27.04	55.94	2.69	0.38	3.67	10.28
M342	27.04	55.94	2.69	0.38	3.67	10.28
M423	27.04	55.94	2.69	0.38	3.67	10.28
M432	27.04	55.94	2.69	0.38	3.67	10.28

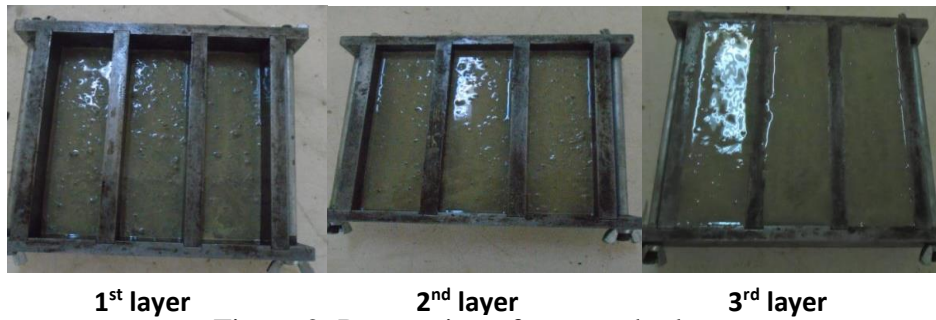
### 2.3 Preparation and curing of samples, test methods

Three specimens of dimension  $40 \times 40 \times 160 \text{ mm}^3$  were made for each mixture by varying the quantity and distribution of the steel fibers. The mixture details of the variants elaborate is illustrated in Table 4. Initially, three mixtures M20, M30 and M40 containing 20, 30 and 40  $\text{kg/m}^3$  of steel fibers respectively were prepared. The fluidity in the fresh state for the variants M0, M20, M30 and M40 was measured.

Next, six variants containing the same amount of  $90 \text{ kg/m}^3$  fiber were prepared by varying the amount of fiber per layer (Figure 2). The prismatic molds were divided into three equal layers (Figure 3) and each layer contained a different amount of fiber compared to the other as shown in Table 5. Finally, we obtained a M0 mortar without fibers, M20, M30 and M40 mortars containing respectively amounts of fibers the following 20, 30 and  $40 \text{ kg/m}^3$  and six variants M234, M243, M324, M342, M423 and M432 of fiber-reinforced mortars contains  $90 \text{ kg/m}^3$  divided into three layers.

**Fresh properties:** After each preparation, the fluidity of the freshly prepared mortar was evaluated to ensure the mini-slump flow diameter suitable for self-compacting concrete according to EFNARC [36].

**Hardened Properties:** For hardened properties of mortars, prismatic ( $40 \times 40 \times 160 \text{ mm}^3$ ) samples were manufactured for each mixture. One day after casting, samples were stored in water under  $21 \pm 1^\circ\text{C}$ . The bulk density of studied mortars has been measured using the mass/volume relationships according to EN standard [37]. The bending tests under load in three points were carried out on the mortars studied at 28 days of maturation according to the European Standard EN [38].



1<sup>st</sup> layer                      2<sup>nd</sup> layer                      3<sup>rd</sup> layer  
 Figure 2: Preparation of mortars by layer

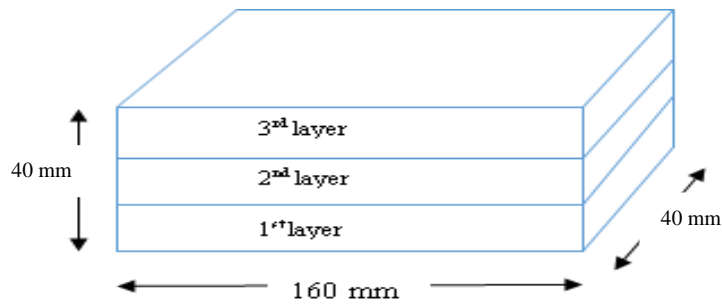


Figure 3: Preparation of mortars by layer in prismatic molds

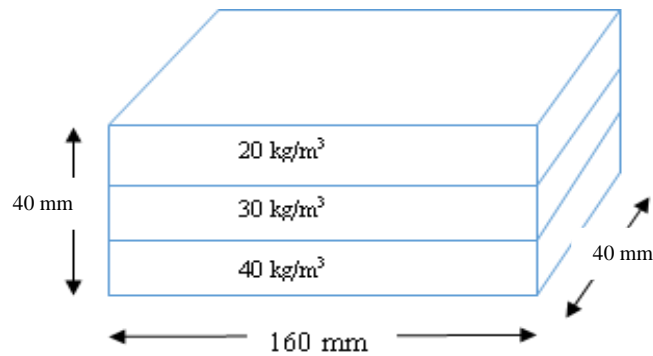

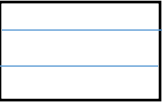


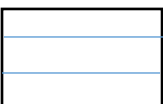



Figure 4: Dosage variation of fibers by layer (Example **M432**)

Table 5 gives all mortar variants having the pouring by layer as well as the quantities of fibers in each layer.

Table 5: Dosage by layer and pouring fiber-reinforced mortars

Variants	Quantity of steel fiber (kg/m <sup>3</sup> )		
	1 <sup>st</sup> layer	2 <sup>nd</sup> layer	3 <sup>rd</sup> layer
40 30 20  <b>M234</b>	20	30	40
20 30 40  <b>M432</b>	40	30	20
20 40 30  <b>M342</b>	30	40	20
40 20 30  <b>M324</b>	30	20	40
30 40 20  <b>M243</b>	20	40	30
30 20 40  <b>M423</b>	40	20	30

### 3 Results and discussion

#### 3.1 Fluidity

Figure 5 illustrates the fluidity of self-compacting mortars prepared with the two types of fibers; straight fibers (T1) and with a fibers end hooked (T2). It is noted that more dosage fiber increases, more the fluidity of mortar decreases. Mortars prepared with the T1 type fibers have better fluidity than those prepared with the second type with end hook. This is explained by the shape of used fibers as well as the presence of hook at ends of the fiber T2. Many research works have shown that the type and end-hooks of steel fibers decrease the fluidity and workability of concretes. Recently, Lee et al. have investigated on the effect of end-hook geometry of steel fibers on the flexural behavior of concrete slabs, three types of hooked-end steel fibers with different end geometries [40, 41]. Indeed during establishment of the mortar, the fibers provided with the hooks brake the flow and decrease the fluidity of the mortar.

Table 6: Flow test result obtained by using the mini-cone

Variants	Spreading in mm	
	T1	T2
M0	195	195
M20	195	189
M30	190	186
M40	187	184

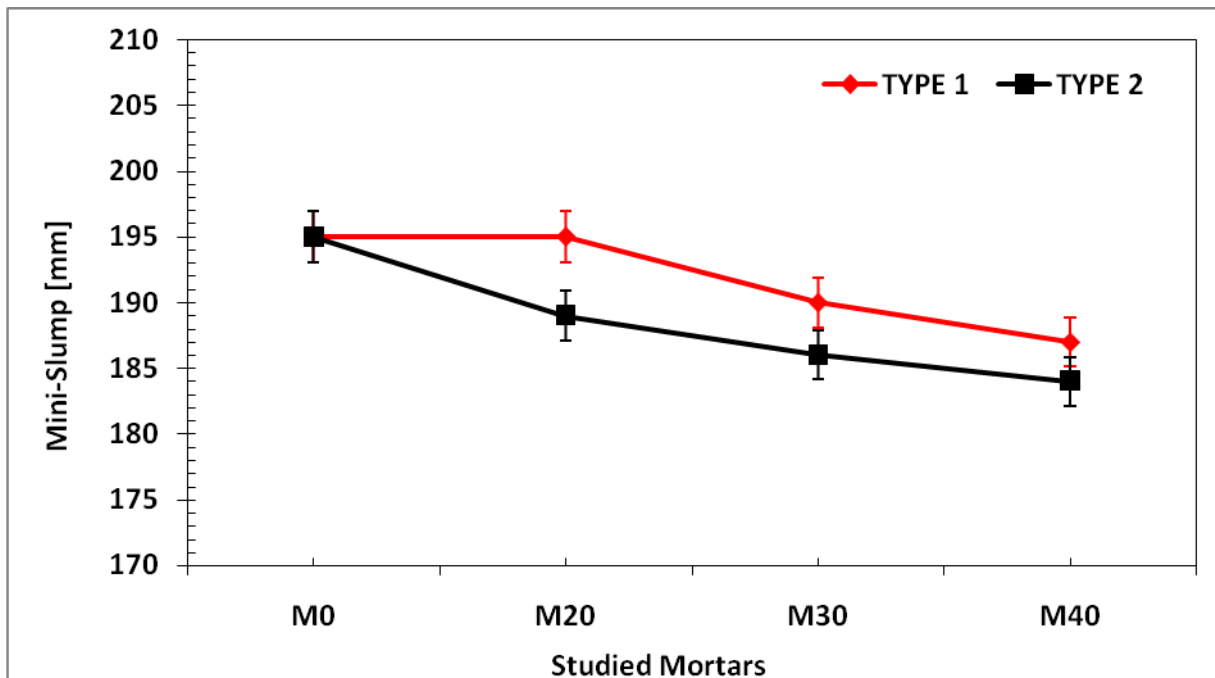


Figure 5: Fluidity of studied mortars

### 3.2 Bulk Density

Table 7 gives the measurement results of apparent density of the studied mortars at 2-days and 28 days of curing age. It was noted that the bulk density has not been changed whatever the curing age but the reinforced mortars with type 2 fibers have a slightly high mass compared to those designed by type 1 fibers. It is explained that the fibers provided with the end hooks favored the compactness of the mortar. It is obvious that the steel fibers increase the bulk density of all mixtures with increasing the fiber content, because of their density. This observation was already verified by several authors [42, 43, 44, 45].

Table 7: Physical properties of the studied mortars

Variants	Bulk density (g/cm <sup>3</sup> )			
	2 d		28 d	
	T1	T2	T1	T2
M20	2.26	2.30	2.28	2.31
M30	2.25	2.30	2.27	2.29
M40	2.29	2.34	2.31	2.35
M423	2.32	2.37	2.34	2.34
M243	2.29	2.40	2.31	2.36
M324	2.28	2.40	2.30	2.37
M342	2.30	2.39	2.31	2.35
M432	2.27	2.39	2.29	2.40
M234	2.27	2.35	2.32	2.35

### 3.3 Bending tensile strength of fiber-reinforced mortars

#### a) Influence of the dosage and types of fibers

Figure 6 show the evolution the bending tensile strength as a function as type and dosage of fibers measured at 28d of age. It can be seen in figure 6 that the bending tensile strength is influenced by the dosage and the type of steel fibers used. The steel fibers increase the bending tensile strength. The more the fiber dosage increases, the more the bending tensile strength increases. From the results obtained, we note that the fiber-reinforced mortars prepare with the type of T2 fibers (end hook) have significantly higher strengths than those produced with the T1 type. The values of the bending tensile strength for the variant M40 containing the type of fibers T1 and T2 are respectively 8.2 and 10.9 MPa.



Table 8: Bending tensile strength of the dosage and type of fiber

Variants	Bending tensile strength (MPa)	
	T1	T2
M0	7.1	7.1
M20	7.7	9.0
M30	7.8	10.1
M40	8.2	10.9

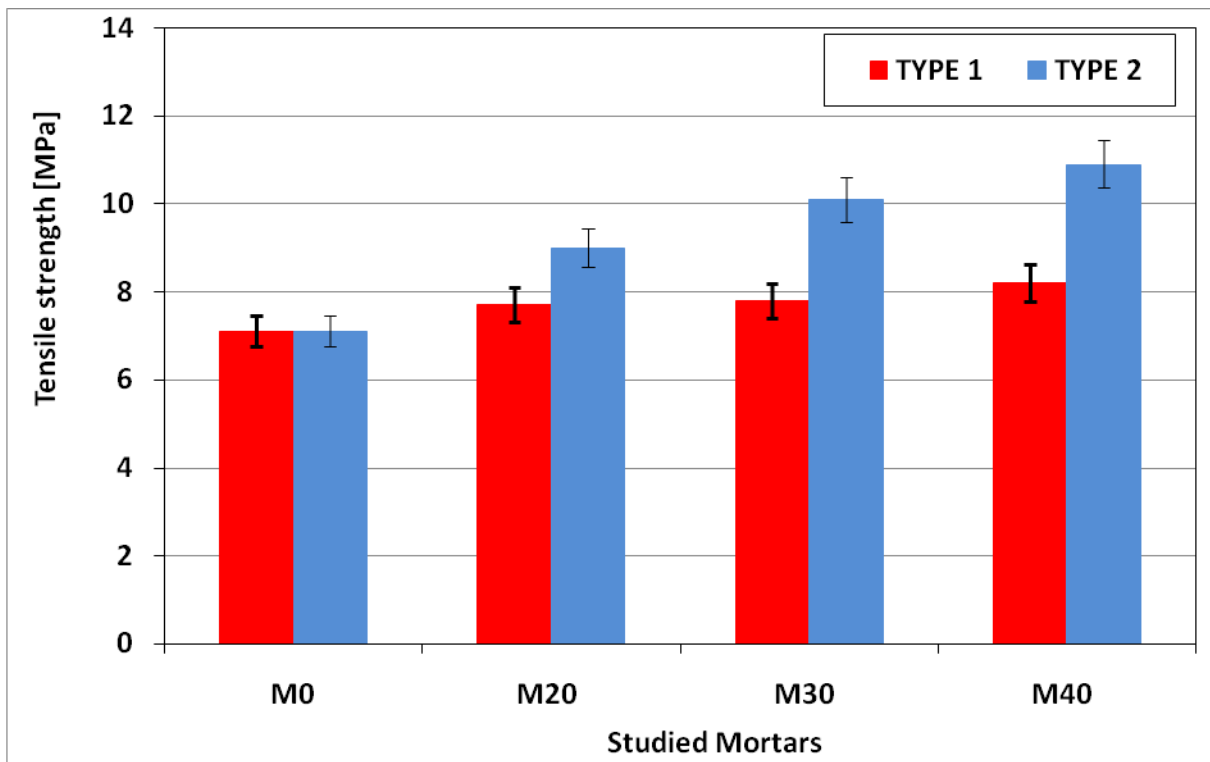


Figure 6: Effect on the bending tensile strength test

### b) Influence of type and distribution of fibers in the mortar

It can be seen in figure 7 that the cement matrices all have the same dosage of steel fibers. However, the bending tensile strength varies as a function of the distribution of the fibers in the cement matrix. For the variants developed with the type of fibers T1, it is noted that for the matrices containing a dosage of 30 or 40 kg/m<sup>3</sup> of fibers in the lower layer of the mold, the resistance is high compared to the other variants with the exception of the M234. This can be explained by the reinforcement with a high percentage of fibers of the tensed area which is at the bottom part of mold. That is to say, the higher the fiber dosage at the bottom part of mold (above 30 kg/m<sup>3</sup>) the more the resistance increases. As for the maximum value of the M234 variant which is 10.7 Mpa this is probably due to the high fluidity of the mortar which

caused the fibers contained in the 40kg/m<sup>3</sup> or 30kg/m<sup>3</sup> layers to descend towards the lower zone of the test piece. This resulted in increased bending tensile strength. For the variants containing the second type of fiber T2, it is found that the values of the resistances are close to each other and much higher compared to the variants elaborate with the type of fiber T1. The bending tensile strength with the type of fibers T2 reaches 12.2 MPa so much said with the type T1 it does not exceed 10.9 MPa. This can be explained by the presence of the hook at the end of the fiber which requires high force and energy to extract it.

Table 9: Bending tensile strength of mortars produced by layer

Variants	Bending Tensile Strength (MPa)	
	T1	T2
M234	10.7	11.2
M432	10.9	11.5
M423	10.4	11.6
M342	9.7	11.8
M243	8.8	12
M324	10.8	12.2

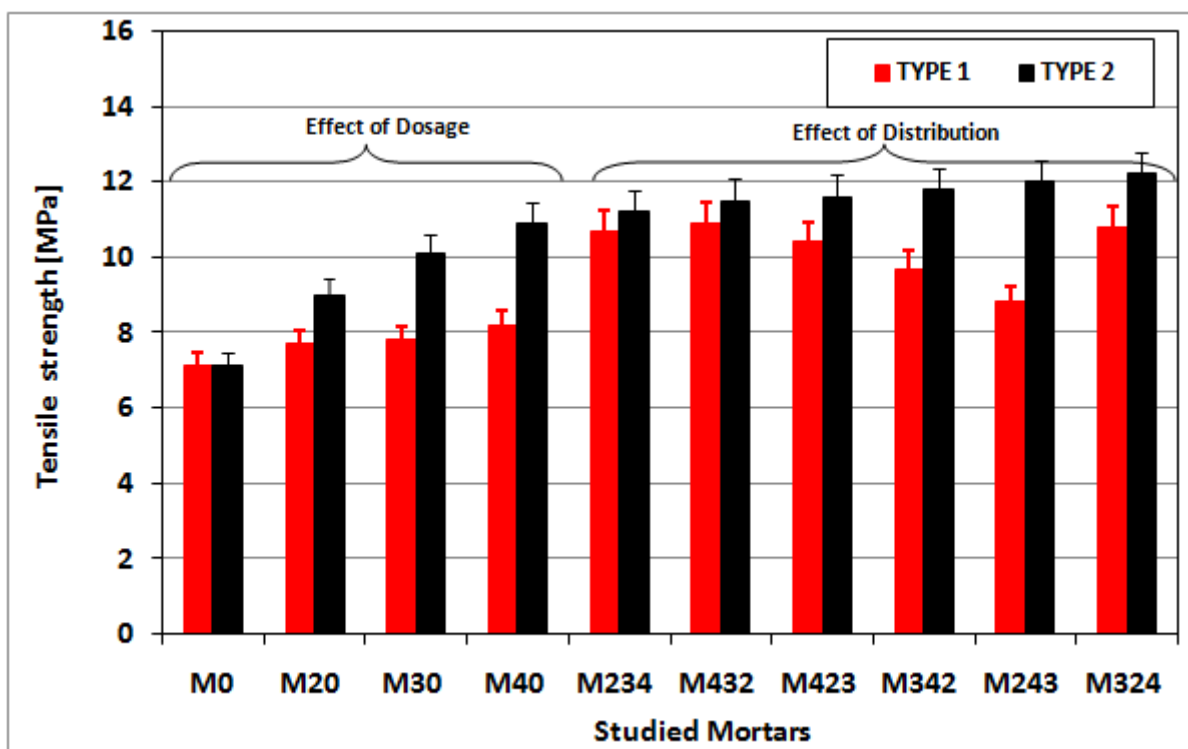


Figure 7: Type and fiber distribution effect on the bending tensile strength of mortars

### c) Gain in bending tensile strength

Figure 8 shows the gain in the bending tensile strength of the fiber-reinforced mortars compared to the mortar without fibers. It is found that the presence of steel fibers improves the resistance. The resistance gain for the M40 variant having a dosage of  $40 \text{ Kg/m}^3$  of steel fibers of type T1 does not exceed 15.49% as long as for the same variant developed with the type of fibers T2, the gain is estimated at 53.52%. For the variants prepared by layer, the gain in strength varies from 23.94 to 52.53% for mortars elaborated with the type of fibers T1 and from more than 57 to 71.83% for the mortars containing the fiber type T2 (end hook). The highest resistance gain is observed for variants M432 and M324 which contain the fiber types T1 and T2 respectively. The variants whose lower layer contains a dosage of high T2 type metallic fibers of 30 or  $40 \text{ kg/m}^3$  have a high bending tensile strength.

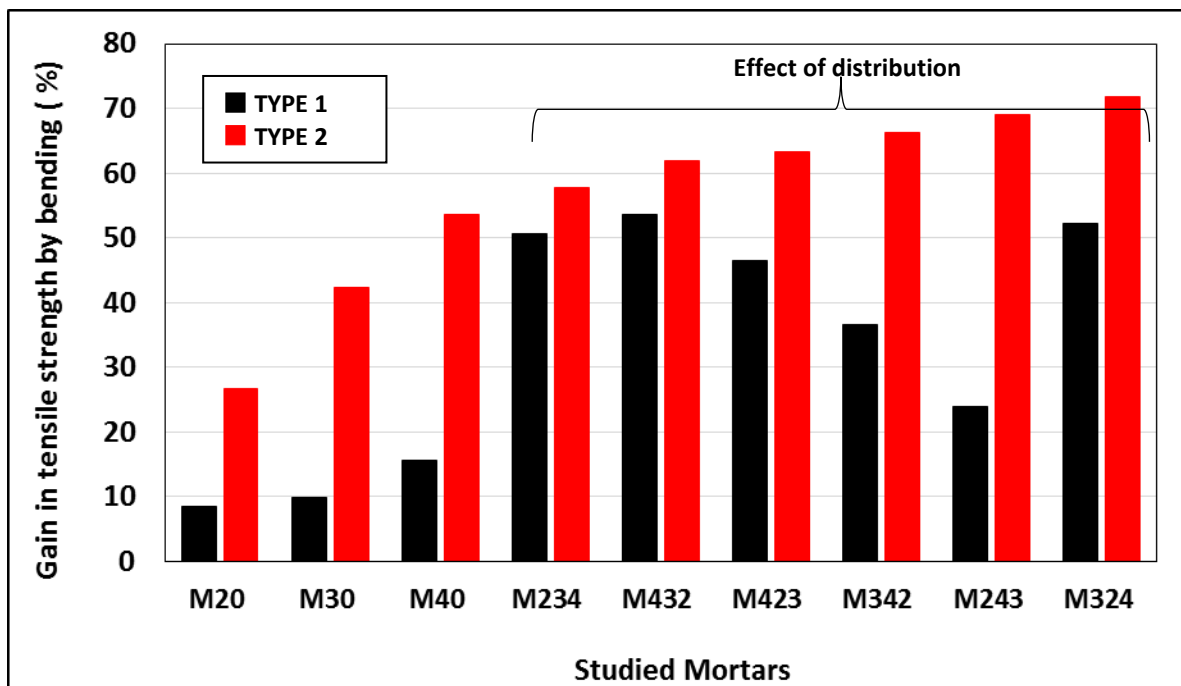


Figure 8: Gain in bending tensile strength as a percentage of fiber mortars made with two types of fibers

### 3.4 Deflection of fiber-reinforced mortars

Figure 9 illustrates the deformation of the prepared mortars, which was measured during the three-point bending tests. The maximum value is 0.44 mm for mortars M20, M30 and M40 and 0.56 mm for variants containing  $90 \text{ kg/m}^3$  of fiber.

It was found that the variants M20, M30 and M40 made using hook fibers have greater deformation than those made with straight fibers. The more the fiber dosage increases, the more the deformation of the hook fiber mortars increases.

The performance of mortars in terms of deformation has been improved by the presence of hooked metal fibers. These results are similar to those obtained by Biao Li et al. [45],

Mahakavi et al. [46] and Malgorzata et al. [47]. These authors have demonstrated the role and effectiveness of dosing and the nature of metallic fibers with hooks to improve the performance of the material.

For mortars made by layer apart from variants M342 and M324 where the deflection value is slightly higher by 0.1 mm for the variants containing straight fibers, the deflection value is greater for the variants containing fibers hook.

The variants containing a quantity of hook fibers of 40 gr in the lower layer M423 and M432 have a deformation of more than 40% than those made with straight fibers. This is explained by the presence of the hook in end of fibers which give more ductility to the mortar.

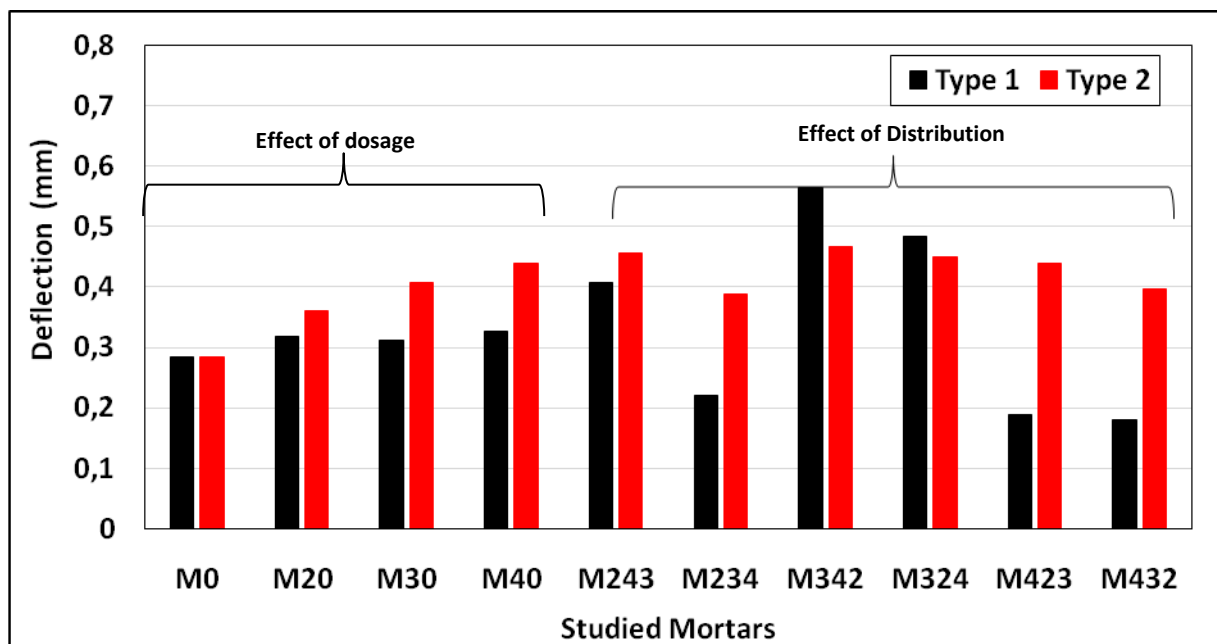


Figure 9: Effect of fiber distribution on the flexural deformation of studied mortars

When the variation of the fiber dosages per layer is applied, different deflection values were recorded. The recorded deflection values are higher for mortars containing hooked fibers compared to mortars made with straight fibers (Fig. 10). In fact, the presence of hooked fibers allowed a difference in deflection value of 0.1 mm to be observed for mortars made with the same proportioning of fibers for the whole sample and 0.3 mm for mortars made per layer. However, the highest flexural deformation values are obtained for fiber-reinforced mortars with hooks compared to those without hooks.

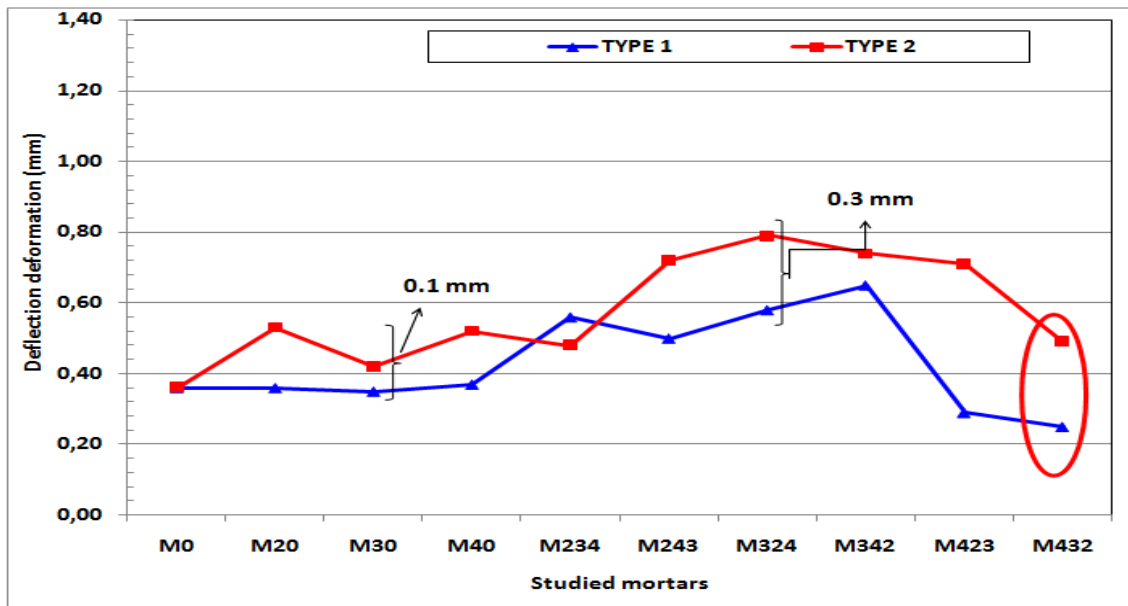


Figure 10: Deflection evaluation of mortar made with two types of fibers

### 3.5 Flexural elastic modulus:

The flexural elastic modulus was determined by relationship commonly used in strength of materials. The modulus of elasticity in bending varies as a function of the variation in the force-deflection ratio. The higher the value of the maximum loading the higher the modulus of elasticity in bending and the smaller the deflection, the larger the modulus.

From the results obtained, it can be seen that the modulus of elasticity in bending for the variants M20, M30 and M40 are almost identical for mortars containing fibers with and without hook.

For samples with different fiber dosing in layers, it should be noted that the elasticity modulus values of mortars M234, M423 and M432 made up of straight fibers is high compared to that containing fibers with hook. This is explained by the fact that the deflection value is higher for mortars containing hook fibers.

For mortar mixtures M243, M324 and M342: the modulus value is higher for those made with hook fibers.

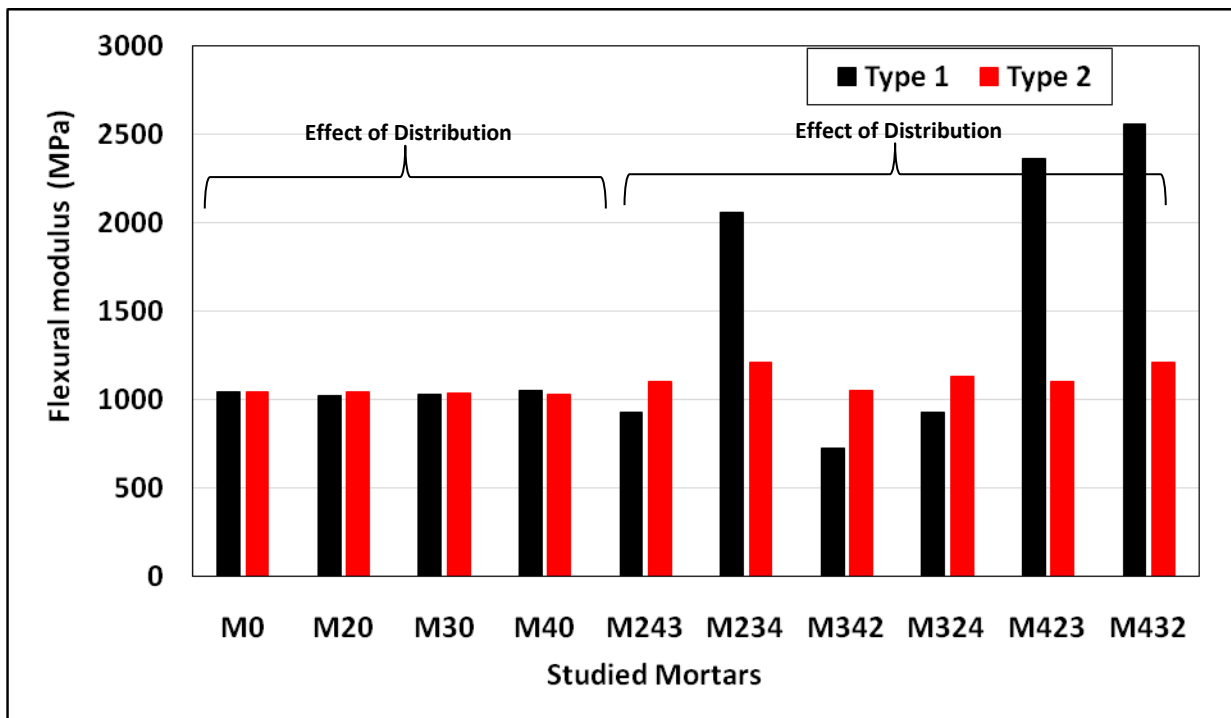


Figure 10: Flexural elastic modulus of mortar made with two types of fibers

#### 4 Conclusion

This paper has presented the highlighting of steel fiber distribution effect on strength and behavior mechanical in bending tensile of self-compacting mortar. The results which could be summarized and concluded as:

A new method of placing mortar in molds by layer has been developed. It improves bending tensile strength by 53.52% for mortars prepare with T1 straight steel fibers and 71.83% for mortars containing steel fibers with a hook at one end.

This method makes it possible to control the distribution of the fibers and to minimize the effects of walls in order to allow them to respond effectively to external solicitations.

The importance of the distribution of steel fibers in the cement matrix is illustrated using this method. The variants entirely contain the same dosage of metallic fibers ( $90 \text{ kg/m}^3$ ) but the bending tensile strength obtained varies according to the dosage of fibers in the layers.

The variants containing a high proportion of steel fibers in the lower layer have a high bending tensile strength.

The type of steel fibers influences the bending tensile strength. The use of steel fibers with a hook at one end made it possible to obtain higher resistances than those obtained with straight steel fibers. This is explained by the presence of a hook which requires significant energy for its extraction.

The bending tensile strength varies according to the distribution of the fibers in the cement

matrix, the dosage and the type of steel fibers used.

## 5 References

- [1] Baqersad, M., Sayyafi, E. A., & Bak, H. M. (2017). State of the art: mechanical properties of ultra-high performance concrete. *Civil Engineering Journal*, Volume 3(3), 190-198. DOI: 10.28991/cej-2017-00000085
- [2] M. Zhou, Wei Lu, Jianwei Song & George C. Lee. (2018). Application of Ultra-High Performance Concrete in bridge engineering. *Construction and Building Materials*. Volume (186), pp.1256-1267. DOI.org/10.1016/j.conbuildmat.2018.08.036
- [3] N.M. Azmee & N. Shafiq. (2018). Ultra-High Performance Concrete: From Fundamental to Applications. Case Studies in Construction Materials., pp.1-21  
doi.org/10.1016/j.cscm.2018.e00197
- [4] Dagenais, M. A., Massicotte, B., & Boucher-Proulx, G. (2018). Seismic retrofitting of rectangular bridge piers with deficient lap splices using ultrahigh-performance fiber-reinforced concrete. *Journal of Bridge Engineering*, 23(2), 04017129.
- [5] Lachance, F., Charron, J. P., & Massicotte, B. (2016). Development of Precast Bridge Slabs in High-Performance Fiber-Reinforced Concrete and Ultra-High-Performance Fiber-Reinforced Concrete. *ACI Structural Journal*, 113(5).
- [6] Elsa Nguyen Phuong Amanjean.(2015).*Développement de Bétons Fibrés Ultra Performants pour la réalisation d'éléments de structure préfabriqués*. Phd Thesis University of Toulouse. France
- [7] Verger-Leboeuf, S., Charron, J. P., & Massicotte, B. (2017). Design and behavior of UHPFRC field-cast transverse connections between precast bridge deck elements. *Journal of Bridge Engineering*, 22(7), 04017031.
- [8] Benjamin A. Graybeal. (2007). *Compressive Behavior of Ultra-High-Performance Fiber Reinforced Concrete*. *ACI Materials Journal*. Volume (104-M17), pp. 146–152.
- [9] S. Abbas, M.L Nehdi & M.A. Saleem. (2016). Ultra-High Performance Concrete: Mechanical Performance, Durability, Sustainability and Implementation Challenges. *Concrete Structures and Materials*. Volume (10), pp. 271–295. DOI.10.1007/s40069-016-0157-4
- [10] H.R. Sobuz, P. Visintin, M.S. Mohamed Ali, M. Singh, M.C. Griffith & A.H. Sheikh.(2016). Manufacturing ultra-high performance concrete utilizing conventional materials and production methods. *Construction and Building Materials*. Volume (111).pp. 251-261  
doi.org/10.1016/j.buildmat.2016.02.102
- [11] Doo-Yeol Yoo, Kyung-Hwan Min, Joo-Ha Lee & Young-Soo Yoon.(2014).Shrinkage and cracking of restrained ultra-high-performance fiber-reinforced concrete slabs at early age. *Construction and Building Materials*. Volume (73).pp. 357–365.doi.org/10.1016/j.buildmat.2014.09.097
- [12] Doo-Yeal Yoo, Soonho Kim & Min-Jae Min.(2018).Comparative shrinkage behavior of ultra-high-performance fiber reinforced concrete under ambient and heat curing conditions. *Construction and Building Materials*. Volume (162).pp. 406–419.doi.org/10.1016/j.buildmat.2017.12.029
- [13] Yi Xu, Jiaping Liu, Jianzhong Liu, Ping Zhang, Qianqian Zhang & Linhua Jiang.(2018).Experimental studies and modeling of creep of UHPC. *Construction and Building*

- Materials. Volume* (175).pp. 643-652.doi.org/10.1016/j.buildmat.2018.04.157
- [14] V.Y. Garas, K.E Kurtis & L.F Kahn.(2012). Creep of UHPC in tension and compression: Effect of thermal treatment. *Cement & Concrete Composites. Volume* (34).pp. 493-502.Doi :10.1016/j.cemconcomp.2011.12.002
- [15] Jun Li, Chengqing Wu & Hong Hao.(2015).Investigation of ultra-high performance concrete slab and normal strength concrete slab under contact explosion. *Engineering Structures. Volume* (102).pp. 395-408.doi.org/10.1016/j.engstruct.2015.08.032
- [16] Ali Als Salman, Canh N.Dang, Gary S. Prinz & W. Micah Hale.(2017).Evaluation of modulus of elasticity of ultra-high performance concrete. *Construction and Building Materials. Volume* (153).pp. 918-928.doi.org/10.1016/j.conbuildmat.2017.07.158
- [17] Masoud Pourbaba, Elyar Asefi, Hamed Sadaghian & Amir Mirmiran.(2018).Effect of age on the compressive strength of ultra-high-performance fiber-reinforced concrete. *Construction and Building Materials. Volume* (175).pp. 402-410.doi.org/10.1016/j.conbuildmat.2018.04.203
- [18] Kequan Yu, Jiangtao Yu & Zhou dao Lu. (2018). Mechanical Characteristics of Ultra High Performance. V. Mechtcherine et al. (Eds.), *Strain Hardening Cementitious Composites*.(RILEM Bookseries,15).
- [19] Yuliarti Kusumawardaningsih, Ekkehard Fehling, Mohammed Ismail & Attitou Amen Mohamed Aboubkr.(2015).Tensile strength behavior of UHPC and UHPFRC. *Procedia Engineering. Volume* (125).pp. 1081-1086. Doi :10.1016/j.proeng.2015.11.166
- [20] Kim Huy Hoang & Nguyen Viet Tue.(2018).Comparative Flexural and Tensile Behaviors of Ultra-High Performance Fiber Reinforced Concrete with Different Steel Fibers.V. Mechtcherine et al. (eds.). *Strain Hardening Cementitious Composites*.(RILEM Bookseries).
- [21] Haber, Z. B., De la Varga, I., Graybeal, B. A., Nakashoji, B., & El-Helou, R. (2018). Properties and behavior of UHPC-class materials (No. FHWA-HRT-18-036). United States. Federal Highway Administration. Office of Infrastructure Research and Development.
- [22] Shivam Gangwar, Suruchi Mishra & H.K.Sharma.(2019).An Experimental Study on Mechanical Properties of Ultra-High-Performance Fiber-Reinforced Concrete (UHPFRC). *Sustainable Construction and Building Materials*. pp. 873–886. doi.org :10.1007/978-981-13-3317-0\_08
- [23] Luis Felipe Maya Duque and Benjamin Graybeal. (2017).Fiber orientation distribution and tensile mechanical response in UHPFRC. *Materials and Structures*. pp 1-17. doi : 10.1617/s11527-016-0914-5
- [24] Huanghuang Huang, Xiaojian Gao, Linshan Li &Hui Wang. (2018).Improvement effect of steel fiber orientation control on mechanical performance of UHPC. *Construction and Building Materials. Volume* (188).pp. 709-721.doi.org/10.1016/j.conbuildmat.2018.08.146
- [25] Huanghuang Huang, Ansuhang Su,Xiaojian Gao & Yingzi Yang.(2019).Influence of formwork wall effect on fiber orientation of UHPC with two casting methods. *Construction and Building Materials. Volume* (215).pp. 310-320.doi.org/10.1016/j.conbuildmat.2019.04.200
- [26] Rui Wang, Xiaojian Gao, Huanghuang Huang & Guangshui Han. (2017).Influence of rheological properties of cement mortar on steel fiber distribution in UHPC. *Construction and Building Materials. Volume* (144).pp. 65-73.doi.org/10.1016/j.conbuildmat.2017.03.173
- [27] Cong Lu & Christopher K.Y Leung. (2017).Theoretical evaluation of fiber orientation and its effects on mechanical properties in Engineered Cementitious Composites (ECC) with various thicknesses. *Cement and Concrete Research. Volume* (95).pp. 240-



246.doi.org/10.1016/j.cimconres.2017.02.024

- [28] Sue Tae Kang, Bang Yeon Lee, Jin-Keun Kim & Yun Yong Kim.(2011).The effect of fiber distribution characteristics on the flexural strength of steel fiber-reinforced ultra-high strength concrete. *Construction and Building Materials. Volume (25)*.pp. 2450-2457.  
Doi:10.1016/j.conbuildmat.2010.11.057
- [29] Qiulei Song, Rui Yu,Zhonghe Shui, Xinpeng Wang, Suduan Rao & Zewen Lin.(2018).Optimization of fibre orientation and distribution for a sustainable Ultra-High Performance Fibre Reinforced Concrete (UHPFRC): Experiments and mechanism analysis. *Construction and Building Materials. Volume (169)*.pp. 8-19.  
doi.org/10.1016/j.conbuilmat.2018.02.130
- [30] Burak Felekoglu, Selçuk Turkel & Yigit Altuntas.(2007). Effects of steel fiber reinforcement on surface wear resistance of self-compacting repair mortars. *Cement & Concrete Composites. Volume (29)*.pp. 391-396.doi.org/10.1016/j.cemconcomp.2006.12.010
- [31] Warun Wongprachum, Manote Sappakittipakorn, Piti Sukontasukkul, Prinya Chindappasirt & Nemkumar Banthia.(2018). Resistance to sulfate attack and underwater abrasion of fiber reinforced cement mortar. *Construction and Building Materials. Volume (189)*.pp.686-694.doi.org/10.1016/j.conbuilmat.2018.09.043
- [32] Aamer Bhutta, Mohamed Farooq & Nemkumar Bathia.(2019).Performance characteristics of micro fiber-reinforced geopolymer mortars for repair. *Construction and Building Materials. Volume (125)*.pp.605-612.doi.org/10.1016/j.conbuilmat.2019.04.210
- [33] T. Simões, H. Costa, D. Dias-da-Costa & E. Julio. (2018). Influence of type and dosage of micro-fibers on the physical properties of fiber reinforced mortar matrixes. *Construction and Building Materials. Volume (187)*.pp.1277-1285.doi.org/10.1016/j.conbuilmat.2018.08.058
- [34] Mingli Cao, Ling Xu & Cong Zhang.(2018).Rheological and mechanical properties of hybrid fiber reinforced cement mortar. *Construction and Building Materials. Volume (171)*.pp.736-742.doi.org/10.1016/j.conbuilmat.2017.09.054
- [35] A. Schwartzentruber & C. Catherine. (2000).Method of the concrete equivalent mortar (CEM)- A new tool to design concrete containing admixture. *Materials and Structures/ Matériaux et Structures. Volume (33)*. pp. 475-482.
- [36] EFNARC (2002).Specification and guidelines for self-compacting concrete. pp 25-35.Free pdf copy downloadable from. Http: //www.efnarc.org.
- [37] European Standard (1999-b) “Methods of test for mortar for masonry, Part 10: Determination of dry bulk density of hardened mortar.” EN 1015-10, European Committee for Standardization CEN, Brussels, August
- [38] European Standard (1999-c) “Methods of test for mortar for masonry Part 11: Determination of flexural and compressive strength of hardened mortar.” EN 1015-11, English European Committee for Standardization CEN, Brussels, August.
- [39] Yoo, D.Y., Kim, S., Park, G.J., Park, J.J. & Kim, S.W.(2017).Effects of fiber shape, aspect ratio, and volume fraction on flexural behavior of ultra-high-performance fiber-reinforced cement composites. *Compos. Struct. Volume (174)*.pp.375-388.
- [40] Lee, S. J., Yoo, D. Y., & Moon, D. Y. (2019). Effects of hooked-end steel fiber geometry and volume fraction on the flexural behavior of concrete pedestrian decks. *Applied Sciences, Volume 9*(6), 1241.
- [41] Yazici, S., Inan, G. & Tabak, V. (2007).Effect of aspect ratio and volume fraction of steel fiber

- on the mechanical properties of SFRC. *Construction and Building Materials, Volume (21)*.pp.1250-1253.
- [42] Danying Gao, Lijuan Zhang, Michelle Nokken & Jun Zhao.(2019). Mixture Proportion Design Method of Steel Fiber Reinforced Recycled Coarse Aggregate Concrete. *Materials. Volume(12)*.p 375
- [43] Gao, D., Zhang, L. &Nokken, M.(2017).Mechanical behavior of recycled coarse aggregate concrete reinforced with steel fibers under direct shear. *Cement and Concrete Composites. Volume (79)*. pp1-8
- [44] Carneiro, J.A., Lima, P.R.L., Leite, M.B. & Toledo Filho, R.D.(2014).Compressive stress-strain behavior of steel fiber reinforced-recycled aggregate concrete. *Cement and Concrete Composites. Volume (46)*.pp 65-72.
- [45] Biao Li, Lihua Xu, Yuchuan Shi, Yin Chi, Qi Liu & Changning Li.(2018).Effects of fiber type, volume fraction and aspect ratio on the flexural and acoustic emission behaviors of steel fiber reinforced concrete. *Construction and Building Materials. Volume (181)*.pp 474-486
- [46] P. Mahakavi & R. Chithra. (2019). Impact resistance, microstructures and digital image processing on self-compacting concrete with hooked end and crimped steel fiber.*Construction and Building Materials. Volume (220)*.pp 651-666.
- [47] Pająk, M., & Ponikiewski, T. (2017). Investigation on concrete reinforced with two types of hooked fibers under flexure. *Procedia engineering*, 193, 128-135.